The Messenger

No. 154 – December 2013

Paranal instrumentation programme
Focus on ESO Public Surveys
Resolving AGN with MIDI

Paranal Instrumentation Programme: 2013–2020 Development Plan

Luca Pasquini[1]
Mark Casali[1]
Adrian Russell[1]

[1] ESO

The development plan for instrumentation at the Paranal Observatory was presented to the ESO Scientific Technical Committee (STC) in April 2013. Its overall goal is to keep Paranal at the forefront of ground-based astronomy. In addition to the completion of the current second generation instruments, the installation of the Adaptive Optics Facility with the imager and spectrometer ERIS, and execution of the Very Large Telescope Interferometer (VLT/I) mid-term implementation plan, it will allow one new instrument, or instrument upgrade, to be initiated per year (provided current projects are completed). The plan is divided into two phases. Over 2013–2017, instruments are selected and developed with the criteria of filling the VLT capabilities and maintaining the balance between dedicated and general purpose facilities. Beyond 2018, the instruments will be deployed in the era of maturity of the European Extremely Large Telescope (E-ELT). The strategy for the second phase derives from analysis of VLT science in the E-ELT era, to be fully shaped in the coming five years. One new instrument is also proposed for the New Technology Telescope at La Silla, fully funded by the community.

Strategic Overview

With the construction of the E-ELT, ESO will offer two main observatories to its community after 2020: Paranal (integrating the VLT and the E-ELT) and the Atacama Large Millimeter/submillimeter Array (ALMA). The fundamental goals for the Paranal instrumentation strategy can be summarised by quoting the strategic goals for ESO formulated by Council in 2004 and 2011:

– ESO must retain European leadership in astronomical research in the era of Extremely Large Telescopes (ELTs) by carefully balancing its investment in its most important programmes.
– The VLT must continue to receive effective operational support, regular upgrades — especially to stay at the forefront of image quality through novel adaptive optics concepts — and efficient new instrumentation in order to maintain its world-leading position for at least another decade; the unique capabilities of the VLTI must be exploited.

The instrumentation development plan does not define the long term strategy for the Paranal Observatory, but rather provides a framework within which to implement new instrumentation in the years 2013–2020, bearing in mind that, for the next ten years, the Paranal Observatory will be the main source of ground-based optical and infrared data for the ESO community. The long-term strategic view is being developed in a white paper, “Paranal in the era of E-ELT”. This white paper, and the process of its development over the coming years, has been recently discussed with STC. This strategy will be fully developed after the E-ELT funding decision, and its development will profit from a thorough discussion with the community at large.

When considering the VLT instrumentation projects currently under construction, in 2018 the second generation VLT and VLT interferometer (VLTI) instruments and the Adaptive Optics Facility (AOF) will be complete, and all VLT/I instruments, but five, will either be new or recently upgraded. This complement of instruments will cover most options in imaging (including adaptive optics [AO] and VLTI working at the diffraction limit) and spectroscopy in the 300–24 000 nm range (c.f. Figure 1). Four integral field unit (IFU) instruments (two AO-assisted) and at least four multi-object spectrographs will be in operation (none AO-assisted). The Paranal Observatory will provide polarimetry, high contrast imaging and coronography, fast photometry and superb astrometry, and also the finest instruments for precise radial velocity (RV) determination. In order to keep the Paranal Observatory competitive, however, a continuous initiative regarding new instrumentation development is planned from 2014.

Considering an overall instrument development time of six to seven years, the plan is separated into two phases, with a cross-over in ~ 2018. The first phase is devoted to providing the VLT with instrumentation that maintains a balance between general purpose and dedicated

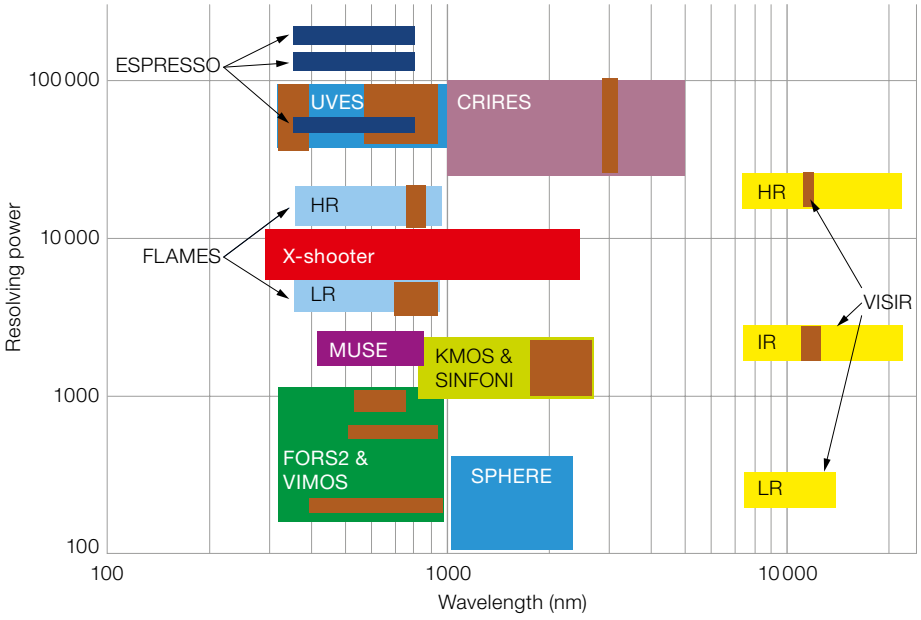

Figure 1. The wavelength–spectral resolving power domain for the VLT instruments (including those at the telescope and those in construction phase).

instruments. The second phase is dictated by the strategy of how the VLT will be used in the E-ELT era.

Phase 1 (Projects initiated before 2018/ deployed before ~ 2025).
There is no indication that the size of the Paranal user community will decrease. On the contrary, new Member States may join ESO, increasing the pressure on the Paranal facilities. Consequently the scientific use and output of Paranal instruments should be optimised. It is important to preserve a balance between specialised instruments and workhorse instruments, with the latter covering a wide range of scientific interests.

Phase 2 (Long-term opportunities in the E-ELT era, after ~ 2025).
This phase is still relatively open and different scenarios can be envisaged. The E-ELT will be fully operational and astronomical research with 8-metre-class telescopes may evolve towards a model where a large fraction of the time is devoted to dedicated experiments and large collaborative projects. In this context the four VLT Unit Telescopes together could provide a unique opportunity to dedicate up to ~ 1200 nights per year to a single problem. This approach could open up new perspectives in astronomical research. The last two instruments of the decade (deployed in 2018/2019), should be fully integrated into this long-term perspective. Their selection will occur after a careful reflection on the scientific use and role of the VLT in the E-ELT era. To this purpose, several scientific conferences will be held in the coming years to direct the choices and finalise the strategy and its implementation.

Programmatic drivers

The instrumentation development plan follows from consideration of a number of basic drivers:

Paranal and E-ELT
The E-ELT will be an additional telescope at the Paranal Observatory, and the strengths of each unit should be maximised. Synergy and the ability to complement E-ELT capabilities are therefore important criteria for the VLT.

Paranal, HST and JWST
By 2018 the Hubble Space Telescope (HST) will most likely no longer be in operation, and the James Webb Space Telescope (JWST) will be about to enter operations. HST capabilities that will be unavailable include ultraviolet (UV) spectroscopy and high-resolution imaging in the *B*- to *R*-bands. An instrument able to provide diffraction-limited observations in the *B*- to *R*-bands over a sufficiently large field could recover an important part of the missing parameter space. Complementarity between the VLT and the JWST in the areas of high resolution spectroscopy, observation of bright sources, diffraction-limited observation at short wavelengths, flexible operations, wide wavelength coverage and use of wide field can be mentioned. It may also be advantageous to provide some overlapping capabilities with JWST.

Paranal and ground-based observatories
The relationship of Paranal with other ground-based observatories (including ALMA) has still to be discussed in depth. In general, the Paranal choices will be driven by the scientific requests of the ESO community rather than by the developments of its competitors.

Maximisation of efficiency/optimal use of observing time
Optimisation can be achieved by concentrating on three main aspects: improved efficiency (throughput and duty cycle); extending the spectral coverage; exploring the possibilities for sharing the available foci. This goal could include the concept (new for the VLT) of instruments designed to be exchanged with a regular cadence.

Instrument development duration
The typical development time for second generation VLT instruments has been almost ten years from the time of conception. This long lead time should not be assumed to be inevitable, and the programme could develop instruments on shorter construction times if this becomes an agreed goal. One interesting possibility would be to create a new class of visitor instrument, operated by the construction team, but also including proposals from the community at large (in the manner of the VLTI instrument PIONIER).

Focus occupancy
With the arrival of ESPRESSO in 2016, all VLT/I foci will be occupied, including the incoherent combined focus. Some instruments (e.g., ISAAC and MIDI) will have been decommissioned as early as 2013–2014 and replaced by second generation instruments (SPHERE, MUSE and GRAVITY). Each time a new instrument is accepted, the instrument to be decommissioned will be identified on the basis of a grid of criteria that includes: scientific potential, complementarity with new instruments, instrument status and future perspectives.

Role of La Silla
It is clear that today the success of 4-metre-class telescopes is often linked to the ability to occupy scientific niches. HARPS at the ESO 3.6-metre telescope is a good example of such a success story. The specific added value of the La Silla 4-metre-class telescopes for ESO can be summarised:
– La Silla continues to be a competitive site in the southern hemisphere providing unique opportunities to its users;
– the ESO community continues to request the ESO 3.6-metre telescope and the New Technology Telescope (NTT) at reasonable to high oversubscription rates and both telescopes continue to produce good publication rates (105 refereed publications from the NTT in 2012, 69 from the ESO 3.6-metre);
– the ESO 3.6-metre telescope and the NTT are maintained to VLT technical standards and provide excellent image quality and efficiency at negligible technical down time;
– a minority of Member States have access to national 4-metre-class telescopes;
– La Silla provides the opportunity to dedicate a 4-metre-class telescope to one, or a few, scientific questions;
– 4-metre-class telescopes with state-of-the-art (workhorse) instrumentation release pressure on the observing time at the VLT (and in the future, possibly for the E-ELT).

Considering that the current NTT instrumentation is reaching the end of its life cycle (EFOSC2 went into operation in 1990, SOFI in 1998), ESO will launch a call in 2014 for a new instrument for the

NTT to be built in the community. This new instrument could replace either SOFI or EFOSC2 or both, and would be available to the ESO community for 50% of the time until 2021. Additional observing time with the new instrument will be available for interested groups through the co-funding of NTT operations.

The NTT call will be open for both specialised instruments, taking advantage of the large amount of dedicated observing time, as well as state-of-the-art workhorse instruments addressing broad needs within the ESO community. Such an instrument is required to be at negligible cost to ESO.

Instrument definition and procurement procedure

Scientific input for the new instruments is provided to the instrumentation programme manager through:
– the "Paranal in the E-ELT era" white paper, as well as other inputs from the VLT programme scientist;
– the community, by either contacting the instrumentation programme manager directly, via the STC, or via *ad hoc* scientific conference(s).

Each proposal will be scientifically evaluated by the VLT programme scientist. In order to ensure community input to the definition of the Paranal instruments, scientific workshops will be organised to address the scientific needs for the VLT in the next decade. The emphasis will be on 8-metre telescope science rather than instruments or technological concepts. These workshops, organised in the period 2013–2017, will define the instrumental capabilities to be developed after ~ 2018.

A working group of about 15 people (five from ESO, five composed of STC members and five community experts) will evaluate the best sequence in which to deploy the 2015–2018 projects. A non-exhaustive list of instrument options, which has emerged so far from the different inputs, is presented in the following sections.

After the various inputs have been collected and elaborated, a proposal consisting of the top-level characteristics for the instruments will be presented to the STC. Once the concept has been recommended a call for tenders for Phase A study will follow.

The Paranal instrumentation programme will not be static, and must be able to react to the evolving scientific and technological landscape and to re-assign priorities. New proposals will be evaluated by the programme manager, in collaboration with ESO management and the STC, against the existing plan. Acceptance of a new project may result either in cancelling/de-scoping or re-phasing planned projects. A similar evaluation will be made if one of the running projects requests a substantial increase in the allocated resources.

New instruments for the VLT

Following a series of Phase A studies and recommendations by the STC, the following new instruments are now in process.

CUBES

In UV spectroscopy from the ground (i.e., 300–380 nm spectral range), a large increase of efficiency with respect to the existing instruments (UVES and X-shooter) is possible. In addition, this spectral range complements that of the E-ELT and JWST. An efficient UV spectrograph can cover a broad science case and could be a world-leading instrument for many years to come. Located at the Cassegrain focus, it could be easily exchanged. The CUBES concept will be developed by a consortium of Brazilian institutes and ESO. The project has passed Phase A review and has been recommended by the STC. The detailed design is ongoing, and construction will commence following the ratification of Brazilian accession to ESO.

CRIRES upgrade

CRIRES is equipped with a pre-disperser and currently delivers a fraction of one echelle order per observation. A cross-disperser could increase the simultaneous wavelength range by a large factor. An upgrade that considers the installation of a set of cross-dispersers and new detectors has passed Phase A and, after positive STC recommendation, is now in the design and construction phase (Oliva et al., 2012). It will answer a number of scientifically pressing questions, and will, in addition, satisfy several of the above considerations (such as complementarity with JWST and improvement of efficiency).

MOONS and 4MOST

The proposal to build a new, powerful multi-object spectrograph (MOS) has been strongly endorsed by the ESO community and advocated in several instances by the STC. After a call for ideas, two competitive MOS Phase A studies were awarded: 4MOST (de Jong et al., 2011) and MOONS (Cirasuolo et al., 2011).

MOONS is a near infrared facility (0.8–1.8 μm) which can host up to 1000 fibres at the Nasmyth focus of the VLT. The field of view is about 500 square arcminutes. It can operate either at lower resolution (R ~ 5000) or at higher resolution (R ~ 20 000) in two selected spectral regions.

4MOST is proposed for the 4-metre VISTA telescope, with a field of view of more than 3 square degrees. It will host up to 2400 fibres and will work in the optical (0.3–0.9 μm). Sixteen hundred fibres will feed two lower resolution spectrographs (R ~ 5000), with 800 fibres to two higher resolution spectrographs (R ~ 20 000).

These two instruments are largely complementary in almost all aspects: spectral coverage, telescope used, field of view and scientific aims. Given the outstanding science cases presented by the two consortia, the enormous range of applications of large field spectroscopy and the strong push by the community to increase ESO's MOS capabilities, together with the strong complementarity with JWST and E-ELT, both instruments have been recommended for design and construction by STC. The work for MOONS has started in 2013 and 4MOST will start in 2014.

Potential new instruments for the VLT/I

After examining the current complement of Paranal instruments at the telescope, or in construction, a number of potential developments can be identified, which are listed below. This list is not intended to be exhaustive.

Workhorse instrument to complement/support FORS2 and X-shooter

FORS2, X-shooter and ISAAC (and also EFOSC at the NTT) are among the most popular and productive ESO instruments. They are typical workhorses and the user pressure on them is very high. It is important that ESO preserves this class of instrument. With the decommissioning of ISAAC, infrared spectroscopy in the 2.4–5 μm regime will no longer be available. Should the new workhorse be a multi-function multi-wavelength instrument? Or a copy (perhaps slightly modified) of one of the existing, most requested instruments? Such questions will be debated by the ESO/STC/community working group.

New Instrument for the AOF

In answer to the STC request for a plan for AO instruments at the VLT, ESO has proposed a development in two phases: ERIS, that will follow-up NACO and feed SPIFFI, the SINFONI spectrograph; a new, ambitious instrument, still to be decided, to fully exploit the potential of the AOF, in the focus occupied by GRAAL and HAWK-I. A high Strehl *B*- to *R*-band imager would be one attractive possibility. A multi-IFU, AO-assisted, large field spectrograph would also be unique, and its scientific merits should be studied.

In either case, the instrument may require a considerable amount of research and development. The scientific discussion about a new AO-assisted instrument of this type should start soon.

New VLTI instrument

The VLTI will continue to provide the highest angular resolution, even in the E-ELT era. The rising demand for imaging capability of stellar surfaces, close circumstellar environments and extragalactic sources sets a clear path for the VLTI medium-term development plan. PIONIER, GRAVITY, MATISSE and the second generation fringe tracker are, and will be, the immediate answers to that request. The continuous and successful effort to improve the VLTI's robustness and performance will be essential too.

However, improving the spectral coverage (visible to mid-infrared) and the imaging capability of VLTI should remain a high priority in the years to come. PIONIER already provides this and GRAVITY will provide observing modes close to the most demanded AMBER ones, but with greater sensitivity and much improved Fourier uv-plane coverage.

While it seems premature to start a new project given the enormous ongoing effort to complete and operate PRIMA, GRAVITY and MATISSE, some avenues to be explored for the VLTI in the coming years include:

1) Securing the continuity of PIONIER and offering it to the community;
2) Continuing to offer a visitor focus at the VLTI;
3) Exploring the six-telescope imaging capabilities of VLTI with the existing infrastructure.

Potential VLT instrument upgrades

Even if most of the VLT/I instruments will be new or recently upgraded, the 15 years of VLT experience demonstrate that there are frequent requests for upgrades (mostly of detectors) and that these have served the community very well.
Upgrades under consideration are:

- X-shooter: Two proposals to upgrade X-shooter have been submitted and have been evaluated.
- FORS2: A proposal to upgrade the FORS2 detector is being prepared. The use of a 4kx4k pixel CCD detector would bring substantial operational benefits.
- SPHERE: The deformable mirror is formally below specification, and a replacement could be needed if its performance deteriorates.

All major upgrades will be treated as any other project, and compared to running or planned instruments in order to decide priorities. It must be clear that starting one project per year implies that either a new instrument or a major upgrade can be initiated, but not both.

Potential new instruments for La Silla

3.6-metre

In 2014 HARPS will be equipped with the Laser Frequency Comb (LFC), but will be out-performed by ESPRESSO at the VLT after ~ 2017. However HARPS has the advantage of using a dedicated telescope and of having built up a long time-series of observations; it should be used for the sources that do not need an 8-metre collecting area. HARPS is highly requested, and its future demand will also depend on the fate of space missions. It is worth recalling that exoplanet science is a young and expanding field.

NTT

The new instrument for the NTT (see above) could either be a dedicated instrument or a multi-function workhorse.

An exciting approach could be to complement HARPS at the ESO 3.6-metre with a near-infrared planet-finder at the NTT, matching the RV precision of HARPS. Several observatories are planning instruments of this kind in the northern hemisphere. High velocity precision could make it unique.

An X-shooter-type instrument for the NTT could be an interesting alternative to EFOSC2 plus SOFI.

Roadmap

Starting from 2013, the resources dedicated to E-ELT instrumentation will progressively increase. This will imply a progressive decrease in the resources available for the Paranal instrumentation programme to a new level that can sustain the "one new start per year" plan. Table 1 shows the proposed timetable. For all instruments, one year of Phase A is foreseen and a development time

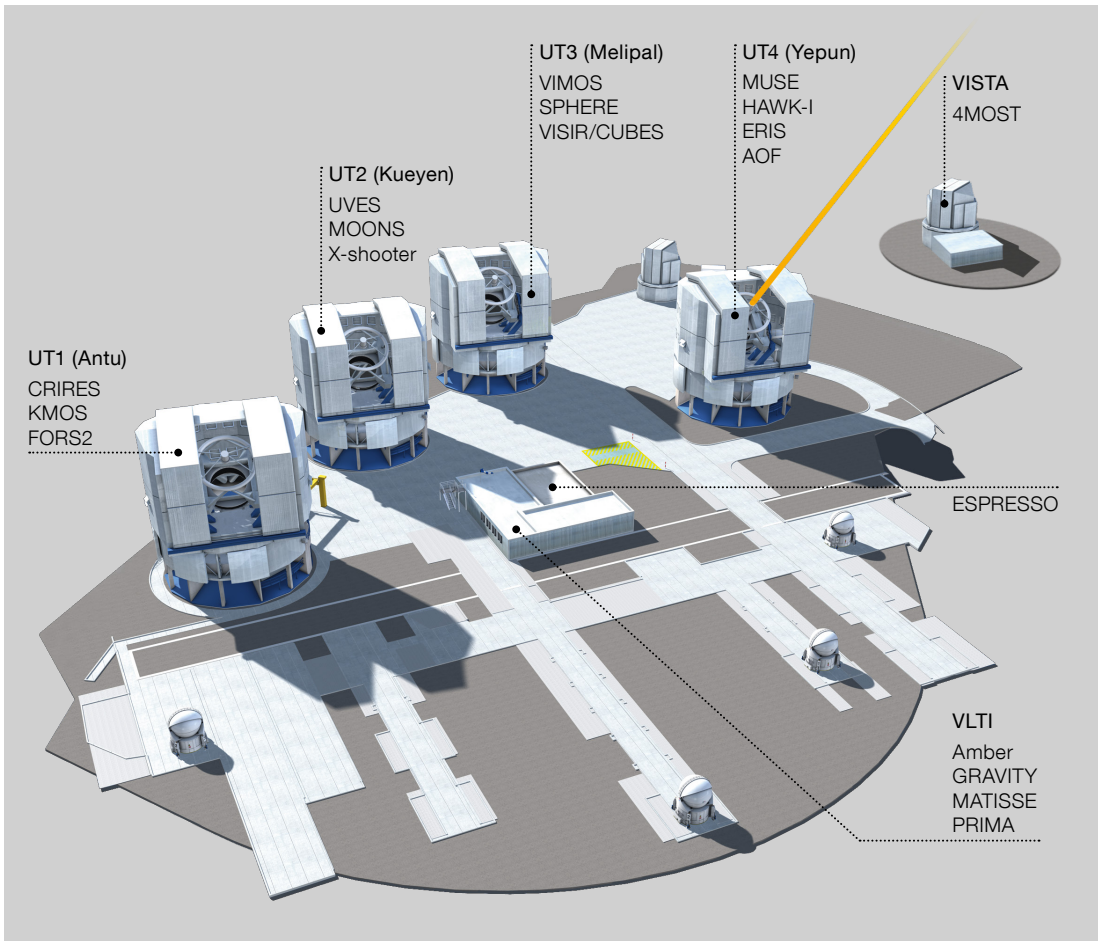

Figure 2. Planned Paranal instrumentation in 2019. One new instrument in integration, four in design and construction and one in Phase A are also planned at this time (see Table 1).

of five years. This is on the short side, but not unrealistic. Figure 2 shows the Paranal instrumentation and the project development in 2019 according to the present plan. In a resource-constrained environment, the beginning of new projects will also have to be subject to satisfactory completion of existing projects. If existing projects run late, the new ones will be re-planned accordingly.

References

Cirasuolo, M. et al. 2011, The Messenger, 145, 11
de Jong, R. et al. 2011, The Messenger, 145, 14
Oliva, E. et al. 2012, Proc. SPIE, 84462N

Links

The agendas of Council and STC meetings can be found on the ESO web pages: http://www.eso.org/public/about-eso/committees/

Year	Phase A	Design & Construction	Delivery
2012	CUBES CRIRES upgrade	ERIS	KMOS VIMOS upgrade
2013		MOONS CRIRES upgrade	MUSE SPHERE
2014	Letter of interest NTT	4MOST	VISIR upgrade PRIMA astrometry GRAVITY LFC for HARPS
2015	New I (NTT?)	CUBES (?)	AOF MATISSE
2016	New II	New I (NTT?)	ESPRESSO VLTI
2017	New III	New II	CRIRES upgrade
2018	New IV	New III	CUBES(?) MOONS
2019	New V	New IV	ERIS 4MOST
2020	New VI	New V	New I (NTT?)

Table 1. Proposed development plan for the Paranal instrumentation programme. One year of Phase A is expected to be carried out, and the overall duration is typically estimated as six to seven years. Delivery in the last column refers to start of integration in Paranal for instruments or to the end of the integration for infrastructure projects (such as the AOF and VLTI).

Revisiting the Impact of Atmospheric Refraction on VIMOS-MOS Observations: Beyond the Two-hour Angle Rule

Rubén Sánchez-Janssen[1]
Fernando Selman[2]
Steffen Mieske[2]
Paul Bristow[2]
Peter Hammersley[2]
Michael Hilker[2]
Marina Rejkuba[2]
Burkhard Wolff[2]

[1] NRC Herzberg Institute of Astrophysics, Canada
[2] ESO

Multi-object spectroscopic (MOS) observations with VIMOS have traditionally been limited to a narrow two-hour range from the meridian to minimise slit losses caused by atmospheric dispersion and differential refraction. We revisit the impact of these effects on the quality of VIMOS-MOS spectra through extensive simulations of slit losses. We show that MOS observations can be effectively extended to plus/minus three hours from the meridian for fields with zenith angles smaller than 20 degrees at culmination — provided a nonstandard rotator offset angle of 0 degrees is used. The increase in target observability will enhance the efficiency of operations, and hasten the completion of programmes — a particularly relevant aspect for the forthcoming spectroscopic public surveys with VIMOS.

Atmospheric refraction in VIMOS-MOS observations

VIMOS (Le Fevre et al., 1998) is a wide field-of-view (four fields of 7 by 8 arcminutes) instrument with imaging, integral field, and multi-object spectroscopic capabilities mounted at the Nasmyth B focus of the Very Large Telescope (VLT) Unit Telescope 3. The instrument operates in the optical wavelength range (360–1000 nm), and is equipped with six sets of grisms, six sets of broadband filters, plus three additional filter sets specifically designed to be used in combination with the grisms to block the second-order spectra. During the last few years the instrument performance has been significantly enhanced (see Hammersley et al., 2012; 2013): changing the detectors to red-sensitive, low-fringing CCDs; replacing the HR-blue grism set with higher throughput volume phase holographic grisms; introducing an active flexure compensation system; redesigning the focusing mechanism and mask cabinet; and introducing a new pre-image-less MOS mode (Bristow et al., 2013). All these improvements have made VIMOS a much more stable instrument, and have extended its lifetime to prepare it for the start of the spectroscopic public surveys for which ESO has recently issued a call.

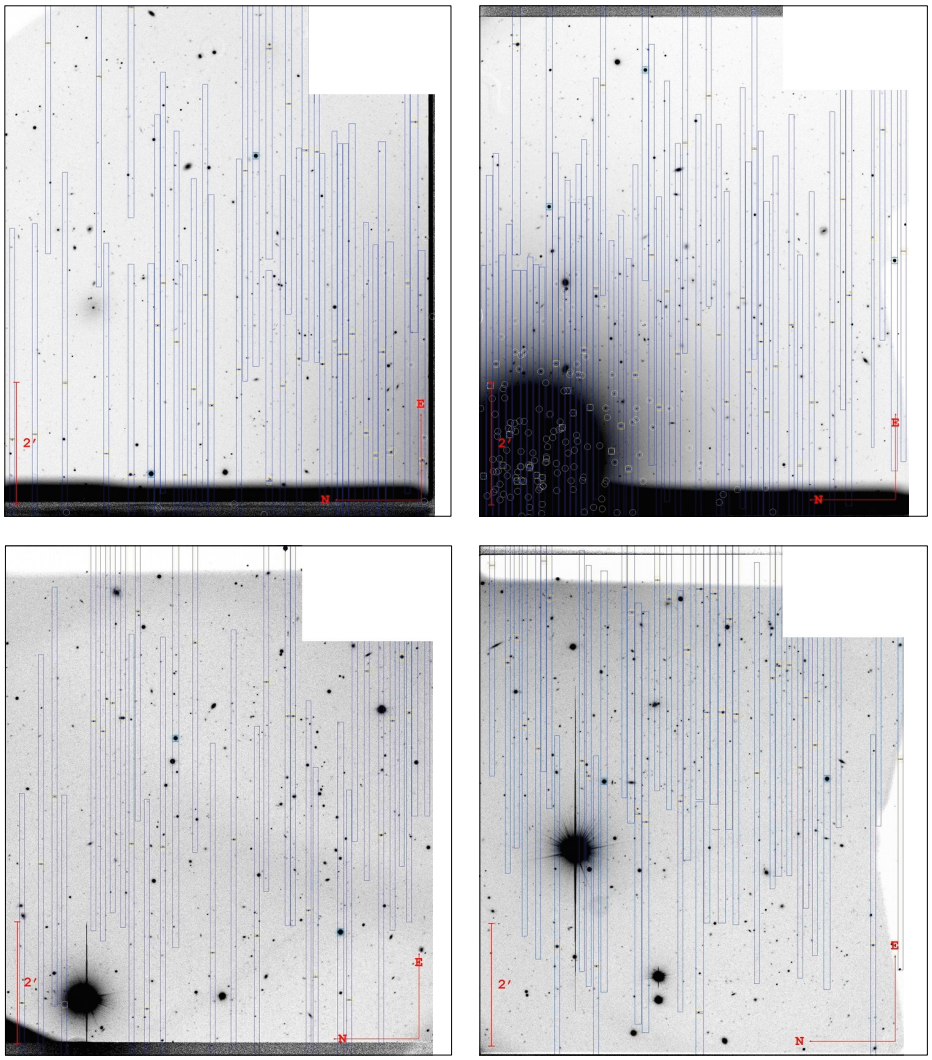

Figure 1. Example of a VIMOS finding chart for MOS observations. Each quadrant is 7 by 8 arcminutes, and they are separated by two arcminute gaps. Allocated slits are overplotted in blue. The blank areas (upper right of each finding chart) are masked out proposal information.

Further work to improve the operational efficiency of the instrument includes the present study, which has, as its main goal, to revisit the need for restricted observability of targets only within plus and minus two hours from the meridian in the MOS mode — the two-hour angle rule. VIMOS is not equipped with atmospheric dispersion compensators (ADCs), and MOS observations are carried out using multi-slit masks (see Figure 1). As a result, atmospheric dispersion (caused by the wavelength variation of the index of refraction of air) and field differential refraction (resulting from airmass variations across the field of view [FoV]) introduce a wavelength-dependent flux reduction, due to slit losses, that cannot be corrected. Unfortunately, field rotation further prevents the alignment of all slits

along the parallactic angle (PA), so that slit losses can only be minimised by a careful optimisation of the observability windows.

The atmospheric effects in VIMOS-MOS were studied with great detail in Cuby et al. (1998). They show that: i) atmospheric dispersion dominates at shorter wavelengths, while differential refraction is not negligible at the red end of the visible spectrum; ii) in the former case, image drifts occur along the meridian; iii) differential refraction can be almost neglected for zenith distances smaller than 25 degrees for exposure times of duration up to two hours from the meridian. In view of these results they recommended that, in order to minimise flux losses, the slits be positioned along the dispersion direction at mid-exposure (north–south), and observations be limited to a narrow two-hour range from the meridian crossing. This guarantees that losses remain below 20% for zenith angles < 50 degrees at culmination.

These rather limiting guidelines have always been in place for all MOS observations since the start of operations in 2003, and, in practice, translate into mandatory airmass constraint limits for the VIMOS-MOS observing blocks. Increasing the observability of targets in the MOS mode provides more flexibility to operations, because the number of masks that can be loaded into the instrument before the beginning of each night is limited. VIMOS is very often used for deep observations of cosmological fields, where very long integrations are taken for the same field. By increasing the target visibility (relaxing the two-hour angle rule), observing programmes can be completed faster.

In this report we revisit the impact of atmospheric refraction on the quality — in terms of slit losses and spectrophotometric distortions — of VIMOS observations for all the different MOS setups. We note that the parameter space of this problem is huge. Irrespective of image quality and weather conditions, slit losses depend on slit orientation and position within the FoV, observed wavelength range, target declination, total exposure time, and hour angle (HA) of the observations. We have tried to condense all this information to provide VIMOS users with clear, optimal recommendations.

A model to address slit losses

In order to investigate potential operational improvements that could enhance the efficiency of VIMOS, we have simulated the effects of slit losses under different circumstances. Our fiducial model assumes a flat input spectrum and nine slits evenly distributed across the entire VIMOS FoV, from the centre to the corners, and with relative separations of seven arcminutes. All slits have a length of 10 arcseconds and width of 1 arcsecond, which is typical for the majority of VIMOS-MOS observations. We assign two different orientations for the slits at meridian crossing, namely north–south (PA = 0 degrees), and east–west (PA = 90 degrees). Here we follow the usual on-sky convention for orientations, but note that this differs from the rotator offset angle described in the VIMOS manual: the default offset angle of 90 degrees corresponds to a north–south on-sky orientation, while a non-standard rotator offset angle of 0 degrees corresponds to east–west on sky.

Alignment and guiding are assumed to be done at either 450 nm (for the blue grisms only) or 700 nm (for the rest), and the seeing point spread function is considered to be wavelength- and airmass-independent, with a Gaussian full width at half maximum of 1 arcsecond. In reality, of course, the seeing will vary as a function of both parameters, but we note that, during actual service mode operations, seeing constraints have to be satisfied at any given airmass and instrument setup — and therefore our assumption provides the closest match to reality. This setup results in a 24% fiducial flux loss due to finite seeing and slit width, and under the assumption that the objects are perfectly centred within the slits. We adopt the average night-time pressure (743 mbar) and temperature (12 C) at the Paranal Observatory within the last five years (courtesy of J. Navarrete) in our computation of atmospheric refraction. Finally, for each of the six VIMOS grisms (and filter combinations) we assume observations with 3600 s exposure times, within four hours from meridian crossing, and for targets in the $-75 \leq \delta \leq +25$ degree declination range.

Figure 2 shows an example of the output from the simulations. Each panel shows, for the nine different positions across the VIMOS FoV, the output spectra obtained after a one hour long integration ($-3 < HA < -2$) on a $\delta = 0$ degree field, and using the LR-red grism. Solid (dotted) lines correspond to slits oriented along the north–south (east–west) direction at meridian crossing. The dashed lines indicate the fiducial maximum flux mentioned above. For each slit we also provide the corresponding values for the two figures of merit with which we characterise the results of the simulations: the total relative flux loss (f), and the spectral distortion ($\Delta = 1 - f_{min}/f_{max}$). In this particular case, even though the two slit orientations result in very similar median slit losses ($f = 0.10$ and $f = 0.09$ for the north–south and the east–west orientation, respectively), the east–west alignment provides more stable results across the FoV, and lower median spectral distortions ($\Delta = 0.07$ *vs.* $\Delta = 0.15$). This should therefore be the preferred orientation.

Figures 3 and 4 illustrate the final results for the entire set of simulations in the case of the LR-blue and the LR-red grisms respectively. In all panels the solid curves show the minimum, median and maximum flux losses, and spectral distortions, of the nine simulated slits as a function of target declination, and for the two different slit orientations at meridian crossing. Each column corresponds to a one hour long integration with target hour angle as indicated at the top. We note that the behaviour of the curves is similar for both grisms, but both losses and distortions are significantly smaller at the red end of the visible spectrum.

The general trends for the two slit orientations can be summarised as follows. For the north–south (PA = 0 degree) orientation, we find that at fixed HA there is a very weak dependence on declination (except for $|HA| > 2$ hr and the bluest wavelengths). The minimum of the loss/distortion distributions increases and moves towards southern declinations at larger HAs. For any given grism, there is a strong dependence with HA, such that

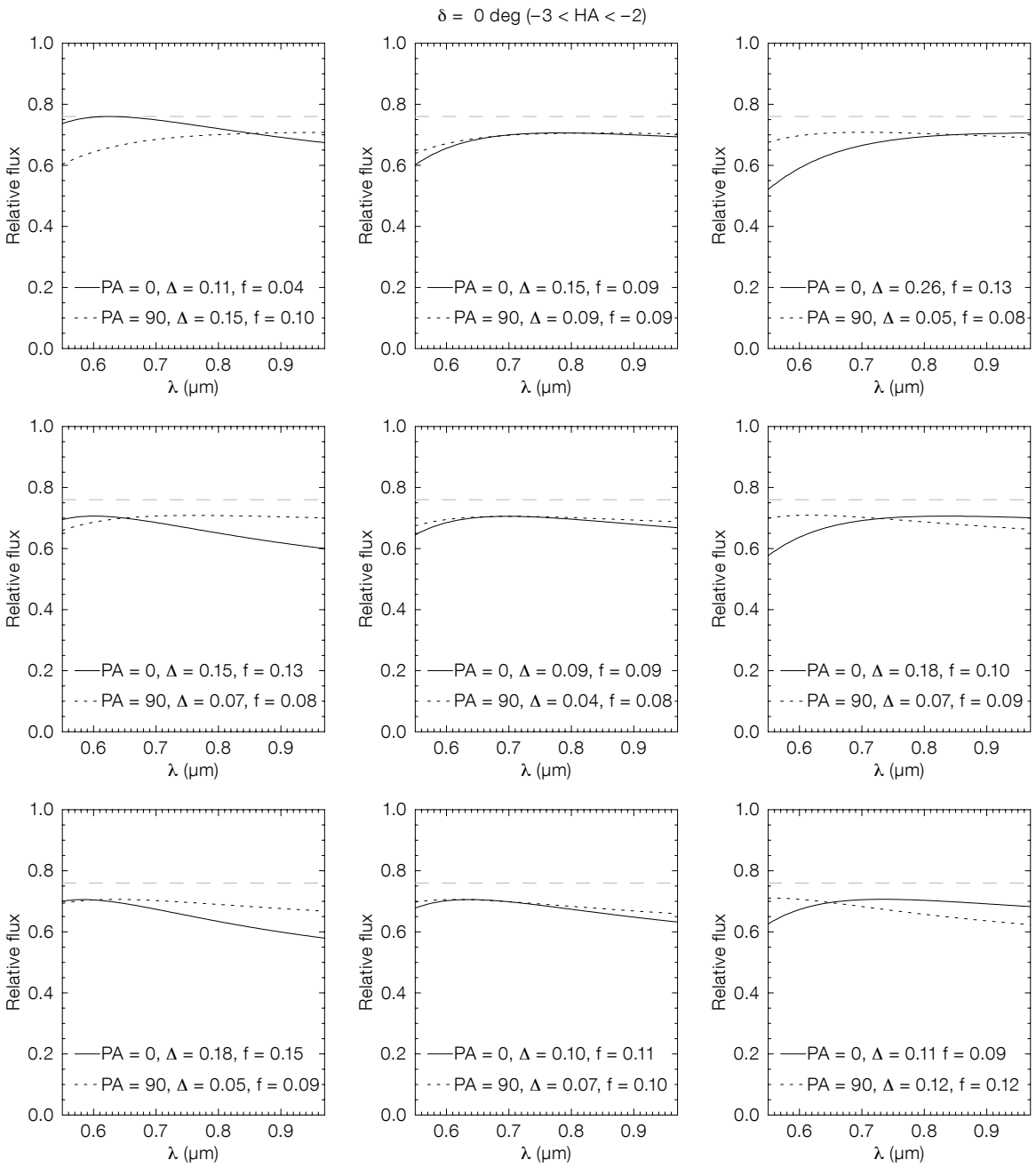

Figure 2. Output simulated spectra for nine different slit positions across the VIMOS FoV. These are the result of a one hour long integration (–3 < HA < –2) on a δ = 0 degree field using the LR-red grism for an input flat spectrum. In each panel we show the spectra for two different slit orientations, as well as the corresponding relative flux loss (*f*) and spectral distortion (Δ).

larger distortions and flux losses occur at larger HAs. Both the amount of losses/distortions, and the dependence on declination, increase for bluer wavelengths.

On the other hand, for the east–west (PA = 90 degree) orientation, we see that at fixed HA there is a very strong dependence on declination, but the behaviour flattens towards redder wavelengths. The minimum of the loss/distortion distributions slightly decreases and moves towards southern declinations at larger HAs. For any given grism, there is very little dependence on HA (except for extreme declinations). Finally, the dependence on declination of losses/distortions increases towards bluer wavelengths.

Beyond the two-hour angle rule

Extracting simple rules from a problem with such a high dimensionality requires a certain level of data compression. Following the previous work by Cuby et al. (1998), we set the tolerance level for losses/distortions at 20%. In Figure 5 we show the declination–hour-angle pairs (colour-coded according to slit orientation) for which the median spectral distortion (top row) or median flux loss (bottom row) across the VIMOS FoV remain below this tolerance value during a one hour long integration. It is evident that for fields culminating at small zenith distances the

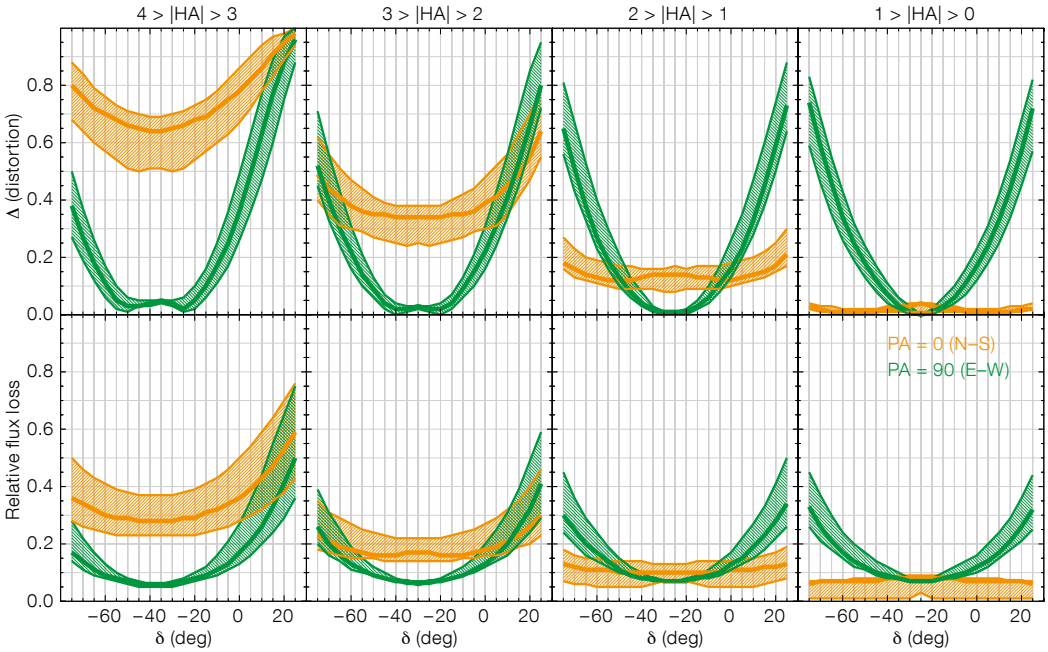

Figure 3. Curves show, for the LR-blue grism, the minimum, median and maximum flux losses (lower row) and spectral distortions (upper row) for the nine simulated slits as a function of target declination. The region between the minimum and maximum, about the median, is shaded. The plots show the effects for two different slit orientations at the meridian (north–south in orange and east–west in green).

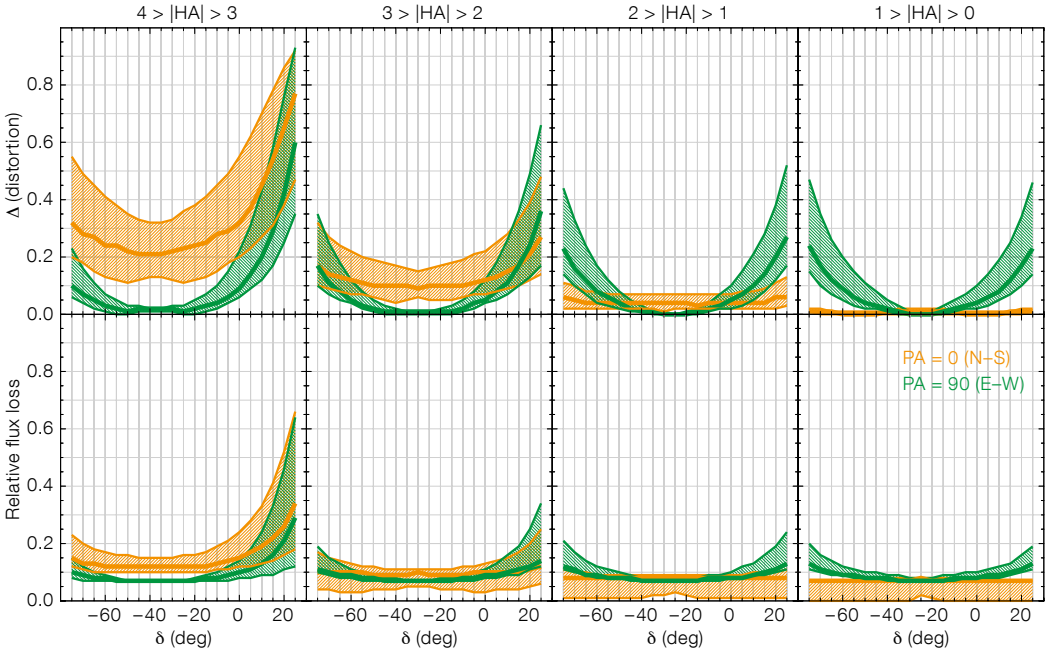

Figure 4. Same as Figure 3, but for the LR-red grism.

optimal slit alignment is the one that follows the east–west direction at meridian crossing. This is expected, as this slit orientation is closer to the parallactic angle at high airmasses, and dispersion is almost negligible close to meridian crossing. We note, however, that the flux loss differences between the north–south and east–west orientations are small for these fields when observed within two hours from the meridian — as was originally pointed out by Cuby et al. (1998). We also note that the most stringent constraints arise from the blue grisms.

In summary, the two-hour angle rule, together with the default north–south slit orientation, provide the most stable results, with slit losses and spectral distortions below 20 % and almost independent of target declination. This should always be the preferred option for users with targets at $\delta \gtrsim -5$ or $\delta \lesssim -45$ degrees. However, for targets within the $-45 < \delta < -5$ degree range, the east–west orientation is generally preferred. This slit orientation allows for observations to go past the two-hour angle rule, and be effectively extended up to |HA| = 3 hours. This holds for all grisms currently offered in VIMOS, provided the acquisition is done with a filter that closely matches the grism wavelength

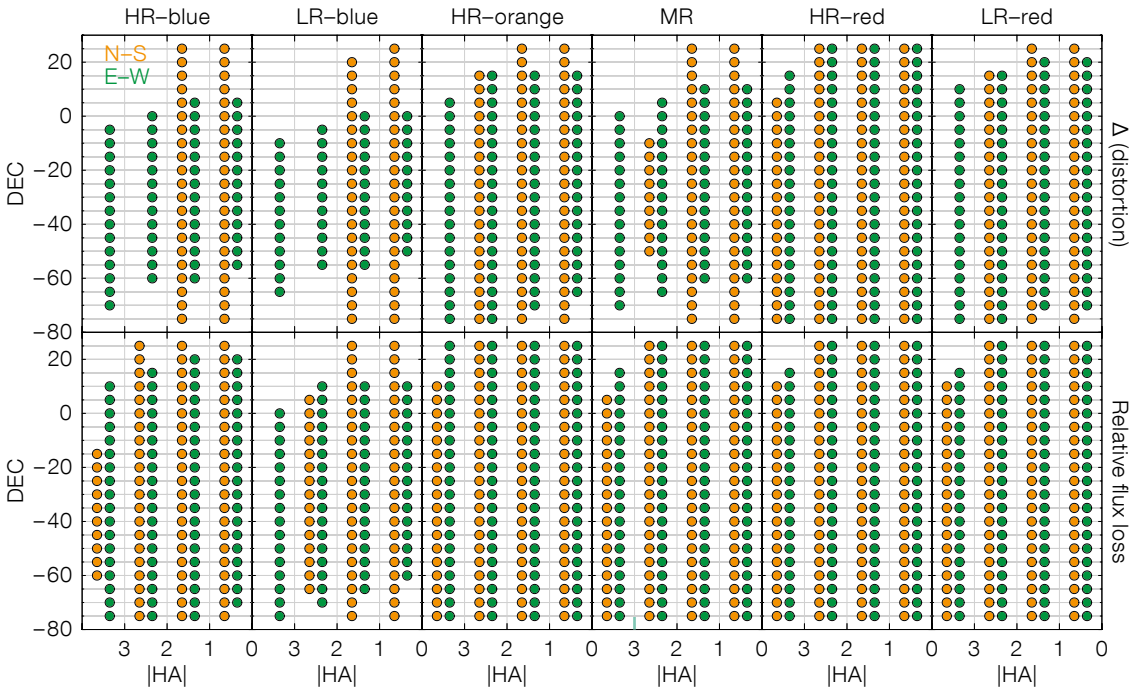

Figure 5. Circles show the declination–hour-angle pairs (colour-coded according to slit orientation — orange for north–south and green for east–west) for which the median spectral distortion (top row) or median flux loss (bottom row) across the VIMOS FoV remain below 20% during a one hour long integration, for all the VIMOS grisms.

range. Figure 6 shows the new airmass constraint limits for MOS observation blocks. They have been significantly relaxed for fields culminating at small zenith distances, thus increasing target observability. This will enhance the efficiency of operations, and speed up the completion of programmes — a particularly relevant aspect for the forthcoming spectroscopic public surveys with VIMOS. These recommendations for MOS observations have already been in place since September 2013. To define the optimal slit position angle for any specific target declination and instrument setup, we refer the users to the summary plots in the slit losses report at the VIMOS news section[1].

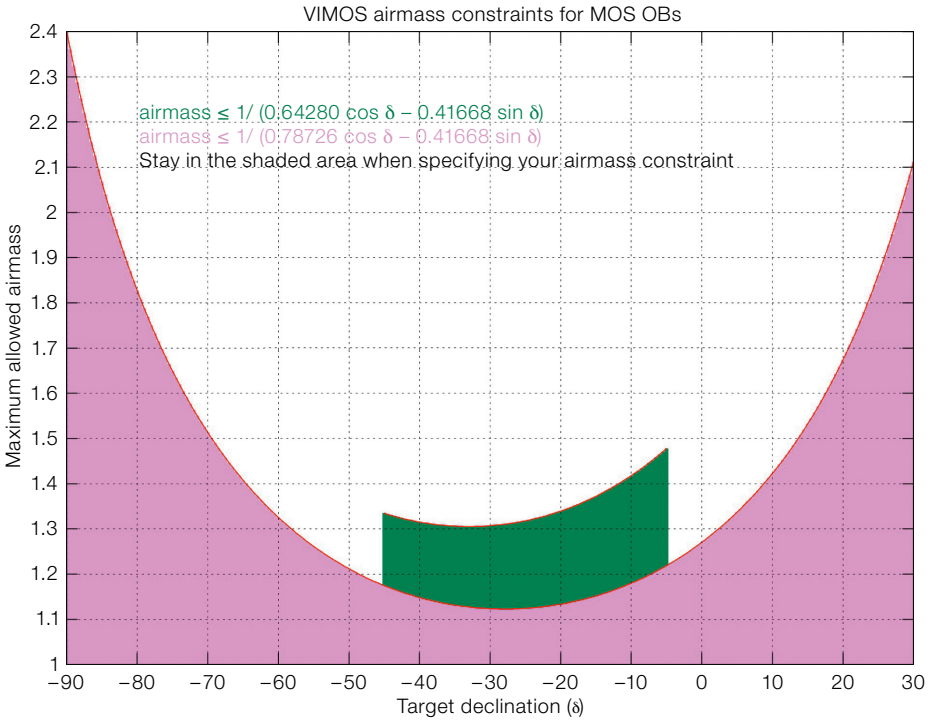

Figure 6. VIMOS airmass constraints for MOS observing blocks. The two different shaded areas correspond to the limits for fields that can be observed with slits having north–south orientations at meridian (purple), or east–west orientations (green). The generating formulae for these curves are shown with the same colour coding.

References

Bristow, P. et al. 2012, The Messenger, 148, 13
Cuby, J.-G. et al. 1998, Proc. SPIE, 3355, 36
Hammersley, P. et al. 2012, The Messenger, 142, 8
Hammersley, P. et al. 2013, The Messenger, 151, 2
Le Fèvre, O. et al. 1998, Proc. SPIE, 3355, 8

Links

[1] Report on VIMOS slit losses: http://www.eso.org/sci/facilities/paranal/instruments/vimos/doc/rsjvimosslitlossessept2013.pdf

OmegaCAM Science Operations

Steffen Mieske[1]
Dietrich Baade[1]
Magda Arnaboldi[1]
Giovanni Carraro[1]
Danuta Dobrzycka[1]
Armin Gabasch[1]
Philippe Gitton[1]
Nicolas Haddad[1]
Michael Hilker[1]
Ronald Holzloehner[1]
Valentin D. Ivanov[1]
Sebastien Morel[1]
Mark Neeser[1]
Loethe Noethe[1]
Ricardo Parra[1]
Andres Parraguez[1]
Monika Petr-Gotzens[1]
Andrew Rakich[1]
Marina Rejkuba[1]
Miguel Riquelme[1]
Fernando Selman[1]
Ricardo Schmutzer[1]
Thomas Szeifert[1]

[1] ESO

The science operations process of the VLT Survey Telescope (VST) camera, OmegaCAM, is described. OmegaCAM is a 267-megapixel CCD camera imaging a 1 × 1 degree field of view with a pixel scale of 0.21 arcseconds. It began operations in October 2011. The telescope and camera provide a survey speed that is five times greater than the now-decommissioned Wide Field Imager on the MPG/ESO 2.2-metre telescope at La Silla. OmegaCAM is currently used for three public surveys, guaranteed time observations for the OmegaCAM and VST consortia, and Chilean programmes. The execution of OmegaCAM observations, real-time quality control and the calibration plan are outlined.

General description of the facility

The VST resulted from a collaboration between the Italian National Institute of Astrophysics (INAF) under the Principal Investigator (PI) Massimo Capaccioli and ESO (see Capaccioli & Schipani [2011] for a description). OmegaCAM[1] was built in a collaboration between ESO and the OmegaCAM consortium (PI, Konrad Kuijken) with contributions from the Netherlands, Germany and Italy and is described by Kuijken et al. (2002) and Kuijken (2011). With OmegaCAM ESO fulfilled its mandate from the ESO Council to provide an optical wide-field imaging capability at Paranal Observatory.

OmegaCAM is the wide-field imager for the Cassegrain focus of the VST on Paranal. The VST is a 2.6-metre modified Ritchey–Chretien alt-azimuth telescope (F/5.5) designed specifically for wide-field imaging, to exploit the good image quality at the Paranal Observatory. OmegaCAM observes from 330–950 nm within a corrected field of view of 1 × 1 degree, four times the size of the full Moon. OmegaCAM samples the VST field of view with a 32-CCD, 16k × 16k detector mosaic with 0.21-arcsecond pixel scale (Figure 2). The CCDs are thinned, blue-sensitive, three-edge buttable CCD44-82 devices from e2v of high (but not perfect) cosmetic quality. In addition to the 32 CCDs making up the science array, OmegaCAM also contains four auxiliary CCDs around the edges of the field that are used for autoguiding and image analysis. Since both guiding and image analysis are performed on the instrument side, the telescope "only" tracks, but does so very well. Outside a zenith-centric circle of about 10 degrees diameter, image quality remains acceptable for up to ~ 2–3 minutes without guiding.

Most data are taken in the five Sloan-like bands *u′*, *g′*, *r′*, *i′* and *z′*, and a narrow-band Hα filter provided by the VPHAS+ consortium. Service mode operations for OmegaCAM started on 15 October 2011. The median full width at half maximum (FWHM) of OmegaCAM images, as measured during the first half year of operation, was about 0.80 arcseconds in *i′*-band, and 0.95 arcseconds in *g′*-band (including the instrumental resolution of 0.4 arcseconds). In the first two years of operations, the sky was clear or photometric 77 % of the time.

Three public surveys are being executed at OmegaCAM (see Figure 3): the Kilo-Degree Survey (KiDS; 1500 square degrees), ATLAS (4500 square degrees), and the VST Photometric Hα Survey (VPHAS+; 2000 square degrees). For their detailed setup and science goals, see the public survey web pages[2] and

ESO/INAF-VST/OmegaCAM/G. Lombardi

Figure 1. Left: The VST on the VLT platform. Right: OmegaCAM (the yellow volume) mounted on the VST.

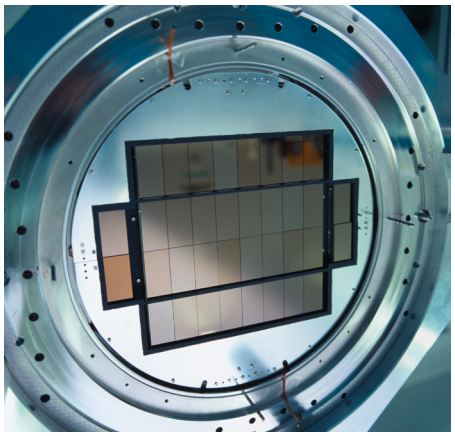

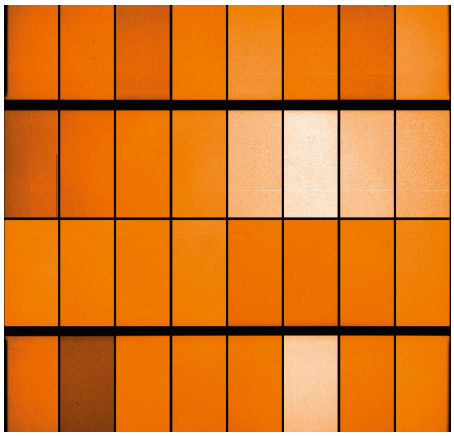

Figure 2. Left: An image showing the 32 (4 × 8) CCD array of OmegaCAM and the four auxiliary CCDs used for guiding and wavefront analysis. Right: OmegaCAM dome flat illustrating individual chip sensitivities, which have a root mean square chip-to-chip variation of ± 6%. The 32 science CCDs cover 92% of the 1 × 1 degree field of view with only small inter-chip gaps. Dither patterns of a few arcminutes total amplitude are used to image the full field of view.

the dedicated articles in this *Messenger* edition. Releases of data from these surveys are available through Phase 3[3]. The execution of these three surveys takes up 50–60% of the available service mode time. The remaining 40–50% is shared between guaranteed time observations (GTO) for the OmegaCAM and VST consortia, Chilean programmes, and calibration observations. The respective shares may evolve over time as a function of programme completion rates.

The survey speed of OmegaCAM is about five times higher than the Wide Field Imager (WFI) at the MPG/ESO 2.2-metre telescope in La Silla (Baade et al., 1999). The good image quality and high blue sensitivity provide a unique window in observational parameter space. Furthermore, it complements very well the near-infrared survey telescope VISTA at Paranal (Emerson & Sutherland, 2010), which is operated at the neighbouring console in the VLT control room. VST and VISTA together cover the entire near-ultraviolet to near-infrared range 0.33–2.35 μm: VST from 0.33–0.95 μm, and VISTA from 0.85–2.35 μm, with an overlap at the *z*′-band that is used by both facilities.

Execution of observations

All observations on the VST are carried out in service mode. The two surveys with short integration times, VPHAS+ and ATLAS, observe most of the time in open loop (no guiding, no image analysis). Due to the high cadence of ~ 1–2 minutes between images taken at different positions on the sky in these two surveys, there is no time to acquire image analysis stars and perform active optics correction at each new position. A new correction is enforced after, at most, half an hour in such open loop observations. The KiDS survey spends more time on a single pointing due to the science requirement of providing a deep and accurate weak lensing map. KiDS observations are, therefore, performed with guiding and closed loop image analysis.

The telescope and instrument are operated at night by one telescope operator, without a night-time astronomer. The short-term scheduling of observations is done by a program called the Observing Tool (OT; see also Bierwirth et al. [2010]). The basic observation unit containing the full description of the observation sequence (acquisition and science exposures), information about the target and the required observing constraints necessary to achieve the scientific objective, is called an Observation Block (OB). At any given time, the OT filters out all OBs that are not observable in the current conditions (due to seeing, airmass, Moon illumination, sky transparency), and then ranks the observable OBs to match, as well as possible, the observing conditions requested by the users, while

Figure 3. The on-sky footprint of the three public surveys executed with OmegaCAM: KiDS (1500 square degrees), ATLAS (4500 square degrees), VPHAS+ (2000 square degrees).

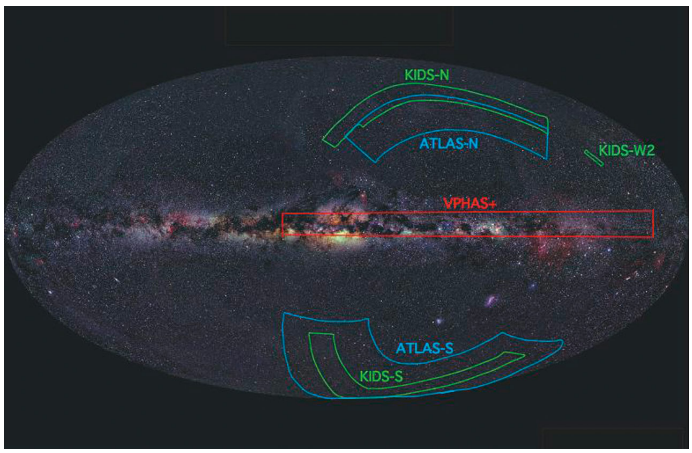

Figure 4. Distinguished visitors at the VST OmegaCAM console: Chilean president Sebastian Piñera and his wife. Also present in the picture is Paranal staff astronomer Fernando Selman.

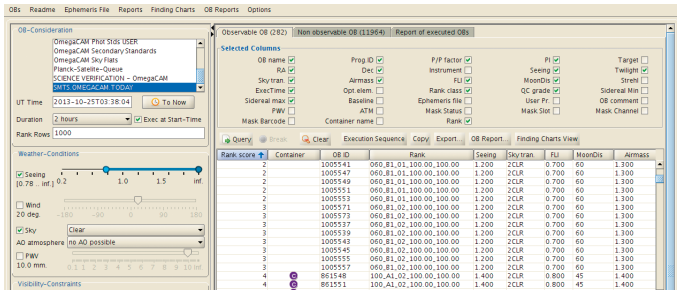

Figure 5. Example screenshot of Observing Block ranking as performed by the Observing Tool.

taking into account relative programme priorities (see Figure 5 for an example of the OT ranking). Users prepare their OBs using the P2PP[4] software which includes the option to define relations between OBs (groups, concatenations and time series). Those higher level constraints are also included in the ranking made by the OT.

It is worth noting that around full Moon there is a scarcity of observable OBs due to the bright sky background, which most of the science cases for optical imaging cannot tolerate. Also, only a few programmes accept the presence of thin clouds. The combination of those two issues has led to a comparably high fraction of 8–10 % idle time at the VST. ESO is taking measures to improve the baffling of the VST which, in turn, will reduce the effect of scattered moonlight on the science images. More detail is provided in the section on challenges and outlook.

Real-time quality control during night-time observations

The high cadence of observations and large number of 32 CCDs (267 megapixels) requires reliable automated quality control. With one person operating both the telescope and the instrument at night, it is not possible to measure manually image quality parameters across the field for all those images, which can amount to several hundred per night. Real-time quality control is performed by using the output log of the OmegaCAM data reduction pipeline, which was assembled by ESO from algorithmic modules provided by the OmegaCAM consortium. There is a 1–2 minute delay between the completion of an image and the availability of the pipeline output log. This allows near real-time assessment of data quality, enables fast decisions to be taken to re-adjust the input parameters for the OT ranking engine, and hence optimise the observation plan for the next hour(s). The pipeline provides measurements of mean point spread function (PSF) FWHM and ellipticities for detected sources in each single chip.

The core of the automated quality control is a dedicated script with some 800 lines of code which reads in the pipeline output log, calculates the specific parameters that are used for quality control assessment (called QC0 at ESO), and suggests quality control grades for each OB to the night-time operator (see Figure 6). Specifically, the script calculates, for each frame across the field of view, the mean FWHM, the mean ellipticity and the IQ variation, which is the variation in the FWHM in the centre of the field *vs.* the FWHM at the edge of the field of view. The script also measures the number of single CCD images affected by ellipticities greater than 0.2. These numbers are then appropriately averaged across an OB, or concatenation of OBs, and the script suggests to the operator the zero-level quality control (QC0) grades (fully/almost/not within constraints). The general QC0 acceptance criteria for an OB are: average seeing ≤ 1.1 × requested seeing; average ellipticity ≤ 0.15; and IQ variation ≤ 25 %.

In addition to these criteria for a single OB, the QC0 script includes a number of nested criteria regarding single images, concatenations of OBs, special cases like GTO and agreements with consortia about deviations from the general QC0 acceptance criteria per OB. The script also contains a number of warning flags which highlight image quality and calibration plan issues to the operator. The full set of these criteria is quite complex and could not realistically be tracked manually by an operator during the night. Therefore the QC0 script is a crucial part of OmegaCAM science operations. It allows fully reproducible quality control according to criteria agreed between ESO and the users that is as independent as possible from variations in human habits. An example output is indicated in Figure 6, left panel.

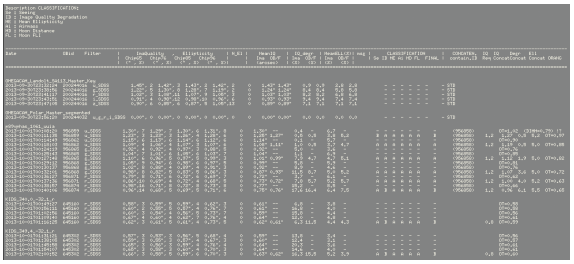

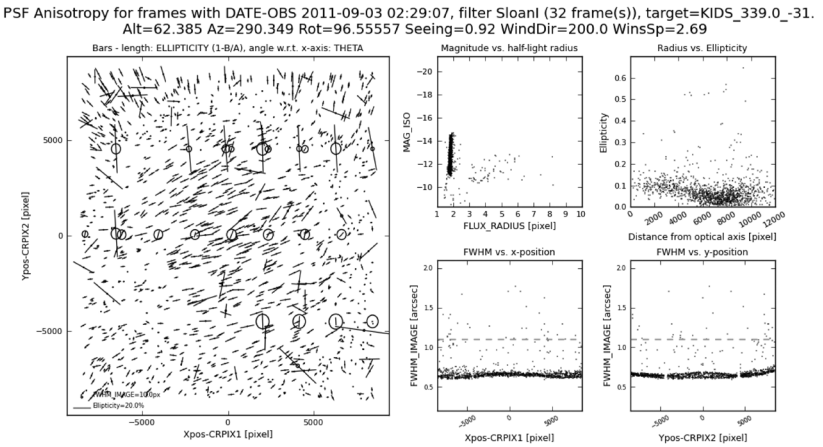

Figure 6. Left: Example output of the real-time quality control script used for OmegaCAM. Each line corresponds to one image. The grouped sets of images correspond to one OB or a concatenation of OBs. Right: PSF anisotropy distribution for a single image of average FWHM 0.65 arcseconds, taken in Early Science.

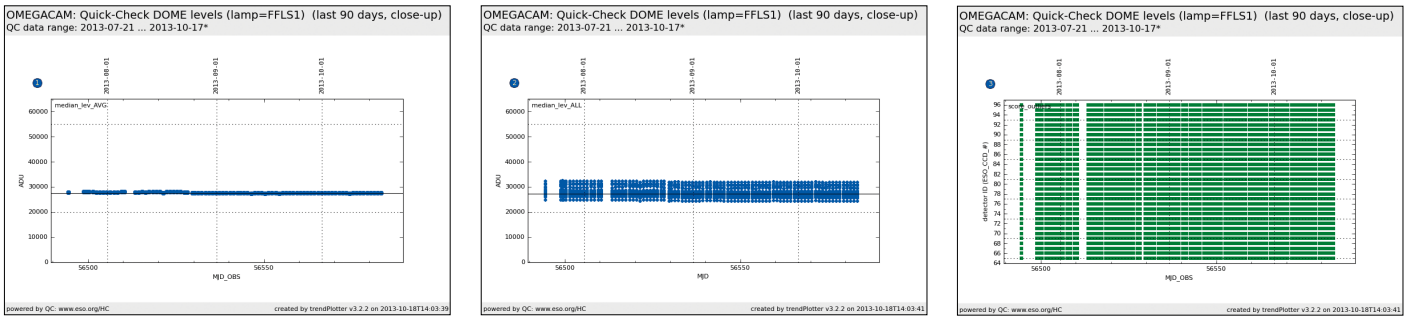

Figure 7. An example of an OmegaCAM health-check scoring performed by the QC group in ESO Garching. The left panel shows the dome flat level averaged over all 32 detectors, while the middle panel shows the median level for each detector. The panel on the right plots the score status of each detector (labelled with their names: ESO_CCD_#65 to ESO_CCD_#96) as a function of time. If the dome flat level falls below or exceeds levels defined for each detector, then the square at that date will turn red.

The set of QC0 criteria applied to OmegaCAM night-time observations ensures that we fulfil our mission statement of providing data of excellent image quality to the users. This very strict adherence to a combination of criteria leads to a slightly larger rate of OB repetitions than for other instruments: for OmegaCAM, about 20% of time in service mode is spent on repeating OBs (note that all data, whether in or out of constraints, is immediately transferred to the ESO archive). The typical fraction for other non-adaptive optics instruments at Paranal is 10–15%. Paranal instruments using adaptive optics, and VLT interferometer instruments, have a greater than 20% fraction of time spent on repeating observations since they very often push out to the instrumental and atmospheric limits. For OmegaCAM, the balance between strict QC0 and quick observing progress is constantly reviewed by the operations team in consultation with the survey consortia.

Calibration plan

The calibration plan of OmegaCAM ensures continuous monitoring of the system throughput in the *u′*, *g′*, *r′*, *i′* and *z′*-bands. Sky flats are taken in two to three filters during each clear evening twilight. Equatorial Landolt photometric standard star fields in *u′* to *z′*-bands are observed at the beginning and in the middle of the night. Furthermore, a short observation close to the southern celestial pole is performed three times per night in a segmented filter with simultaneous *u′*, *g′*, *r′* and *i′* coverage. These high airmass observations guarantee continuous monitoring of the extinction, complementing the low-airmass Landolt field observations. Other filters like Johnson *B* and *V* or Hα are calibrated with Landolt standards only if science data are taken in these filters. Based on dedicated dither observations of the Landolt fields in all chips and under photometric conditions, the OmegaCAM consortium has built up secondary standard star catalogues (currently with more than 315 000 stars) in the key bands for the full 1 × 1 degree field of view.

Daytime calibrations consist of daily bias and dome flats, and weekly gain/linearity measurements. Quality control during the day focuses on monitoring the chip sensitivities, bias levels, dark current levels, readout noise, gain and linearity, flat lamp intensities, twilight flat levels, magnitude zeropoints and image quality (FWHM and ellipticity). A description of the OmegaCAM health checks[5] and the resulting scores and plots[6] is maintained. This follows the classic ESO approach of scored health checks maintained by the QC group in Garching (Hanuschik et al., 2008). An example of the detector-monitoring health check is shown in Figure 7.

Challenges and outlook

VST operations have non-negligible overheads, impacting the completion progress of the public surveys, which were planned before the telescope and camera performance parameters were measured. Most notably, the time used to bring and keep the telescope focal plane to its best shape is higher than originally expected. In the first two years of OmegaCAM operations, about 30% of the available science time was used for acquisition, mainly image analysis. This can be compared to 10% for VISTA. Related to this, OmegaCAM has a larger fraction of direct interaction with the system for the telescope operator when compared to VISTA.

Work is ongoing, in collaboration with the instrument and telescope consortia, to improve the control procedures of the VST main and secondary mirrors, and to optimise image analysis algorithms on the OmegaCAM side. The aim is to move closer towards fully automated operations, including automatic acquisition of guide and image analysis stars.

Another area of improvement is the sky concentration effect that produces rotationally asymmetric features of 5% amplitude in the sky flats (see the OmegaCAM user manual[7]), and reflection/scattering features in images close to the Moon (within a few tens of degrees). Calibrating out the sky flat variations requires great care in data reduction (see the consortium report on sky concentration correction[7]). Additional baffling for the VST will be tested at the end of 2013; this will improve the reproducibility of the sky concentrations in sky flats, and permit observations closer to the Moon, thus reducing idle time.

Survey progress and first results

In Figure 8 the progress of the VST public surveys during the first two years of operations is shown. In total, about 1000 hours of observing time per year have been spent on executing public survey OBs within user constraints.

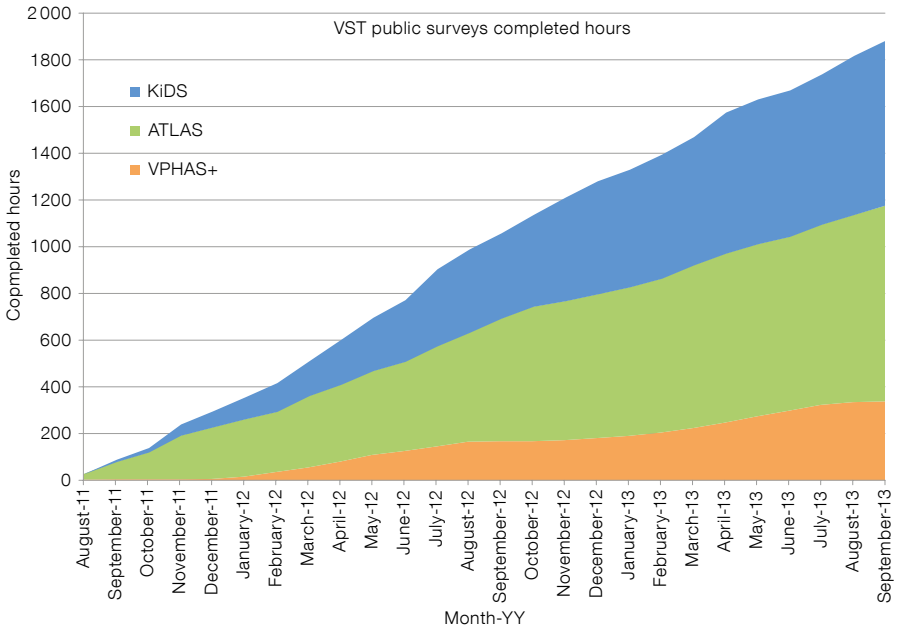

Figure 8. Cumulative number of hours, since start of operations, spent on completed OBs for the three VST OmegaCAM public surveys. About 50–60% of the available service mode time at VST is spent on public surveys. The rest is shared between GTO and Chilean programmes.

In Figure 9, a few first science results from VPHAS+ and KiDS, kindly provided by the survey teams, are illustrated. In the VPHAS+ example (left), an ionised nebula surrounding the extreme red supergiant, W26, begins to be resolved (from Wright et al., 2013). As the only known example of a compact ionised nebula around a red supergiant, this represents a unique opportunity to study the mass loss of red supergiants, using the tools of nebula astrophysics. The right panel shows one example of the nine-band *u′* to *Ks* photometry of KiDS (OmegaCAM) and VIKING (VISTA Kilo-Degree Infrared Galaxy Survey) being used to hunt for high-redshift quasi-stellar object (QSO) candidates which drop-out in the KiDS *i′*-band ($z > 5.7$) and VIKING *z*-band ($z > 6.5$); from Venemans et al. (2013). The histogram shows the redshift distribution of all published quasars at $z > 5.7$ (in grey). Currently, more than 50 quasars at $z > 5.7$ have been discovered in various surveys. The red histogram bars show the redshift distribution of the quasars found in the combined KiDS/VIKING survey thus far. The number of quasars expected in the total KiDS/VIKING area of 1500 square degrees is about 40, with > 10 above $z = 6.5$.

Figure 9. Left: A composite *g′*-Hα-*i′* image of the dense, very massive cluster Westerlund 1, taken as part of VPHAS+, is shown. This image allows the study of the ionised nebula surrounding the extreme red supergiant, W26 (Wright et al., 2013). The zoomed part of the image (centre), shown in orange, is Hα only. Right: High-redshift QSOs detected by combining KiDS (OmegaCAM) and VIKING (VISTA) data (Venemans et al., 2013), indicated as red in the histogram. See text for more details.

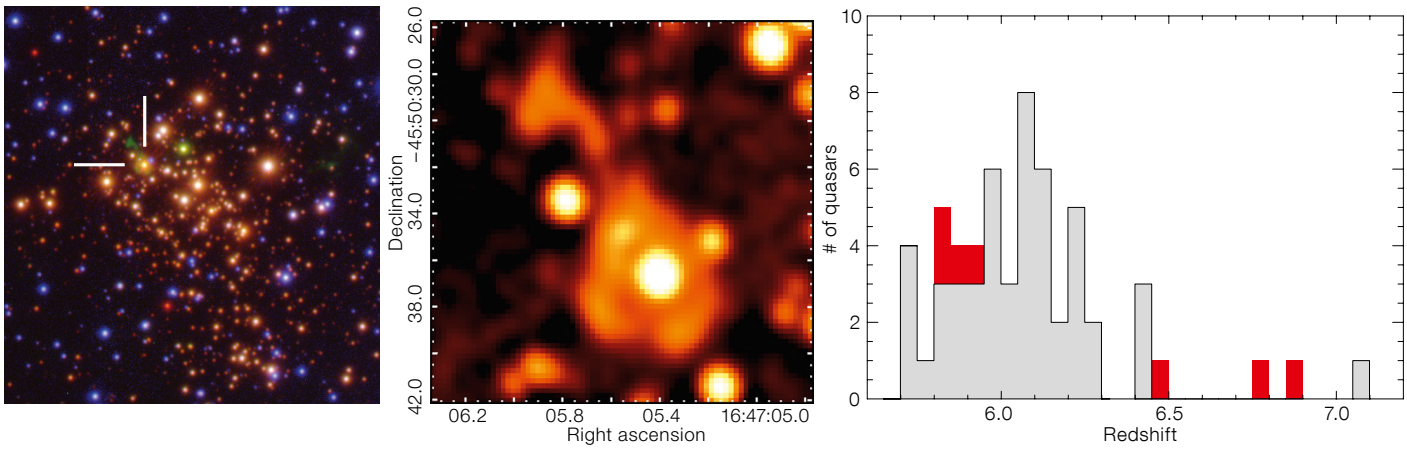

References

Baade, D. et al. 1999, The Messenger, 95, 15
Bierwirth, T. et al. 2010, SPIE, 7737E, 19
Capaccioli, M. & Schipani, P. 2011, The Messenger, 146, 2
Emerson, J. P. & Sutherland, W. 2010, SPIE, 7737E, 4
Hanuschik, R. W. et al. 2008, SPIE, 7016E, 22
Kuijken, K. 2002, The Messenger, 110, 15
Kuijken, K. 2011, The Messenger, 146, 8
Venemans, B. et al. 2013, ApJ, 779, 24
Wright, N. J. et al. 2013, MNRAS, in press, arXiv:1309.4086

Links

[1] ESO OmegaCAM webpage: http://www.eso.org/sci/facilities/paranal/instruments/omegacam
[2] Setup and goals of the VST public surveys: http://www.eso.org/sci/observing/PublicSurveys/sciencePublicSurveys.html
[3] ESO Phase 3 page: http://www.eso.org/sci/observing/phase3.html
[4] Phase 2 P2PP software: https://www.eso.org/sci/observing/phase2/P2PP3.html
[5] OmegaCAM quality control pages: http://www.eso.org/observing/dfo/quality/OMEGACAM/qc/qc1.html
[6] Health check scores and plots: http://www.eso.org/observing/dfo/quality/OMEGACAM/common/score_overview.html
[7] OmegaCAM user manual and consortium report on sky concentration correction: http://www.eso.org/sci/facilities/paranal/instruments/omegacam/doc/

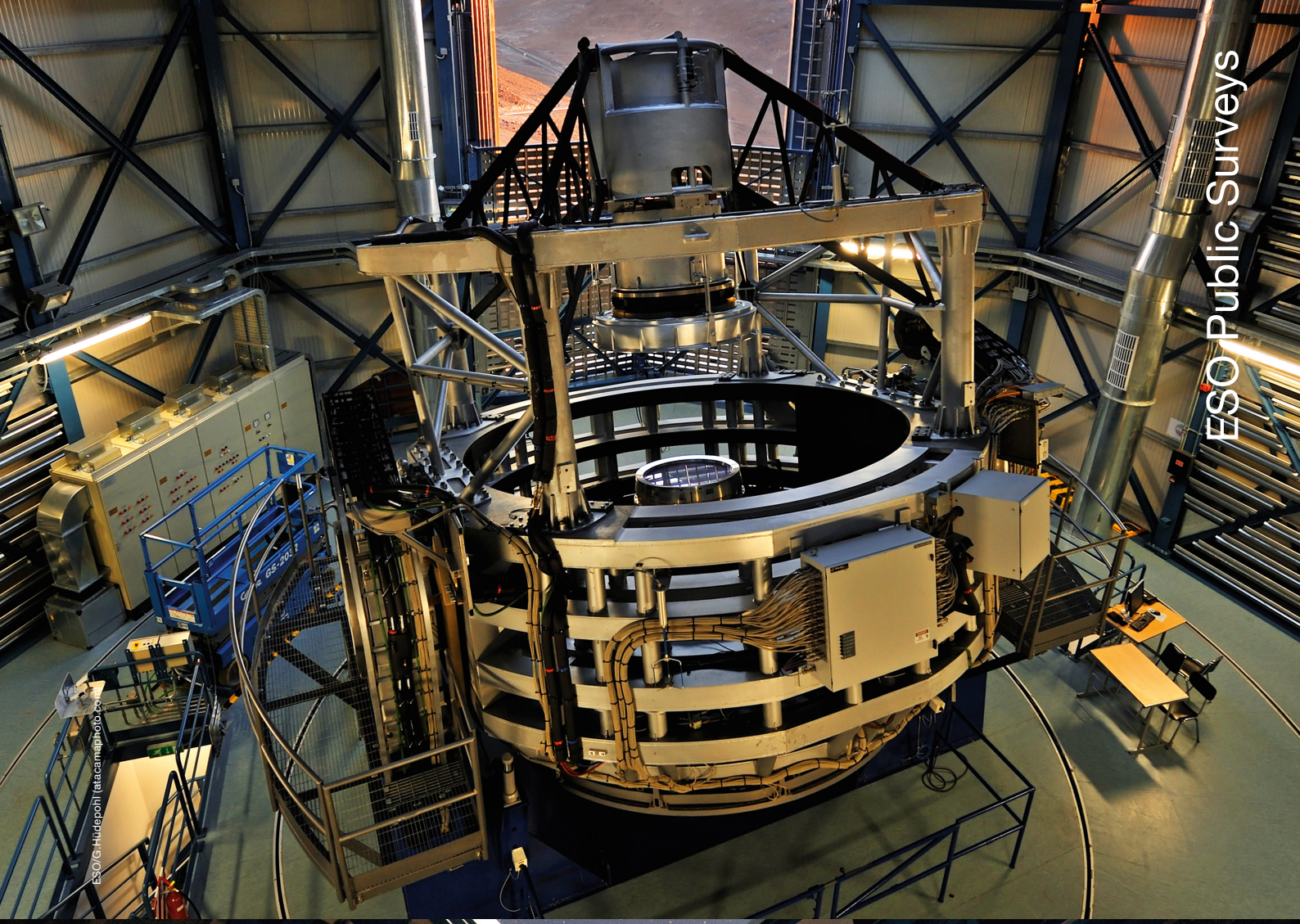

ESO/G.Hüdepohl (atacamaphoto.com)

The two VLT imaging survey telescopes: the Visible and Infrared Survey Telescope for Astronomy (VISTA, upper) and the optical VLT Survey Telescope (VST, lower).

ESO/G.Hüdepohl (atacamaphoto.com)

The ESO Public Surveys — Review of Milestones and Completion

Magda Arnaboldi[1]
Marina Rejkuba[1]
Jörg Retzlaff[1]
Nausicaa Delmotte[1]
Stephan Geier[1]
Reinhard Hanuschik[1]
Michael Hilker[1]
Wolfgang Hummel[1]
Gaitee Hussain[1]
Valentin D. Ivanov[1]
Alberto Micol[1]
Steffen Mieske[1]
Mark Neeser[1]
Monika Petr-Gotzens[1]
Thomas Szeifert[1]

[1] ESO

In 2013 the eleven currently ongoing ESO public surveys successfully completed the submission and publication of their science data products via the ESO Science Archive Facility. An overview of the public survey projects in terms of telescope time allocation, observation progress and expected date of completion is presented. The science data products available in the ESO archive and their usage by the astronomical community are discussed with regard to the legacy value and scientific impact of these projects. This overview represents a natural introduction to the special section of the *Messenger* dedicated to the ESO public survey projects, in which the survey teams present their scientific aims and selected results in a series of dedicated articles.

Introduction

The ESO public surveys are very large programmes that last longer than two years and provide a legacy for the astronomical community at large. The start and implementation of the public surveys is linked to the operational deployment of the dedicated survey telescopes at ESO. The first suite of public survey programmes specifically designed for the VLT Infrared Survey Telescope for Astronomy (VISTA) and the VLT Survey Telescope (VST) started in 2010 and 2011, respectively, as these telescopes entered operations. With the successful start of these imaging public surveys, ESO also initiated spectroscopic public surveys on two other telescopes at the La Silla Paranal Observatory.

The six near-infrared (NIR) imaging public surveys on VISTA (VHS, UltraVISTA, VIDEO, VVV, VMC and VIKING) and three optical imaging public surveys on VST (KiDS, VST ATLAS and VPHAS+) have strong synergies between their wavelength and area coverage (Arnaboldi et al., 2007). These projects range from shallow whole hemisphere — wide area — to deep pencil beam surveys, and their scientific drivers include a broad range of fundamental astrophysics topics, ranging from the nature of dark energy, the formation and evolution of galaxies, detailed studies of the structure of the Milky Way, to the universality of the stellar initial mass function. Two spectroscopic surveys started in 2012: the Gaia–ESO survey is devoted to the dynamics and chemical evolution of the Milky Way; the PESSTO survey investigates transient objects and, in particular, the physics of supernova explosions. For an overview of the scientific goals of the public surveys, their observing strategies and first results, readers are directed to the following contributions of the survey teams in this issue. (For the survey VISTA Variables in the *Via Lactea* [VVV], a half-way progress report will be presented in the next *Messenger* issue.)

The main difference between the public surveys and the other ESO observing programmes (in particular Large Programmes that may also have observations spanning several years) is that all raw data are immediately public and available worldwide through the ESO Science Archive Facility (SAF) and, even more importantly, the commitment made by the survey teams to deliver science data products and catalogues to ESO with yearly releases. The reduced and calibrated images and/or spectra, as well as catalogues listing physical properties of surveyed targets, are made available to the astronomical community through the SAF. In this article, we present the current status of the surveys and estimate the year of completion for the imaging public surveys that are carried out in service mode. The delivery and publication of data products through the SAF closes the loop with the community and we present the current status of the Phase 3 delivery for the eleven public surveys. We conclude with an overview of the data downloaded by the community in terms of data volume and data product types.

Telescope time allocation to ESO public surveys

The VISTA surveys started after the end of the dry-run period on 1 April 2010. VISTA has a 4.1-metre diameter primary mirror and is equipped with a near infrared camera VIRCAM (VISTA InfraRed CAMera) with a 1.65-degree diameter field of view (Emerson et al., 2006). The six VISTA public surveys are well into their fourth year of operation. The overall time allocations for these surveys are comparable, except for the VHS (VISTA Hemisphere Survey), which requires 3400 hrs for completion, according to its survey management plan. The VHS takes up 23 % of the telescope time, while about 13 % goes on each of the other surveys; in addition up to 5 % of the time is allocated to Chilean and 5 % to open-time programmes. Figure 1 shows a summary pie chart of the time allocation to the surveys and Chilean and open time as a percentage of the total available VISTA time.

The VST public surveys started on 15 October 2011 in service mode, following the successful commissioning of the VST on Paranal. The VST is a 2.6-metre modified Ritchey–Chrétien alt-azimuth telescope (Arnaboldi et al., 1998) equipped with a 1 × 1 degree optical imager

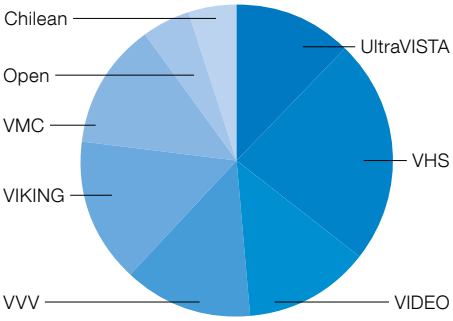

Figure 1. Pie chart showing the time allocation as a percentage of the total available time to the six imaging surveys and open time on VISTA.

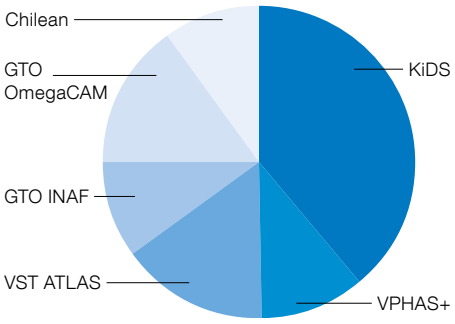

Figure 2. Pie chart showing the time allocation as percentage of the total available time for the VST.

OmegaCAM (Kuijken, 2011). An overview of OmegaCAM's scientific operations is given in Mieske et al. in this issue (p. 12). The VST surveys are starting their third year of operation. KiDS is the largest survey, requiring 3225 hrs to completion, or 39% of the time, followed by 15% for VST ATLAS and 11% for VPHAS+. The time allocated to Chilean programmes (10%), and Guaranteed Time Observations (GTO) of the OmegaCAM consortium (15%) and the Italian National Institute of Astrophysics (INAF; 10%) make up for a sizable fraction of the available telescope time, which has an important impact on the speed of completion. Figure 2 is a summary pie chart of the time allocation of the VST surveys as a percentage of the total available VST time for the public surveys, Chilean and GTO programmes.

The first spectroscopic public survey, the Gaia–ESO survey, started operation on 1 January 2012 on FLAMES at the VLT Unit Telescope 2 (Kueyen) on Paranal. The data acquisition for this survey is carried out in visitor mode and the time allocation of the survey entails 60 nights each year, for an overall assignment over four years initially, with another year pending a review of the survey progress and delivered data. Thus far 105 nights have been allocated to the Gaia–ESO survey. The PESSTO survey started operation on 1 April 2012, on EFOSC and SOFI at the New Technology Telescope (NTT) on La Silla. The data acquisition for this survey is also carried out in visitor mode. The time allocation for the survey includes 90 nights each year, with an allocation of 60/30 nights in odd and even periods respectively, for an overall assignment over four years, also with another year pending a successful review. Thus far 120 nights have been allocated to this project.

Progress and estimated completion time for imaging surveys

An integral part of the approval of public survey projects is the review of their survey management plans (SMPs), which outline the plans for telescope time allocation and observing constraints over the years. Additional information on quality control and pipeline data reduction, survey resource allocation for the survey execution (full-time equivalent [FTE] allocation), the timeline for the delivery and the description of the data products for publication in the SAF are all part of the SMPs. Hence the SMPs have become the benchmark that is used to compute the progress of the public surveys and they represent the basis for estimating their completion time. In service mode, the basic observation unit is the observation block (OB) and the time charged to the programme is accounted for in terms of the number of successfully completed OBs. This includes the shutter open time (exposure time) and the relevant overheads provided in the execution time reporting module, which is part of the observation preparation software (P2PP3).

Successfully completed OBs are executed observations that fulfil the requested observing constraints according to stringent quality control (QC) criteria that are explained extensively elsewhere[1]. Further information on the VST/OmegaCAM QC process, which was designed following the QC for VISTA/VIRCAM observations, is given in the article by Mieske et al. (p. 12). In the following, the fraction of the completion for a survey is computed as a fraction of the total execution time in hours for the completed OBs normalised by the total time in hours requested in the approved SMPs. The cumulative diagrams for the percentage of completion are shown in Figures 3 and 4 for the VISTA and VST surveys, respectively.

VISTA — The six VISTA surveys are progressing at a similar pace. As for any new telescope the start of VISTA operations required some adjustments. After

Figure 3. Graph of the percentage completion for the VISTA surveys as a function of date.

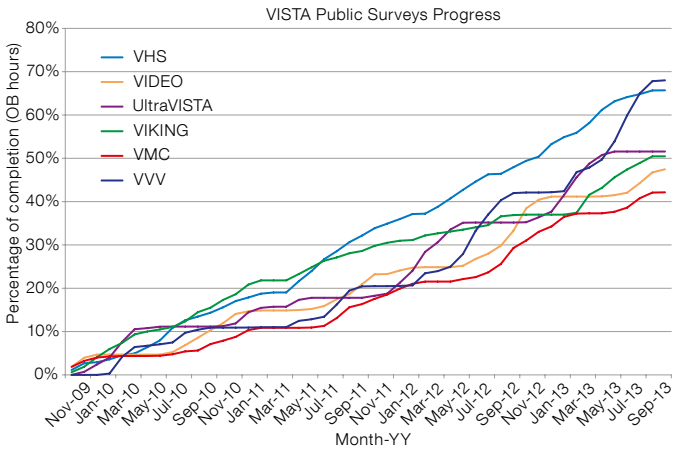

Figure 4. Graph of the percentage completion for the VST surveys as a function of date.

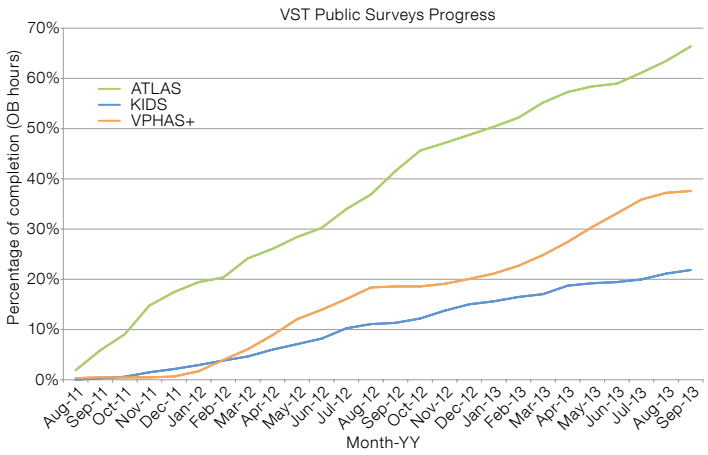

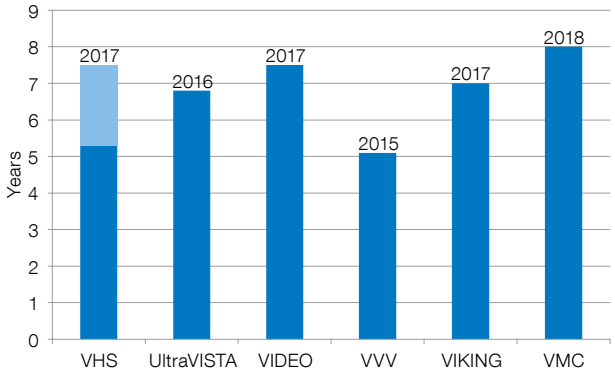

Figure 5. Expected completion time, in years and by year of completion, for the VISTA surveys. For VHS the time to completion for the whole area coverage is indicated in light blue. T = 0 refers to the start of scientific operations, i.e., April 2010.

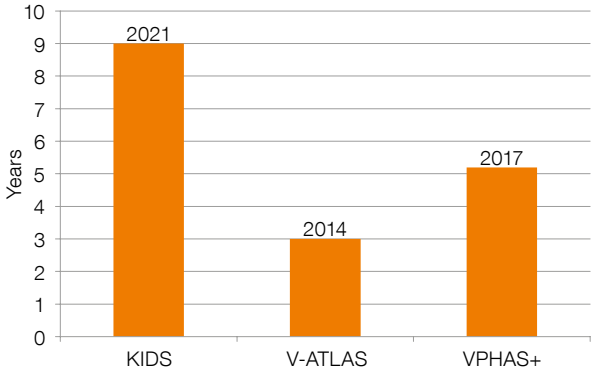

Figure 6. Expected completion time, in years and by year of completion, for the VST surveys. T = 0 refers to the start of scientific operations, i.e., October 2011.

major technical interventions in 2010 (camera shim installation and horizontal re-centring) and 2011 (primary and secondary mirror recoating and extended recovery), operational procedures were adopted to increase the speed of execution and reduce the number of repeated OBs. The current completion rate for the VVV and VHS surveys is more than 67 %, while the percentage of completion is in the range 52 % to 42 % for the other surveys (UltraVISTA, VIKING, VIDEO and VMC).

VST — For the VST surveys, the percentages of completion are 66 % for VST ATLAS, 22 % for KiDS and 38 % for VPHAS+. Of the three VST surveys, KiDS has the tightest requirements in terms of Moon illumination (dark time) and seeing constraints. It is also, by far, the largest survey on the VST and thus, even if it uses a comparable fraction of time per year to the other surveys, its overall completion is much smaller. Furthermore the right ascension/declination distribution of the target fields overlaps with those of approved GTO projects. Strategies are being implemented to mitigate the competition, and speed up the data acquisition for KiDS, and also improve the overall observation progress on the VST. For more details see Mieske et al. (p. 12).

Taking account of the above percentages of completion for each survey and the start of operation of each survey telescope, and assuming the same observation progress as previously, we can evaluate the date of completion for the VST and VISTA surveys. Figures 5 and 6 show the expected completion time in years and the year of completion for the nine imaging surveys. We expect the VVV, VHS and VST ATLAS to be completed by 2015, with the other surveys coming to completion in the following years, with KiDS completed in 2021. For VHS, two numbers are shown in Figure 5: the completion in 2015 is based on the 3400 hours requested in the SMP, but since the overheads were not known at the time of writing the SMP, this survey will actually need about two years longer to cover the entire southern hemisphere, as shown by the light blue bar. It is important to point out that these projections do not automatically translate into telescope time allocated to these surveys. These estimates are upper limits since, as one survey finishes, the others may progress faster, which is not explicitly taken into account in the simple extrapolation above. The legacy value and the scientific excellence of the survey programmes are considered by the public survey panels organised by ESO and these completion dates are presented at major peer reviews. The public survey panels are asked to issue informed recommendations on the continuation of survey programmes, or their termination, should they consider any of them not scientifically competitive at the time of the review.

Publication and download of science data products from ESO public surveys

The ESO policies in place to manage the public survey projects monitor the delivery of data products for ingestion and publication via the SAF. Additional allocation of telescope time is conditional on the submission of data products via Phase 3. Phase 3 concludes the process started with the submission of the letter of intent, followed by Phase 1 (proposal preparation and submission) and the preparation and submission of OBs for observations in service mode, i.e., Phase 2. As a result of Phase 3, the community can access and download the data products from the SAF and is able to carry out independent science projects in addition to those targeted by the survey teams (c.f., Arnaboldi et al., 2011).

Survey	Bands	Sky coverage* (sq.deg)	Data volume (GB)
VHS	*YJHKs*	4210	8511
VIKING	*ZYJHKs*	235	288
VVV	*ZYJHKs*	564	2877
VMC	*YJKs*	3.6	26
Ultra-VISTA	*YJHKs*	1.8	86
VIDEO	*YJHKs*	1.8	24
ATLAS	*ugriz*	2341	3015
VPHAS+	*ugri,* Hα	375	747
KIDS	*ugri*	56	701

Table 1. Summary of VISTA and VST public survey products in the ESO science archive (Status: 25 October 2013).

*The quoted sky coverage is the total geometric area of images, which normally differs from the nominal survey area.

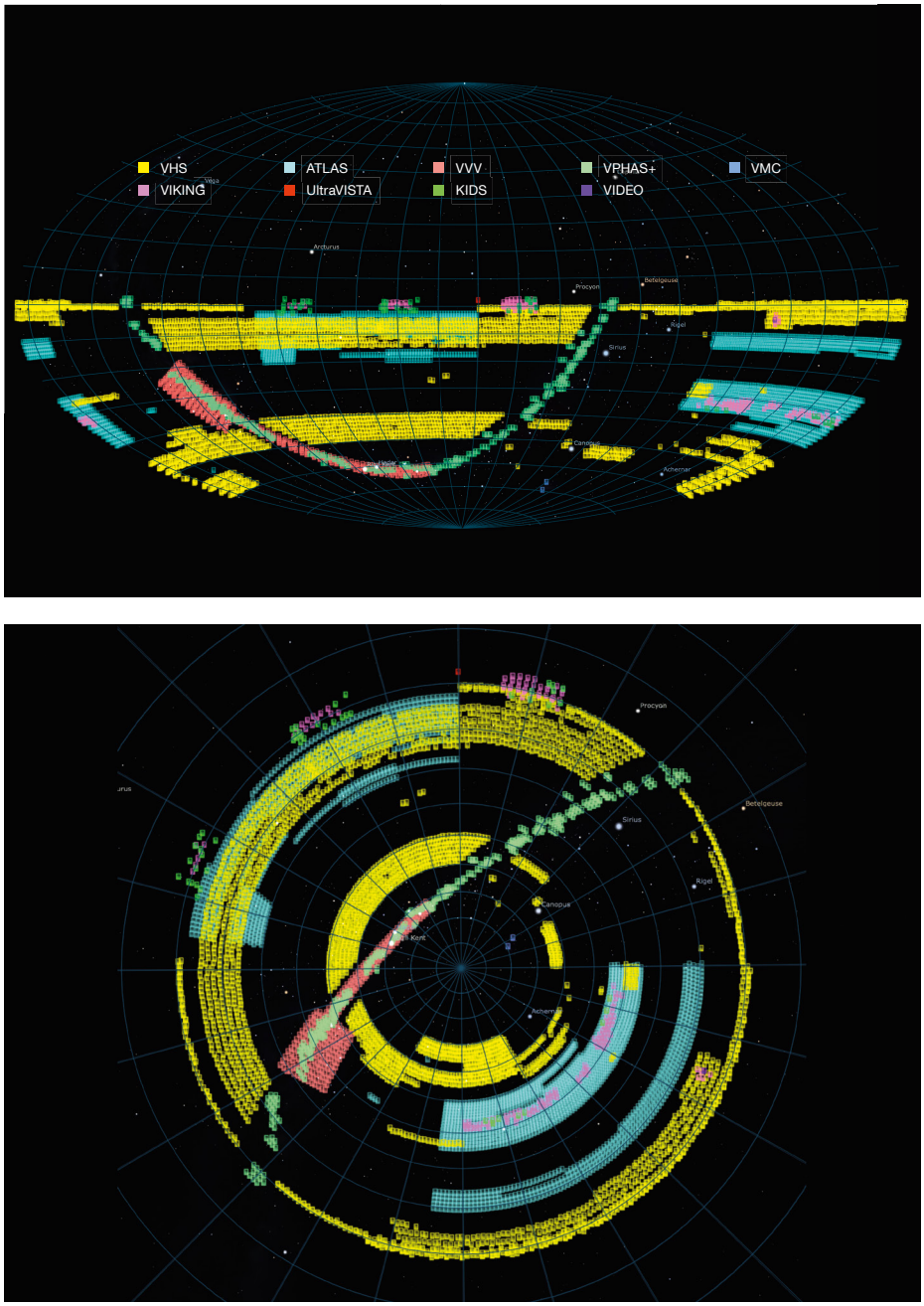

Figure 7. Sky coverage of ESO public survey products is shown in two projections. Upper: Full sky (Hammer–Aitoff projection); lower: Southern hemisphere (stereographic projection).

The year 2013 has been very important for Phase 3 activities, as all eleven ESO public surveys submitted and published their data products via the SAF. The milestones for Phase 3 were the second VISTA submission for images and source lists, and the first submission for catalogues. The first data release of the VST surveys was announced in September 2013. The spectroscopic public surveys are actively going through the process of content validation and it is planned that they will reach publication via the SAF by December 2013. Thus far, a total volume of 16 TB of data products — images, weight maps, source lists and catalogues — is now available and fully searchable via dedicated query interfaces. In Table 1 we provide an overview of the data volume, wavelength and sky coverage of the data releases from the imaging surveys. Further information and detailed descriptions of the data releases from the ESO public surveys are available[2].

Public survey data are published through the ESO archive interfaces conjointly with other products such as the stream for the ultraviolet and visual echelle spectrograph (UVES) data that results from the in-house generation of science data products. All Phase 3 data products comply with the established standard for ESO science data products, thereby guaranteeing uniformity in terms of data format and characterisation across the ESO archive.

Figure 7 illustrates the current sky coverage of the ESO survey products in two projections. More than 4500 square degrees in the NIR bands and 2400 square degrees in the optical bands have been covered by data products, which are now accessible via the query interfaces of the SAF.

Merit parameters for ESO public surveys are the number of refereed publications by ESO survey teams and archive users, the number of press releases and the cumulative download of data products from the ESO archive. There are now 71 refereed publications from the survey teams with a significant increase in the number of refereed publications (+ 200 %) since November 2012, including from four archive users, i.e., researchers who are not members of the survey teams. The contribution by Wegg & Gerhard (p. 54) is an example of exciting scientific results achieved using ESO archive data products (in this case from the VVV survey). There also are more than ten press releases based on VISTA data and more than four press releases for the VST.

The parameters on the data download by the community also demonstrate a strong interest. The cumulative download from the SAF since December 2011 amounts to more than 6.8 TB of data products and ~ 27 000 files. In Figures 8 and 9 these numbers are differentiated per survey project and data product type, respectively. The community is clearly eager to access the data, with the largest

volume download coming from VVV, UltraVISTA and KiDS; see Figure 8. The largest volume download for products is for the source lists, followed by the tile images. We believe that catalogues will represent very valuable assets, as they are the highest level products for the surveys. In this respect, we are working hard to reach a critical data volume soon, with the ingestion of the VIKING, VVV and VMC catalogues so that the community can benefit even more from the joint effort of ESO and the survey teams.

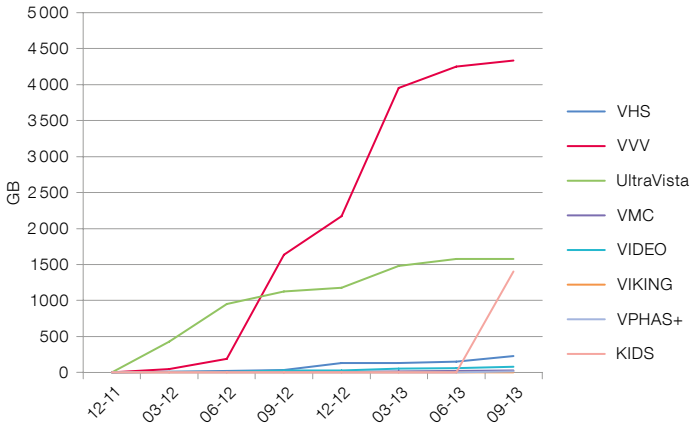

Figure 8. Data volume download for the imaging public surveys.

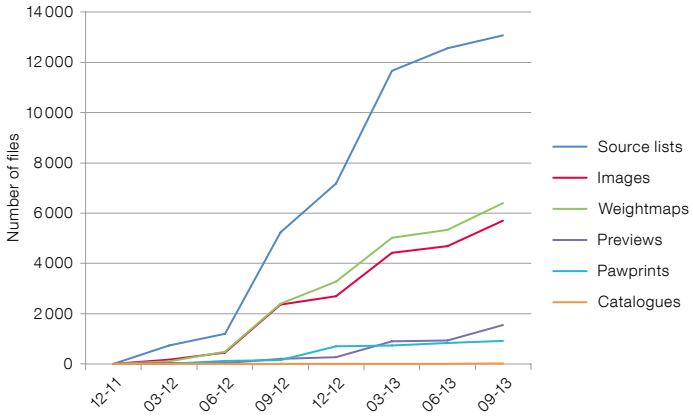

Figure 9. Number of files downloaded for the different data product types from the ESO SAF for the public imaging surveys.

References

Arnaboldi, M. et al. 1998, The Messenger, 93, 30
Arnaboldi, M. et al. 2007, The Messenger, 127, 28
Arnaboldi, M. et al. 2011, The Messenger, 144, 17
Emerson, J., McPherson, A. & Sutherland, W. 2006, The Messenger, 126, 41
Kuijken, K. 2011, The Messenger, 146, 8

Links

[1] Quality control criteria: http://www.eso.org/sci/observing/phase2/SMGuidelines/ConstraintsSet.VIRCAM.html
[2] Phase 3 data releases: http://www.eso.org/sci/observing/phase3/data_releases.html

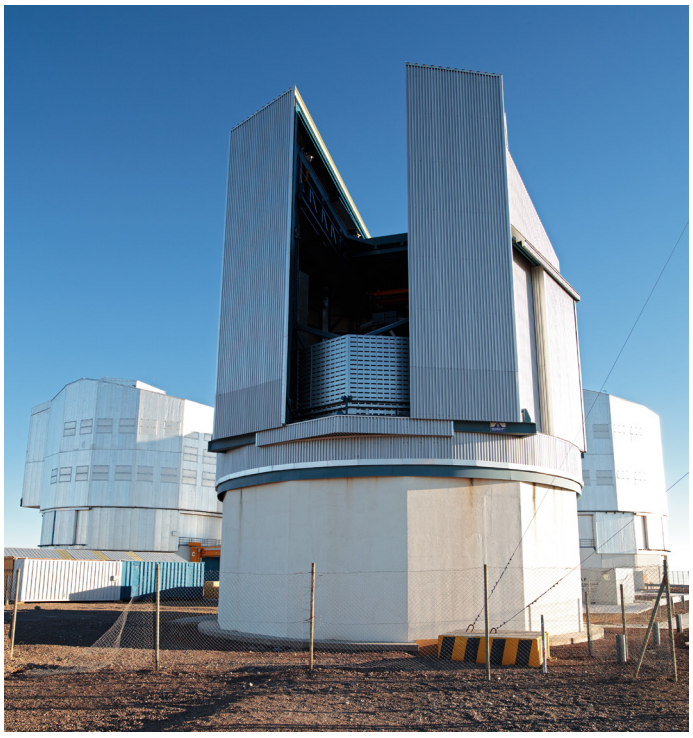

The 2.6-metre VLT Survey Telescope (VST) is shown in its enclosure on Cerro Paranal. In the background are the nearby VLT Unit Telescopes 3 (Melipal, to the right) and 4 (Yepun, left).

The VMC ESO Public Survey

Maria-Rosa L. Cioni[1,2]
Peter Anders[3]
Gemma Bagheri[1]
Kenji Bekki[4]
Gisella Clementini[5]
Jim Emerson[6]
Chris J. Evans[7]
Bi-Qing For[4]
Richard de Grijs[8]
Brad Gibson[9]
Léo Girardi[10]
Martin A. T. Groenewegen[11]
Roald Guandalini[12]
Marco Gullieuszik[10]
Valentin D. Ivanov[13]
Devika Kamath[12]
Marcella Marconi[14]
Jean-Baptiste Marquette[15]
Brent Miszalski[16]
Ben Moore[17]
Maria Ida Moretti[14]
Tatiana Muraveva[5]
Ralf Napiwotzki[1]
Joana M. Oliveira[18]
Andrés E. Piatti[19]
Vincenzo Ripepi[14]
Krista Romita[20]
Stefano Rubele[10]
Richard Sturm[21]
Ben Tatton[18]
Jacco Th. van Loon[18]
Mark I. Wilkinson[22]
Peter R. Wood[23]
Simone Zaggia[10]

[1] University of Hertfordshire, United Kingdom
[2] Leibniz-Institut für Astrophysik Potsdam, Germany
[3] National Astronomical Observatory of China, China
[4] ICRAR, University of Western Australia, Australia
[5] INAF, Osservatorio Astronomico di Bologna, Italy
[6] Queen Mary University London, United Kingdom
[7] Astronomy Technology Centre, Edinburgh, United Kingdom
[8] Peking University, China
[9] University of Central Lancashire, United Kingdom
[10] INAF, Osservatorio Astronomico di Padova, Italy
[11] Royal Observatory of Belgium, Belgium
[12] Institute of Astronomy, KU Leuven, Belgium
[13] ESO
[14] INAF, Osservatorio Astronomico di Capodimonte, Italy
[15] Institut d'Astrophysique de Paris, France
[16] South African Astronomical Observatory, Cape Town, South Africa
[17] University of Zurich, Switzerland
[18] Lennard-Jones Laboratories, Keele University, United Kingdom
[19] Observatorio Astronómico, Universidad National de Córdoba, Argentina
[20] University of Florida, USA
[21] Max-Planck-Institut für extraterrestrische Physik, Germany
[22] University of Leicester, United Kingdom
[23] Australian National University, Australia

The VISTA near-infrared *YJKs* survey of the Magellanic Clouds system (VMC) has entered its core phase: about 50 % of the observations across the Large and Small Magellanic Clouds (LMC, SMC), the Magellanic Bridge and Stream have already been secured and the data are processed and analysed regularly. The initial analyses, concentrated on the first two completed tiles in the LMC (including 30 Doradus and the South Ecliptic Pole), show the superior quality of the data. The photometric depth of the VMC survey allows the derivation of the star formation history (SFH) with unprecedented quality compared to previous wide-area surveys, while reddening maps of high angular resolution are constructed using red clump stars. The multi-epoch *Ks*-band data reveal tight period–luminosity relations for variable stars and permit the measurement of accurate proper motions of the stellar populations. The VMC survey continues to acquire data that will address many issues in the field of star and galaxy evolution.

The VMC survey

The VMC survey observations are obtained with the infrared camera VIRCAM mounted on VISTA and reach stars down to a limiting magnitude of ~ 22 (5σ Vega) in the *YJKs* filters. The VMC strategy involves repeated observations of tiles across the Magellanic system, where one tile covers approximately uniformly an area of ~ 1.5 square degrees in a given band with three epochs at *Y* and *J*, and 12 epochs at *Ks* spread over a time range of one year or longer. Individual *Ks* epochs refer each to exposure times of 750 s and reach a limiting magnitude of ~ 19 for sources with photometric errors < 0.1 mag. The VMC data are acquired under homogeneous sky conditions, since observations take place in service mode, and their average quality corresponds to a full width at half maximum < 1 arcsecond. The VISTA astrometry, which is based on 2MASS, results in positional accuracies within 25 milliarcseconds (mas) across a tile. The VMC data are reduced with the VISTA Data Flow System (VDFS) pipeline and are archived both at the VISTA Science Archive and at ESO. Further details about the VMC survey[1] are given in Cioni et al. (2011).

Stellar populations

One of the main goals of the VMC survey is the identification and characterisation of the mixture of stellar populations that have made up the Magellanic system over time. The star formation history of field stars, the physical parameters of stellar clusters, the links between these and the structure and dynamical processes are all embedded in the VMC data. Extracting a comprehensive picture of the system represents our major challenge, but fortunately we have access to sophisticated tools with which to do the job. In Rubele et al. (2012), we demonstrated that by using two colour–magnitude diagrams (CMDs) simultaneously, and a grid of models at various ages and metallicities, we could derive spatially resolved SFHs where systematic errors in the star formation rate and age–metallicity relations are reduced by a factor of two, relative to previous work, after accounting for the geometry of the galaxy. In our study we independently derive the mean extinction and distance modulus for twelve subsections of the original tiles.

In Figure 1 we show the CMD of a tile in the SMC including the Milky Way (MW) globular cluster 47 Tuc, highlighting the complexity of the SFH analysis in decomposing the different stellar populations. Using custom-derived point spread function photometry, we can push the sensitivity of the VMC data to highly crowded regions. Together with the wide area covered by VMC we will be able to investigate not only substructures in the LMC and SMC, but also streams attached to the 47 Tuc cluster, for example, as well as detecting the members of hundreds of stellar clusters in the Magellanic system waiting to be characterised.

The reddening map of the 30 Doradus field

Dust causes uncertainties in the measurements of the SFH and the structure of galaxies. Red clump stars (0.8–2 $M_{\odot}$ and 1–10 Gyr old) are useful probes of interstellar reddening because of their large number and relatively fixed luminosity. Red clump stars belonging to the tile LMC 6_6 are selected from their location in the (*J–Ks*) *vs*. *Ks* CMD. Then, the amount of total reddening (along the line of sight and within the LMC) in terms of colour excess is obtained for each of ~ 150 000 stars with respect to its intrinsic colour. The latter is derived accordingly from stellar evolution

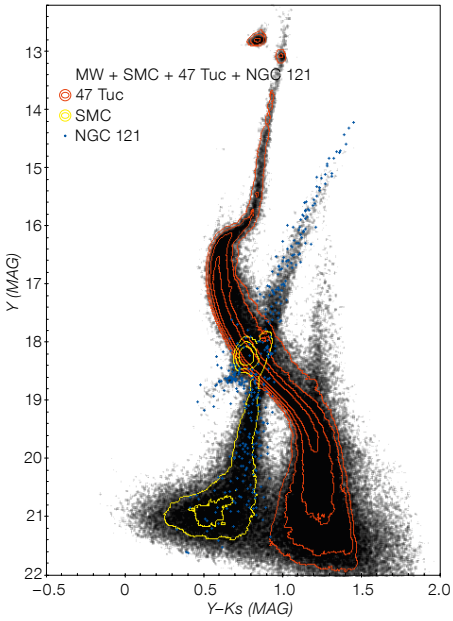

Figure 1. Colour–magnitude diagram of stellar sources in tile SMC 5_2. All sources are shown in grey; stars belonging to the SMC cluster NGC 121 are indicated in blue; the field population of the SMC is indicated with yellow contours; and the stars of the Milky Way cluster 47 Tuc are shown with red contours.

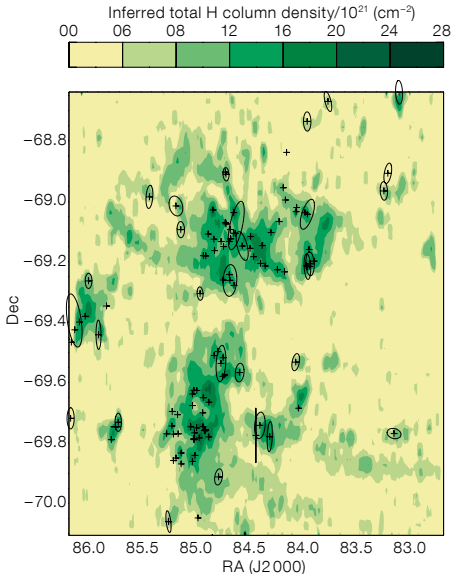

Figure 2. Hydrogen column density map inferred from VMC data in tile LMC 6_6 identifying regions where $N_{HI} > 8 \times 10^{21}$ cm^{-2}. Crosses represent molecular clouds catalogued in the literature and ellipses highlight those with measured properties.

models, accounting for variations with age and metallicity. Extinction is subsequently converted into hydrogen gas column density. Compared to reddening maps produced using the same method at optical wavelengths, the near-infrared VMC data are more sensitive to higher extinction. Compared to H I observations we derive that, on average, half of the stars lie in front of the H I column and hydrogen becomes molecular in the dustiest clouds; the transition begins at $N_{HI} \cong 4 \times 10^{21}$ cm^{-2}. Figure 2 shows the location of molecular clouds superposed on the distribution of hydrogen column density inferred from the VMC data. There is overall agreement with maps of dust emission at 24 μm and 70 μm (see Tatton et al., 2013). Reddening maps will be created for other tiles in the VMC survey allowing red clump stars to be de-reddened; these results will be used in calculating the three-dimensional (3D) structure of the Magellanic system.

Variable stars

The other main goal of the VMC survey is the measurement of the 3D structure of the Magellanic system. Classical Cepheids are primary distance indicators and in the near-infrared obey period–luminosity (PL) relations that are less affected by reddening, chemical composition and nonlinearity than those at optical wavelengths, resulting in smaller intrinsic dispersion. First results for classical Cepheids in the tiles LMC 6_6 (Figure 3, left) and 8_8 have been presented in Ripepi et al. (2012). The identification of the variables is derived from the EROS-2 and OGLE-III catalogues and their VMC *Ks* light curves are very well sampled, with at least 12 epochs, and high precision, with typical errors of 0.01 mag, or better, for individual phase points. The *Ks* mag of the faintest Cepheids in the LMC, which are mostly first overtone pulsators, was measured for the first time thanks to the VMC observing strategy. Photometry for the brightest fundamental mode Cepheids (periods > 23 days), exceeding the linearity regime of VMC data, are taken from the literature. The dispersion of the PL relations is ~ 0.07 mag.

Anomalous Cepheids (1.3–2.1 $M_{\odot}$ and [Fe/H] ≈ –1.7 dex) also play an important role both as distance indicators and stellar population tracers. The VMC survey has already observed many of the anomalous Cepheids discovered by the OGLE project in the LMC. These stars obey a tight PL relation in the *Ks*-band with a dispersion of 0.10 mag (Figure 3, right) that is shown for the first time in Ripepi et al. (2013).

Cepheids (< 200 Myr old) are mainly concentrated towards the bar and in a northwest spiral arm of the LMC as well as in the central region of the SMC. Eclipsing binaries composed of main sequence stars trace a similar distribution, but with clustering mainly occurring in regions of recent star formation. On the other hand, RR Lyrae variable stars (> 10 Gyr old) are smoothly distributed and likely trace the haloes of the galaxies. These stars also follow a PL relation that is tight in the *Ks*-band. The VMC properties and the strategy to measure distances and infer the system 3D geometry of different age components from the variable stars is described in Moretti et al. (2013).

The magnitude of the brightest VMC objects ($10 < Ks < 12$), which may be saturated in their central regions, is well recovered by the VDFS pipeline by integrating the flux in the outer parts. Most of these sources are asymptotic giant branch (AGB) stars. By fitting spectral energy distributions, created from the combination of VMC data and data at other wavelengths, with dust radiative transfer models, it is possible to derive mass-loss rates, luminosities and spectral classifications that offer strong constraints on AGB evolutionary models (Gullieuszik et al., 2012). These variable stars obey PL relations that may also be useful as distance and structure indicators.

The proper motion of the LMC

The astrometric accuracy and the photometric sensitivity of observations made with VISTA are of sufficient quality to select a large sample of targets and measure their proper motion. The proper motion of the LMC is measured from the combination of 2MASS and VMC data that span a time range of ~ 10 years and from VMC data alone across a time baseline of ~ 1 year (Cioni et al., 2013b). Different types of LMC stars (e.g., red giant branch, red clump and main sequence stars, as well as variable stars) are selected from their location in the (*J–Ks*) *vs*. *Ks* CMD, and from lists of known objects, where MW foreground stars and background galaxies are also easily distinguished (Figure 4, left). The proper motion of ~ 40 000 LMC stars in the tile, with respect to ~ 8000 background galaxies, is $\mu_{\alpha}\cos(\delta) = +2.20 \pm 0.06$ mas yr^{-1} and $\mu_{\delta} = 1.70 \pm 0.06$ mas yr^{-1}. This value is in excellent agreement with previous ground-based measurements but our statistical uncertainties are a factor of three smaller and are directly comparable to uncertainties derived with the Hubble Space Telescope. The error budget is at present dominated by systematic uncertainties (a few mas yr^{-1}), but these will decrease due to the improved reduction of the VISTA data and the increase in the time baseline.

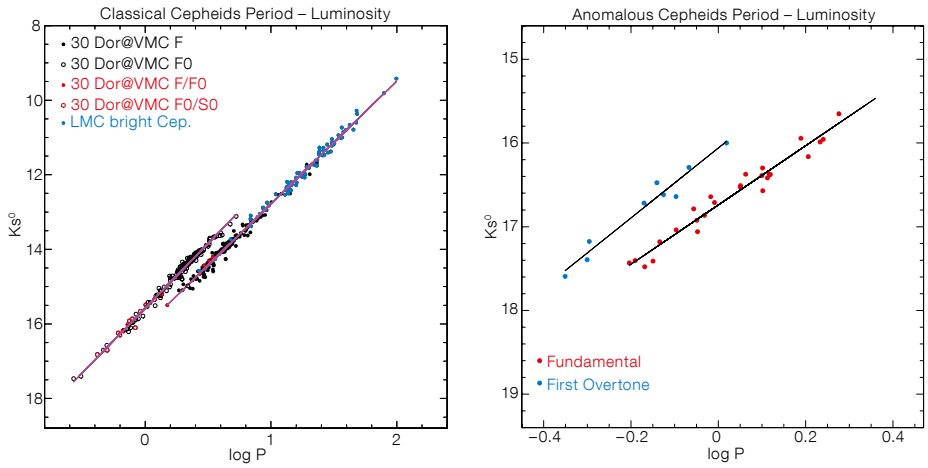

Figure 3. *Ks*-band period–luminosity relation for classical Cepheids in the 30 Dor field (left) and for LMC anomalous Cepheids (right). Fundamental and first overtone pulsators are indicated in blue and red respectively, and the solid lines are the result of least squares fits to the data.

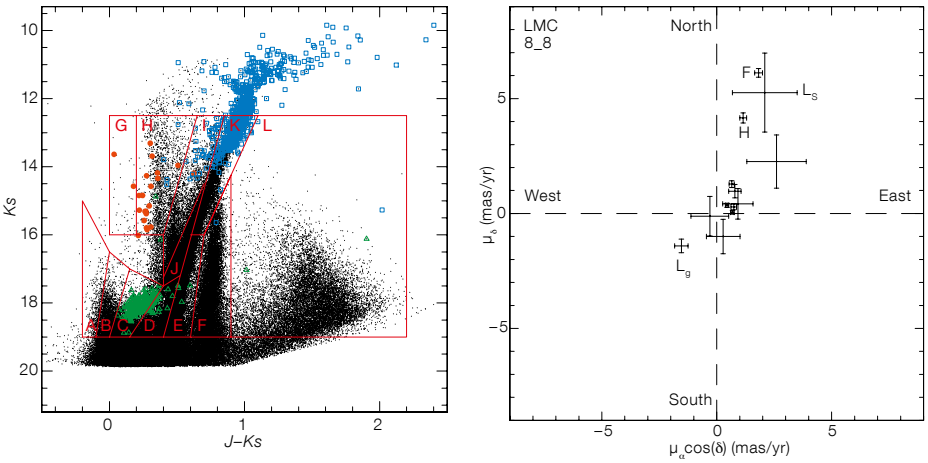

Figure 4. Left: Colour–magnitude diagram (CMD) of VMC sources in tile LMC 8_8. Region boundaries distinguish stars of different types. Colours highlight Cepheids (red), long period variables (blue) and RR Lyrae stars (green). Right: Proper motion derived from stars in each CMD region. Points corresponding to Milky Way stars (F, H and L_s) and to background galaxies (L_g) are indicated, while, for clarity, those corresponding to LMC stars are not labelled.

The mean proper motion of stars in each CMD region is shown in Figure 4 (right). The proper motions of LMC stars are clustered around zero except for region A, despite the large uncertainty. The proper motion of MW stars (regions F and H) is clearly distinct from those of LMC stars and background galaxies (region L_g). The latter refers to a sub-group of objects in region L with a galaxy-like morphology. Those with a stellar-like morphology are likely late-type MW dwarfs, since their proper motion value (L_s) is consistent with that of other MW stars. Using the best fitting model from Rubele et al. (2012) we can associate an age to each CMD region. We then measure a decrease of the proper motion with age where young stars stretch out to the northeast and old stars to the southwest. This difference is linked to both kinematic differences between young and old stars and to different hosting structures.

An alternative and established reference system is made of background quasars and hundreds of them have already been found behind the central regions of the Magellanic Clouds as a result of spectroscopic observations of candidates identified from the OGLE light curves. The combination of VMC colours and *Ks*-band variability is also a valuable method to identify candidate quasars (Cioni et al., 2013a). The contamination by background galaxies, foreground late-type dwarf stars, young stellar objects and planetary nebulae, for which some nebular morphologies are revealed for the first time with VMC data (Miszalski et al., 2011), is reduced to ~ 20 %.

Perspective

The first years of observations have shown that the VMC data meet expectations and our understanding of the SFH across the Magellanic system will no longer be limited to small area observations. With the approaching completion of the SMC and Bridge areas it will be possible to start comparing theoretical predictions with observations on the age and metallicity distributions and their relations with the interaction between the LMC and SMC, the formation of the Bridge and the existence of stripped stars. The VMC survey has a high legacy value and represents the sole counterpart in the *Ks*-band to current and future ground-based (STEP at the VST, SkyMapper, SMASH at the Blanco 4-metre, Large Synoptic Survey Telescope [LSST]) and space-based imaging missions (e.g., Gaia and Euclid) targeting or including the Magellanic system. It also provides a wealth of targets for wide-field spectroscopic follow-up investigations, e.g., with the Apache Point Observatory Galactic Evolution Experiment (APOGEE)-South, High Efficiency and Resolution Multi-Element Spectrograph (HERMES) at the Anglo-Australian Observatory, 4-metre Multi-Object Spectroscopic Telescope (4MOST) and Multi-Object Optical and Near-infrared Spectrograph (MOONS) at ESO.

References

Cioni, M.-R. L. et al. 2011, A&A, 527, A116, Paper I
Cioni, M.-R. L. et al. 2013a, A&A, 549, A29, Paper VI
Cioni, M.-R. L. et al. 2013b, A&A, accepted, Paper IX
Gullieuszik, M. et al. 2012, A&A, 537, A105, Paper III
Miszalski, B. et al. 2011, A&A, 531, A157, Paper II
Moretti, M. I. et al. 2013, A&A, accepted, Paper X
Ripepi, V. et al. 2012, MNRAS, 424, 1807, Paper V
Ripepi, V. et al. 2013, MNRAS, accepted, Paper VIII
Rubele, S. et al. 2012, A&A, 537, A106, Paper IV
Tatton, B. et al. 2013, A&A, 554, A33, Paper VII

Links

[1] VMC survey: http://star.herts.ac.uk/~mcioni/vmc/

The VISTA Deep Extragalactic Observations (VIDEO) Survey

Matt J. Jarvis[1,2]
Boris Häußler[1,3]
Kim McAlpine[2]

[1] Astrophysics, Department of Physics, Oxford, United Kingdom
[2] Physics Department, University of the Western Cape, Bellville, South Africa
[3] Centre for Astrophysics, Science & Technology Research Institute, University of Hertfordshire, Hatfield, United Kingdom

The VIDEO survey is designed to answer key questions regarding the formation and evolution of galaxies, in particular the role of accretion onto black holes and how galaxy evolution may vary depending on environment. VIDEO undertakes deep near-infrared imaging over three well-observed extragalactic fields allowing in-depth study of galaxy evolution over $1 < z < 4$, linking the shallower VST and VISTA surveys with the UltraVISTA survey. The area and depth of the VIDEO survey enables the detection of the bulk of the luminosity density arising from galaxies over 90% of the history of the Universe, as well as the most massive galaxies at all epochs and any associated accretion activity. A few scientific highlights from the early VIDEO data are provided.

How and when were massive galaxies formed?
When did they assemble the bulk of their stellar mass and how?
Where does this mass assembly occur?
These are the crucial questions that VIDEO is designed to answer.

VIDEO enables us to perform an in-depth study of the Universe over the redshift range $1 < z < 4$, linking the shallower surveys such as the VISTA Hemisphere Survey (VHS) and the VISTA Kilo-Degree Survey (VIKING; see de Jong et al. p. 44) with the deeper UltraVISTA survey (McCracken et al. p. 29). The depths of the VIDEO survey have been chosen to detect all "typical" elliptical galaxies out to redshifts of $z \sim 4$, and much fainter galaxies at around a tenth of the luminosity of a typical elliptical galaxy at $z \sim 1$, thereby enabling us to detect the bulk of the luminosity density arising from galaxies over 90% of the history of the Universe, and the most massive galaxies at the highest redshifts.

Thus we are able to investigate in exquisite detail which galaxies are in place first, and address the issue of downsizing in the mass function of forming galaxies, where the massive early-type galaxies appear to be in place before the less massive galaxies.

The epoch for which VIDEO is aimed is also a crucial one in the history of the Universe, as this is when the bulk of the star formation and accretion activity took place. VIDEO is therefore the ideal survey with which to investigate the effects that star formation and accretion activity have on galaxy evolution in general.

Moreover, the intrinsic rarity of the most luminous active, starburst and elliptical galaxies means that it is important to survey a large enough area, from which the luminosity function and clustering of particular galaxy populations can be measured. VIDEO covers 12 square degrees, improving on previous area-limited surveys that have measured the clustering of various galaxy populations to scales of < 0.5 degrees. Crucially, VIDEO will have sufficient area to carry out these investigations as a function of both redshift and environment.

VIDEO not only can detect the galaxies which contribute the bulk of the luminosity density at these redshifts, but the five near-infrared (NIR) filters, along with ancillary data from visible-wavelength surveys and the Spitzer Space

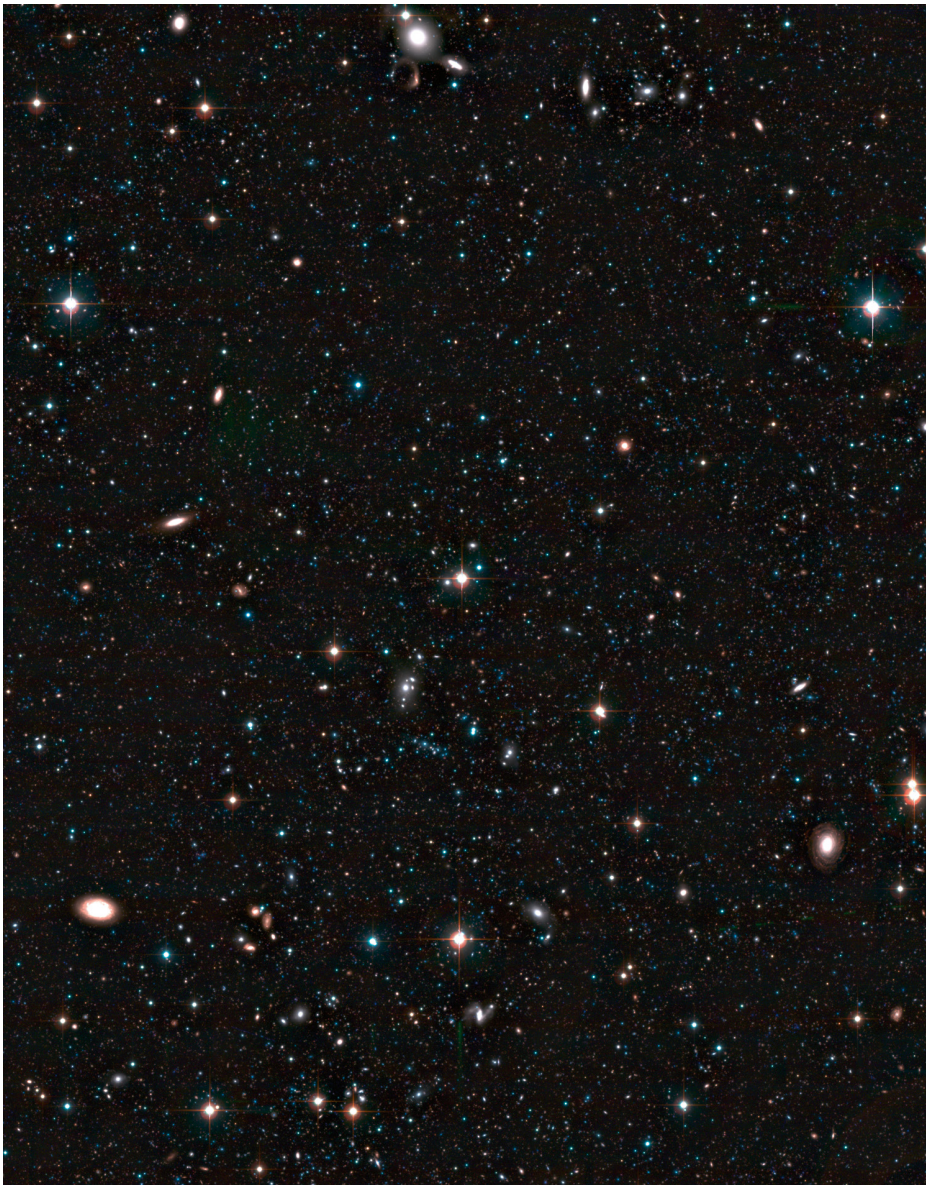

Figure 1. Colour image containing around 1/100 of the total 12 square degree area of the VIDEO field, centred on a region within the XMM-LSS field.

Telescope, will provide photometric redshifts for galaxies all the way out to $z \sim 6$ for the most massive galaxies.

Survey fields

The VIDEO survey is being carried out over three of the most widely observed high Galactic latitude fields: these are two VISTA tiles (3 square degrees) in the ELAIS-S1 field; three VISTA tiles (4.5 square degrees) in the XMM-Newton Large Scale Structure (XMM-LSS) field; and another three tiles in the extended Chandra Deep Field South. The total area covered is ~ 12 square degrees. A small fraction of the VIDEO survey data is shown in Figure 1. The three fields have a wealth of data from the X-ray through to the radio waveband, and are, along with COSMOS/Ultra-VISTA, the primary fields for observation with future facilities in the southern hemisphere.

Figure 1 in Jarvis et al. (2013) shows the footprint of the VIDEO observations in each of these three fields. The design of these positions was driven by the need to cover the wealth of ancillary data available in these fields, including Spitzer (e.g., Mauduit et al., 2012) and Herschel (Oliver et al., 2012), in addition to future ground-based optical data from both the VST and the Dark Energy Survey. Further in the future these areas will also be targeted with the deepest radio observations by the Square Kilometre Array precursor telescope MeerKAT (Jarvis, 2012) and also form part of the Large Synoptic Survey Telescope (LSST) deep drilling fields.

Photometric redshift accuracy

One of the key elements of the VIDEO survey is to provide the NIR data needed to obtain accurate photometric redshifts over all cosmic epochs, but particularly at $z > 1$, where the spectral break at 4000 Å is redshifted beyond the visible wavelength window. These photometric redshifts underpin much of the science that is and will continue to be carried out with the VIDEO survey data. To show the accuracy to which we can measure photometric redshifts with VIDEO, we cross-match the publically released deep-imaging data in the VIDEO-XMM3 field with the latest release of the VIMOS-VLT Deep Survey (VVDS) spectroscopic survey (Le Fevre et al., 2013) over the same region of sky. We select all of those spectroscopic sources with very secure spectroscopic redshifts and compare them with their photometric redshifts derived from the VIDEO photometry, combined with optical data from the Canada France Hawaii Telescope (CFHT), resulting in 1403 galaxies at $0 < z < 3.5$. By only using those sources that were classified as galaxies by the Le Phare photometric redshift code (Ilbert et al., 2006) we find that the normalised median absolute deviation of $(z_{spec} - z_{phot})/(1 + z_{spec})$ is 0.014 and the catastrophic outlier fraction, defined as $|z_{spec} - z_{phot}|/(1 + z_{spec}) > 0.15$, is just 0.65%. In Figure 2 we show the spectroscopic redshifts from the VVDS against the photometric redshifts from VIDEO.

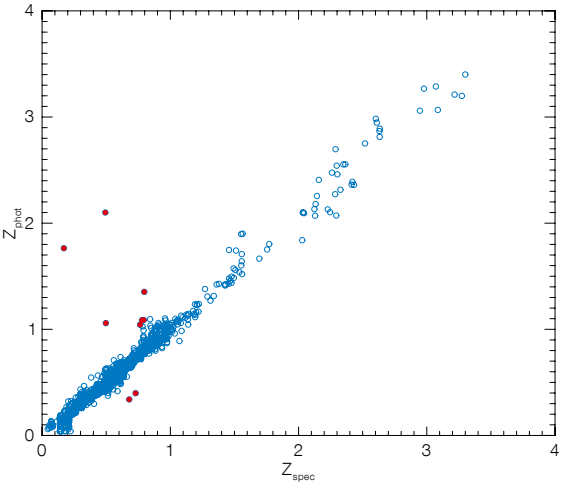

Figure 2. Photometric redshifts from VIDEO+CFHT data (z_{phot}) are plotted versus high-reliability spectroscopic redshifts (z_{spec}) from the VVDS spectroscopic survey. Filled red circles denote the nine sources classified as catastrophic outliers.

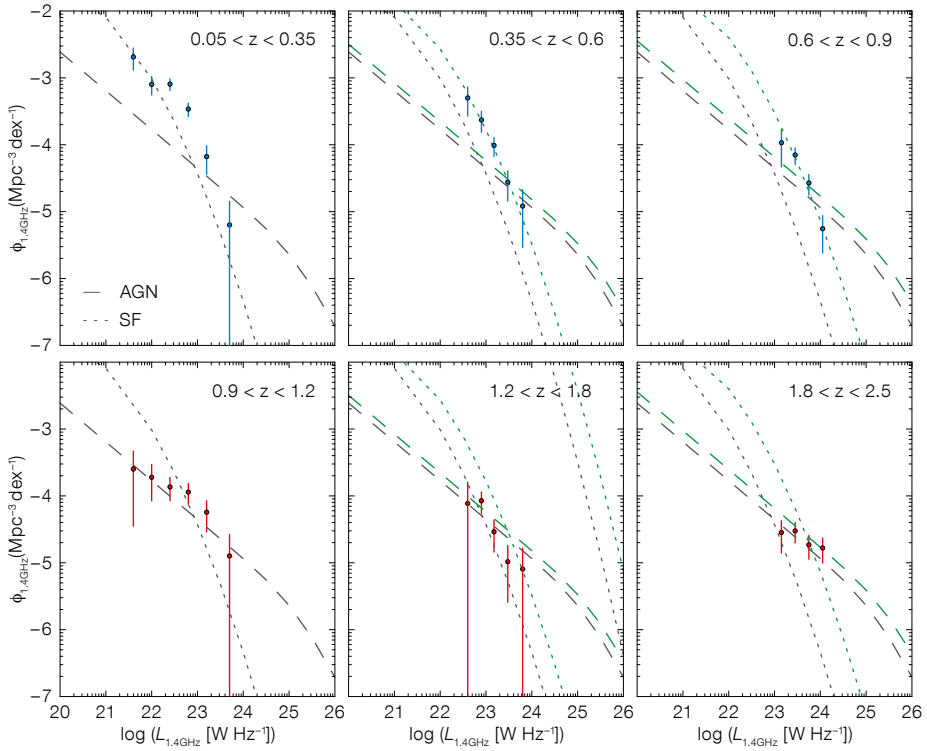

Figure 3. The star-forming (top panel — blue points) and active galactic nuclei (AGN; bottom panel — red points) radio luminosity function (RLF) in three redshift bins. Star-forming galaxies are identified as objects fitted by blue templates in the photometric redshift fitting procedure. The local luminosity function for star-forming galaxies and AGN from Mauch & Sadler (2007) are plotted as black dotted and dashed lines respectively. The green dotted line is the evolved RLF of star-forming galaxies and the green dashed line is the evolved RLF of AGN assuming the evolution parameters from McAlpine et al. (2013).

Disentangling low luminosity radio AGN from star-forming galaxies to $z \sim 2$

Over the past decade it has become clear that active galactic nuclei (AGN) may provide a critical feedback process that truncates star formation in massive galaxies. In particular, radio-loud AGN may provide an additional form of feedback via the mechanical deposition of energy resulting from jets. The predominantly low luminosity AGN, which are thought to be responsible for the bulk of mechanical feedback at $z < 1$, and are believed to be powered by inefficient accretion of hot gas, appear to inhabit gas-poor, quiescent massive galaxies. On the other hand the higher luminosity sources that are efficiently accreting cold gas tend to reside in similarly massive galaxies, but with indications of recent star formation activity. However, decoupling the low luminosity AGN activity from star formation activity at radio wavelengths can be challenging, due to the large overlap in radio luminosity between the lowest luminosity AGN and moderately star-forming galaxies. However, with deep optical imaging coupled with the NIR imaging provided by VIDEO, we may have an efficient method of tracing the evolution of these different populations.

McAlpine, Jarvis & Bonfield (2013) used a combination of visible imaging, NIR imaging from VIDEO and deep radio data from the Jansky Very Large Array to decouple the evolution of star-forming galaxies and AGN traced by radio emission. In Figure 3 we show the radio luminosity function in three redshift bins for galaxies classified as a) star-forming, and b) quiescent, based on their optical–NIR spectral energy distributions. We can see that this split is consistent with the differential evolution of both populations with redshift, showing that it is possible to use multi-colour imaging data to categorise AGN and star-forming galaxies. Given the rarity of AGN and the most luminous star-forming galaxies, with the full VIDEO survey area we will have a unique dataset with which to answer the key questions on AGN evolution and its impact on galaxy evolution.

Additionally the area coverage of VIDEO allows us to study the environments of such AGN. In Karouzos, Jarvis & Bonfield (2013) we find that such radio sources tend to reside in environments of increased density with respect to a stellar-mass matched sample of elliptical galaxies. This in turn implies that the fuelling source for low luminosity radio sources may indeed come from the hot intracluster medium.

The high-redshift Universe

VIDEO is uniquely placed to quantify the density and spatial clustering of the most massive galaxies at the earliest epochs. Initial work on this topic by Willott et al. (2013) used VIDEO data to show that the bright end of the galaxy luminosity function at $z \sim 6$ follows an exponential decline and that these massive galaxies appear to be both larger and dustier than their fainter counterparts discovered in deep Hubble Space Telescope (HST) imaging. VIDEO data will be crucial in helping to pin down the luminosity function of high-redshift ($z > 6$) galaxies. Although much shallower than the very deep NIR surveys conducted with the HST Wide Field Camera 3 (WFC3), the area is such that we can measure the shape of the bright end of the galaxy luminosity function within the epoch of reionisation and gain a full picture of the galaxy population at these high redshifts.

With the full VIDEO survey area we will be able carry out the first statistically significant clustering analysis of massive galaxies towards the epoch of reionisation, providing a direct link between the underlying dark matter distribution and galaxy populations and how this evolves up to the highest redshifts. The VIDEO survey will detect a factor of ~ 10 more $M > 10^{11}\ M_{\odot}$ galaxies than UltraVISTA at $z \sim 6$, as the limiting factor is area rather than depth.

Acknowledgements

We would like to thank David Bonfield for the tremendous amount of work that he put in for the first few years of the VIDEO survey.

References

Ilbert, O. et al. 2006, A&A, 457, 841
Jarvis, M. J. 2012, African Skies, 16, 44
Jarvis, M. J. et al. 2013, MNRAS, 428, 1281
Karouzos, M., Jarvis, M. J. & Bonfield, D. G. 2013, MNRAS, submitted
Le Fèvre, O. et al. 2013, A&A, 55, 14
Mauch, T. & Sadler, E. M. 2007, MNRAS, 375, 931
Mauduit, J.-C. et al. 2012, PASP, 124, 714
McAlpine, K., Jarvis, M. J. & Bonfield, D. G. 2013, MNRAS, 436, 1084
Oliver, S. et al. 2012, MNRAS, 424, 1614
Willott, C. J. et al. 2013, AJ, 145, 4

ESO/C. Malin

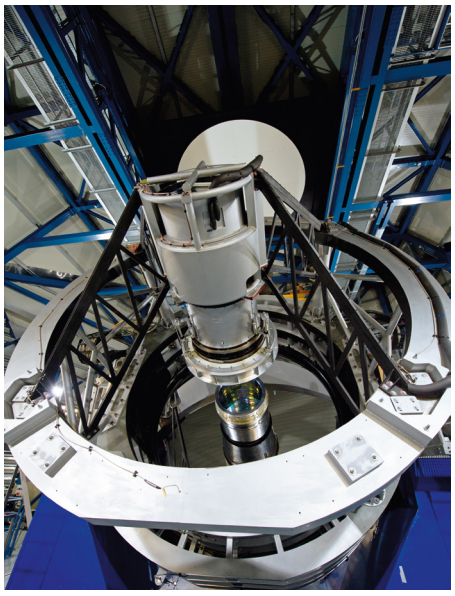

A view from the top of the VISTA telescope showing the secondary mirror assembly and the primary mirror. The dome screen for flat field illumination is seen at the rear.

UltraVISTA: A VISTA Public Survey of the Distant Universe

Henry J. McCracken[1]
Bo Milvang-Jensen[2]
James Dunlop[3]*
Marijn Franx[4]*
Johan P. U. Fynbo[2]*
Olivier Le Fèvre[5]*
Joanna Holt[4]
Karina I. Caputi[3,6]
Yuliana Goranova[1]
Fernando Buitrago[3]
Jim Emerson[7]
Wolfram Freudling[8]
Olivier Herent[1]
Patrick Hudelot[1]
Carlos López-Sanjuan[5]
Frédéric Magnard[1]
Adam Muzzin[4]
Yannick Mellier[1]
Palle Møller[8]
Kim K. Nilsson[2]
Will Sutherland[7]
Lidia Tasca[5]
Johannes Zabl[2]

* co-PI

[1] Institut d'Astrophysique de Paris, UMR7095 CNRS, Université Pierre et Marie Curie, Paris, France
[2] Dark Cosmology Centre, Niels Bohr Institute, University of Copenhagen, Denmark
[3] SUPA, Institute for Astronomy, University of Edinburgh, Royal Observatory, Edinburgh, United Kingdom
[4] Leiden Observatory, Leiden University, the Netherlands
[5] Laboratoire d'Astrophysique de Marseille, Aix-Marseille Université, France
[6] Kapteyn Astronomical Institute, University of Groningen, the Netherlands
[7] Astronomy Unit, School of Physics and Astronomy, Queen Mary University of London, United Kingdom
[8] ESO

Large samples of distant galaxies covering degree-scale areas are an unparalleled source of information concerning the first sources that ionised the Universe and the origin of cosmic structures. The UltraVISTA public survey, using the unique capabilities of the VISTA telescope, aims to assemble a unique sample of remote, very high-redshift galaxies. The characteristics of the first UltraVISTA data release (DR1) and the upcoming DR2 data products are described. The DR1 data, comprising just a few months of observing time, already equals or exceeds in depth all previous wide-field near-infrared images taken on the COSMOS field in the last decade. The first scientific results from UltraVISTA are presented, including new measurements of the high redshift (z ~ 7) galaxy luminosity function and an accurate determination of the type-dependent galaxy stellar mass function from z ~ 0 to z ~ 4. DR2 will reach one to two magnitudes deeper in all bands and provide our clearest picture of the structure and composition of the Universe at high redshifts.

Introducing UltraVISTA

In the last two decades, the utility of deep-field observations for extragalactic astrophysics has been conclusively demonstrated. These surveys, typically comprising effective exposure times totalling tens or hundreds of hours per pixel, have revolutionised our knowledge of the high-redshift Universe, leading to the detection and subsequent spectroscopic confirmation of significant numbers of high-redshift (z ~ 3) and very high-redshift (z > 4) objects. However, the largest ultra-deep fields probed by space-based observatories, whilst reaching very faint magnitude limits (typically AB ~ 27) using the Wide-Field Camera 3 on the Hubble Space Telescope typically have contiguous areas of only a few tens of arcminutes, leaving the region of parameter space comprising square degree angular coverage and moderate depth in near-infrared (NIR) wavelengths unexplored.

This combination of depth, wavelength and areal coverage is crucial for a number of reasons. Firstly, as the first structures in the Universe form at the peaks of the underlying dark matter density field, the numbers of objects at megaparsec scales will fluctuate significantly. Secondly, because the number densities of galaxies fall off exponentially at the bright end of the galaxy luminosity function, a wide-area survey is essential to yield a useful sample of high-redshift galaxies of sufficient brightness for spectroscopic follow-up with the current generation of large telescopes. Finally, this combination of depth and areal coverage will find large numbers of objects suitable for spectroscopic follow-up with the James Webb Space Telescope and the next generation of ground-based extremely large telescopes. The characterisation of these high-redshift, moderately bright objects is essential to understand the nature of the sources that re-ionised the Universe and which are the origin of the seeds of present-day large-scale structures.

The arrival of the VISTA telescope, and the prospect of a substantial time allocation for public surveys, prompted four independent responses to the initial call for VISTA surveys of the very distant Universe, each capitalising on the strengths of VISTA and the excellent observing conditions at Paranal. Given the factor of three or four speed improvement with VIRCAM, compared to existing cameras such as WIRCAM (Canada France Hawaii Telescope [CFHT]) or WFCAM (United Kingdom Infra-Red Telescope), it became possible, for the first time, to think of a ground-based survey reaching to AB limiting magnitudes of 25–26 over ~ 0.9 square degrees in the time envelope allocated to VISTA surveys. These independent proposals were merged to form the UltraVISTA survey[1], which was subsequently allocated 1800 hours of telescope time. Survey operations started in December 2009. UltraVISTA lies in the COSMOS field (Scoville et al., 2007), where a rich data heritage means that a wealth of secondary science has been enabled by UltraVISTA observations.

The UltraVISTA project comprises two components: a deep survey covering the central 1.6 square degrees of COSMOS, and an ultra-deep part covering 0.9 square degrees in four parallel stripes, each of which is separated by one VIRCAM detector width. Observations are made in four broadband filters, *Y*, *J*, *H*, and *Ks*, as well as a narrowband filter. By blocking bright OH sky-lines, this narrowband (NB) filter enables the most extensive search to date for Lyman-α emitters at z ~ 8.8 (Milvang-Jensen et al. [2013] describe this filter in detail). In addition to Lyman-α emitters at very high redshift, the NB survey will detect hundreds of [O II]-emitters at z = 2.2 and thousands of Hα emitters at z ~ 0.8. A dedicated survey using this filter only on the ultra-deep stripes has been incorporated into the UltraVISTA survey plan.

The projected AB depths at survey completion are ~ 25 (5σ for 2 arcseconds) for the deep part and ~ 26 for the ultra-deep part. As of the time of writing (October 2013), the deep survey has been largely completed, and around 40 % of the ultra-deep survey has been finished. At this rate of progress, we expect the survey to be completed by around 2017.

UltraVISTA DR1: The first VISTA survey of the high-redshift Universe

The first UltraVISTA data release, DR1[2], which took place in February 2012, contains stacks created from data taken during approximately the first five months of survey operations (around 8000 images) and contains only deep survey data. As the survey's primary scientific objective relies on detecting objects several orders of magnitude fainter than the bright NIR sky, the principal processing challenge

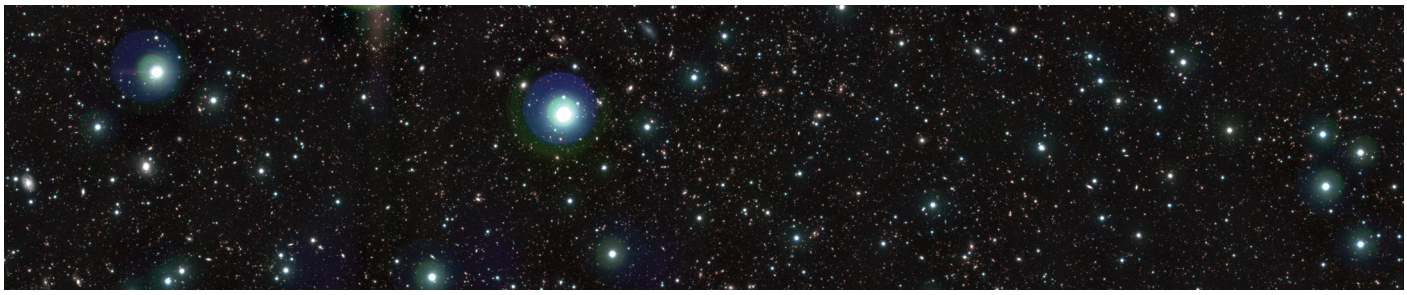

TERAPIX/CNRS/INSU/CASU

Figure 1. UltraVISTA DR2 ultra-deep image. This colour image comprises *Ks*, *J*, *Y* (RGB) stacks with an effective exposure time per pixel in each band of 82, 35 and 53 hours respectively.

involves an accurate and uniform sky-subtraction. To do this, we used the normal two-pass sky background subtraction method, starting from individual images pre-processed by the Cambridge Astronomy Survey Unit (CASU), adding back the already-subtracted sky, and using an object mask computed from the stacked image in each band to compute and subtract an individual sky frame for each of the 8000 images.

The same techniques have been applied to the upcoming DR2 release, containing almost 20 000 images. Such a computationally intensive technique was possible thanks to the use of the TERAPIX facility at the Institut Astrophysique de Paris. The advantage of this method is that the stacked images are extremely flat and uniform. They also bear testament to the excellent optical design of the VIRCAM camera and the high quality of the detector and amplifier chain (almost all remaining instrumental effects can be removed in software either at TERAPIX or CASU). Figure 1 shows a tiny area of one of the "deep stripes" observations from the upcoming DR2 release, where objects as faint as *Ks* ~ 23 AB mag are easily visible. This image is a colour composite of separate *Y*, *J* and *Ks* stacks.

DR1 images have appeared in an ESO press release[3] and also featured prominently on Phil Plait's well-known *Bad astronomy* blog[4], attracting hundreds of comments. Catalogues extracted from these images were released by ESO as part of the DR1 Phase 3 catalogue release in September 2012[2]. The processing steps used to create and validate these images and catalogues are described fully in McCracken et al. (2012).

The UltraVISTA DR1 represents a significant advance over previous NIR data in the COSMOS field. In only five months of operations, the depths in each of the broadband images meets or exceeds all previous near-infrared images taken in COSMOS over the past ten years. In bluer wavebands (*Y* and *J*) it is more than two magnitudes deeper. This enhanced sensitivity in bluer wavelengths (and overall better NIR wavelength coverage) is one of the defining features of UltraVISTA compared to previous NIR surveys at this depth and areal coverage. It ensures that lower-redshift ($z \sim 2$) interlopers for high-redshift galaxies can be reliably rejected and that secure photometric redshifts at $z \sim 1$–1.5, free from systematic errors, can be computed. At the time of writing, it remains the deepest NIR survey of the sky on square-degree areas, and is likely to remain so for the foreseeable future. Thanks to queue-scheduled observations and stringent seeing control, all final stacked images have seeing better than 1 arcsecond full width at half maximum, with variation in seeing between the bands less than 20%, further limiting the impact of systematic photometric errors.

Mass assembly and the high-redshift galaxy luminosity function

Scientific exploitation of this first release has proceeded rapidly. Bowler et al. (2012), by combining DR1 UltraVISTA images with multi-band data from the Subaru Observatory, the CFHT and the Spitzer Space Telescope, searched for UltraVISTA objects undetected in optical wavelengths and derived a new list of ten candidate high-redshift ($z > 6.5$) galaxies. Stacking the four most robust of these candidates, they derived a photometric redshift of $z \sim 7$ and (thanks to UltraVISTA *Y* and *J* data) show that low-redshift galaxy contaminants and T-dwarf star solutions are convincingly rejected. These are the first robust, bright very high-redshift galaxies discovered in COSMOS. This demonstrates also how future UltraVISTA data releases will place stringent limits on the bright-end slope of the high-redshift luminosity function (Figure 2).

The overall depths of the initial DR1 release precluded the discovery of significant numbers of high-redshift objects (although nevertheless demonstrating that our filter selection could reliably find such objects). However, for the redshift $z \sim 2$ population it represents a considerable advance over the existing COSMOS datasets, making possible the most precise assessment to date of the build-up in stellar mass in the Universe from $0 < z < 4$, and providing new constraints on the evolution

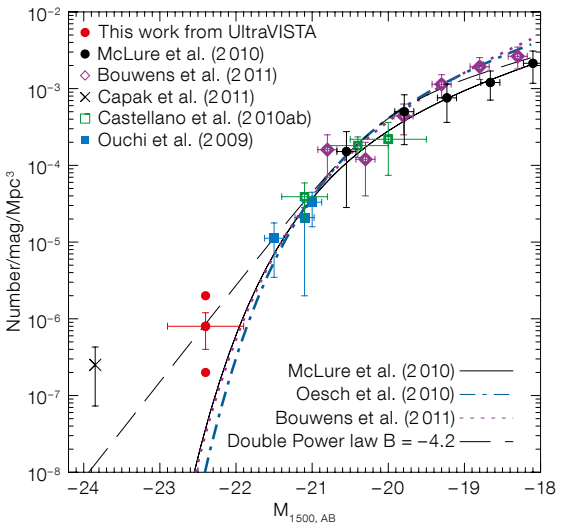

Figure 2. Ultraviolet $z \sim 7$ galaxy luminosity function (from Bowler et al., 2012). The red point shows UltraVISTA measurements if ten, four or one of the candidate objects are at $z \sim 7$. A literature compilation of similar measurements and Schechter function fits to fainter data is also shown.

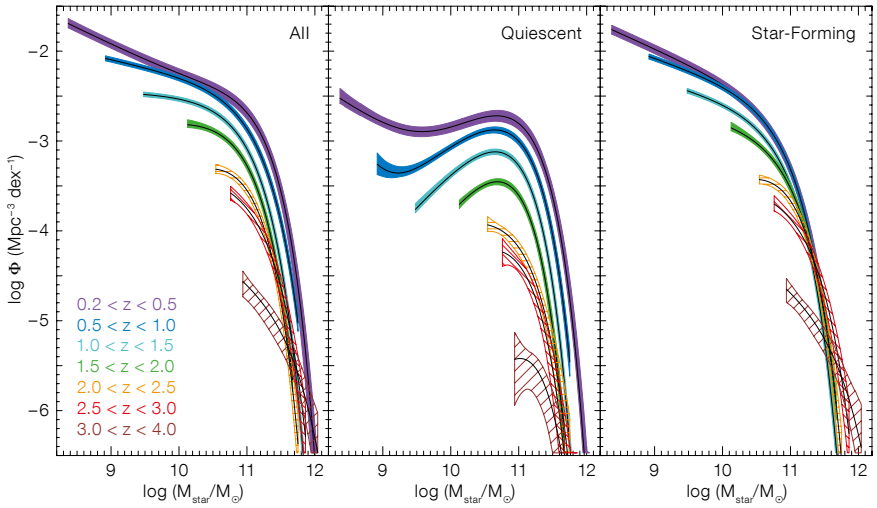

Figure 3. UltraVISTA galaxy stellar mass functions separated by star formation activity and redshift (colour-coded) are shown (from Muzzin et al., 2013).

of the faint-end slope of the mass function several magnitudes below M*. In addition, the galaxy population can be separated into star-forming and non-star-forming (quiescent) objects, the first time that this has been possible over such a large redshift range. The uniquely rich spectral coverage of the COSMOS field (more than 25 bands) and large numbers of extremely difficult-to-acquire spectroscopic redshifts in the $1 < z < 2$ redshift range, means that we can compute the most accurate photometric redshifts to date over a wide redshift baseline with low numbers of catastrophic failures.

Two independent papers (Ilbert et al., 2013; Muzzin et al., 2013) derived UltraVISTA–COSMOS photometric redshifts and used them to compute how the amount of mass in stars per cubic megaparsec (the stellar mass function) evolves as a function of cosmic time and star formation activity (Figure 3). Both confirm that most of the evolution in the stellar mass function is driven by a rapidly changing population of quiescent galaxies and that this evolution is mass-dependent. Massive galaxies are already in place at early times and the amount of stellar mass in these systems evolves only slowly. In contrast, the rapid build-up of mass in quiescent galaxies in the lower redshift Universe seems to be the result of different physical processes, which stop star formation in more massive galaxies at higher redshifts and less massive galaxies at lower redshifts. Furthermore, the cosmic evolution of the stellar mass density inferred from these measurements has now been shown to be consistent with the latest measurements of the evolution of the star formation rate (green shaded area in Figure 4). These photometric redshift catalogues and stellar mass measurements have been made publicly available[5].

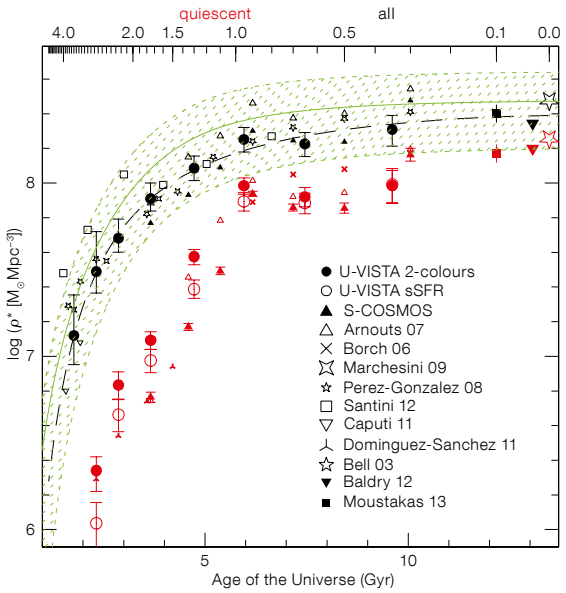

Figure 4. The total stellar mass density as a function of cosmic time as measured in UltraVISTA is shown (filled circles; from Ilbert et al., 2013) for all galaxies (in black) and for quiescent galaxies (in red). Other measurements from the literature are also shown.

Further and deeper: UltraVISTA DR2

Today, DR2 data processing has been completed, and the forthcoming release will contain all data taken during the first three years of operations. The deep survey component remains approximately the same depth as DR1. The ultra-deep stripes, however, have much longer integration times (30–50 hrs per pixel) and now reach *Ks* ~ 25 AB mag (5σ, 2 arcsecond).

The UltraVISTA–COSMOS field remains unparalleled in wavelength coverage and in the next four years several supplementary datasets will enhance the unique legacy value of the UltraVISTA dataset. Ultra-deep Spitzer observations will extend current CH1 and CH2 observations by the Infrared Array Camera (IRAC) to AB ~ 25.5 mag (the SPLASH programme), enabling reliable stellar mass measurements at z ~ 4. In addition, in 2014 the COSMOS-UltraVISTA field will be observed by the Hyper-Suprime-Cam on Subaru, increasing depths in optical bands by one to two magnitudes. Coupled with the complete UltraVISTA dataset, this will provide an unparalleled picture of representative volumes of the high-redshift Universe until the advent of Euclid in 2020.

References

Bowler, R. A. A. et al. 2012, MNRAS, 426, 2772
Ilbert, O. et al. 2013, A&A, 556, A55
McCracken, H. J. et al. 2012, A&A, 544, A156
Milvang-Jensen, B. et al. 2013, arXiv:1305.0262
Muzzin, A. et al. 2013, ApJ, in press, arXiv:1303.4409
Scoville, N. et al. 2007, ApJS, 172, 1

Links

[1] UltraVISTA web page: http://home.strw.leidenuniv.nl/~ultravista/
[2] UltraVISTA DR1 public release: http://www.eso.org/sci/observing/phase3/data_releases/ultravista_dr1.html
[3] ESO Release 1213: http://www.eso.org/public/news/eso1213/
[4] Phil Plait's Bad astronomy blog: http://www.slate.com/blogs/bad_astronomy.html
[5] UltraVISTA catalogue availability: http://terapix.iap.fr/article.php?id_article=844

The VISTA Kilo-degree Infrared Galaxy (VIKING) Survey: Bridging the Gap between Low and High Redshift

Alastair Edge[1]
William Sutherland[2]
Konrad Kuijken[3]
Simon Driver[4,5]
Richard McMahon[6]
Steve Eales[7]
Jim P. Emerson[2]

[1] Deptartment of Physics, University of Durham, United Kingdom
[2] Astronomy Unit, School of Physics and Astronomy, Queen Mary University of London, United Kingdom
[3] Leiden Observatory, Leiden University, the Netherlands
[4] ICRAR, University of Western Australia, Crawley, Australia
[5] SUPA — School of Physics and Astronomy, University of St. Andrews, United Kingdom
[6] Institute of Astronomy, University of Cambridge, United Kingdom
[7] School of Physics and Astronomy, Cardiff University, United Kingdom

VIKING is a medium-deep survey of 1500 square degrees over two areas of the extra-galactic sky with VISTA in *zYJHKs* bands to sample the restframe optical for galaxies at $z \gtrsim 1$. VIKING complements the two other surveys — VHS with its large area but shallower depth and VIDEO with its greater photometric depth and smaller spatial coverage. In addition to a $0.7 < z < 2$ galaxy survey, the area and depth of VIKING enables other studies, such as detection of distant quasars and low-mass stars and many galaxy clusters and superclusters. The early results are summarised and future prospects presented.

The remarkable improvement in the near-infrared survey speed that VISTA delivers offers the opportunity to study a volume of the distant ($z > 1$) Universe in the restframe optical bands that is many times larger than the Sloan Digital Sky Survey (SDSS). A survey of the full southern sky to reach a depth to detect an L^* galaxy requires more time than is available, but even a few percent of the available area is sufficient for the vast majority of projects.

It was with the goal of creating a legacy dataset with a wide range of science goals that we proposed the VISTA Kilo-degree Infrared Galaxy (VIKING) survey. In conjunction with its sister survey KiDS (Kilo-Degree Survey; Principal Investigator [PI]: K. Kuijken) on the VST, VIKING will cover 1500 square degrees in five bands (*z*, *Y*, *J*, *H* and *Ks*) to an AB depth of 23.1, 22.3, 22.1, 21.5 and 21.2 respectively. This combination of depth and area reaches our science goals for the $z > 1$ Universe and sits neatly between the VISTA Hemisphere Survey (VHS) and VIDEO surveys.

The VIKING survey area is split into two areas: an equatorial strip between right ascension 9 and 15.8 hours and 8 degrees wide; and a strip over the South Galactic Pole between right ascension 22 and 3.5 hours and 10 degrees wide. Our choice of survey area was made to maximise the overlap with existing multi-wavelength datasets that cover > 100 square degrees. The most prominent of these are the Galaxy And Mass Assembly (GAMA) survey (PIs: S. Driver and A. Hopkins) and the Herschel Astrophysical Terahertz Large Area Survey (H-ATLAS) (PIs: L. Dunne and S. Eales) covering over 148 and 360 square degrees of the VIKING area respectively.

Synergy with other surveys — GAMA, H-ATLAS and KiDS

The primary focus of GAMA science is on the combination of imaging and spectroscopy for $z < 0.2$ galaxies to determine the structure and evolution of galaxies over a wide range of mass and environment. The quality of the imaging data is particularly important in this context as the balance of bulge to disc in galaxies is key to our understanding of galaxy structure, but the stellar populations in the two components can differ significantly. Therefore, performing bulge–disc decomposition analysis at many different wavelengths can be used to constrain the evolution of the stellar population in the two components of the galaxy independently. To do this requires relatively deep photometry to constrain the lower surface brightness outer regions of the galaxy. Figure 1 illustrates the improvement in image quality going from the Two Micron All Sky Survey (2MASS), UKIRT InfraRed Deep Sky Surveys: Large Area Survey (UKIDSS LAS) to VIKING for a single galaxy (Andrews et al., 2013). The importance of depth to enhance the science potential in the lower-redshift Universe is just as significant as it is at higher redshift.

H-ATLAS represents the largest investment of time into any Herschel project and it has returned results from the lowest redshift (Burton et al., 2013) to lensed high-redshift galaxies (González-Nuevo et al., 2012). The dusty nature of far-infrared (FIR) selected galaxies means that it is particularly important to use near-infrared (NIR) imaging to identify these sources. Fleuren et al. (2012) find counterparts in VIKING for at least 51% of all 250 µm sources and a substantially higher fraction of sources with FIR fluxes consistent with lower redshift. This fraction is 40% higher than equivalent matches in the optical *r*-band. The VIKING depth is sufficient to make a matched detection with at least the deepest band in the KiDS survey for any $z < 1$ galaxy. However, for more distant galaxies, particularly systems with a low specific star formation rate, then many will be too faint to be detected at the KiDS depth of 24 mag AB. Fortunately, for the equatorial strip, the Subaru Hyper SuprimeCam (HSC) Survey (PI: A. Miyazaki) will cover the same area to at least 1–1.5 mag deeper. This will allow for the selection of an unprecedentedly large sample of Extremely Red Objects (EROs; $[i–Ks]_{AB} > 2.45$) that are known to cluster very strongly (Kim et al., 2011) and also trace the most distant clusters of galaxies at $z > 1.6$ (Stanford et al., 2012).

QSO and low-mass star discrimination

The combination of deep optical data and moderately deep NIR data are particularly important when considering the selection of the most distant quasars and the lowest-mass stars. The discovery of the first $z > 7$ quasar (QSO) from the UKIDSS LAS by Mortlock et al. (2011) demonstrated the potential of NIR selection to push back the detection of the most distant active galactic nuclei (AGN), with all the associated insights they provide on the reionisation of the Universe. The combination of depth and area makes VIKING very well suited to the selection of $z > 6.4$ QSOs that fall beyond the grasp of silicon detectors in the optical. Venemans et al. (2013) have amply demonstrated this by the selection of the second, third and fourth most distant QSOs at $z = 6.89$, 6.75 and 6.61 respectively (see Figure 2). The selection of these three QSOs from the first 300 square degrees of the VIKING area required a significant investment of ESO New Technology Telescope (NTT) follow-up time to remove the contamination of low-mass stars and dusty, lower-redshift galaxies, as the KiDS survey had not started in 2011. Now that KiDS has covered the same area as VIKING, this additional screening is not required, so future target selection will be significantly faster. Venemans et al. (2013) predict the discovery of ~ 20 QSOs at $6.44 < z < 7.44$, so the prospects for future constraints on the evolution of QSOs into the epoch of reionisation are very promising.

At the opposite extreme, VIKING offers an excellent combination of bands to select low-mass stars. The differentiation between

low-mass stars and distant QSO candidates in (*Z-Y*) *vs*. (*Y-J*) colour space means that VIKING data can make a clean selection of L- and T-dwarfs. Adding in Wide-Field Infrared Survey Explorer (WISE) photometry and KiDS/HSC *i*-band data, means that VIKING will recover a significant number of these stars, allowing constraints on their scale height given the range of Galactic latitude and longitude covered by VIKING.

Galaxy and cluster surveys

The bulk of the galaxies detected in VIKING will be at redshifts of 0.7 to 2.0. The volume sampled between these two limits is ~ 20 Gpc^3 which is nearly an order of magnitude larger than that of the SDSS DR10 within $z < 0.3$. Therefore rare objects such as clusters and superclusters will be recovered in large numbers. Given the overlap with Sunyaev–Zel'dovich surveys such as the Atacama Cosmology Telescope (ACT; Marriage et al., 2011) and the substantial increase in X-ray survey depth provided by eROSITA (Predehl et al., 2009), VIKING will provide an important resource for the confirmation of cluster candidates from other techniques, as well as providing clusters selected from their member galaxies alone. The selection of more distant clusters is of particular importance when

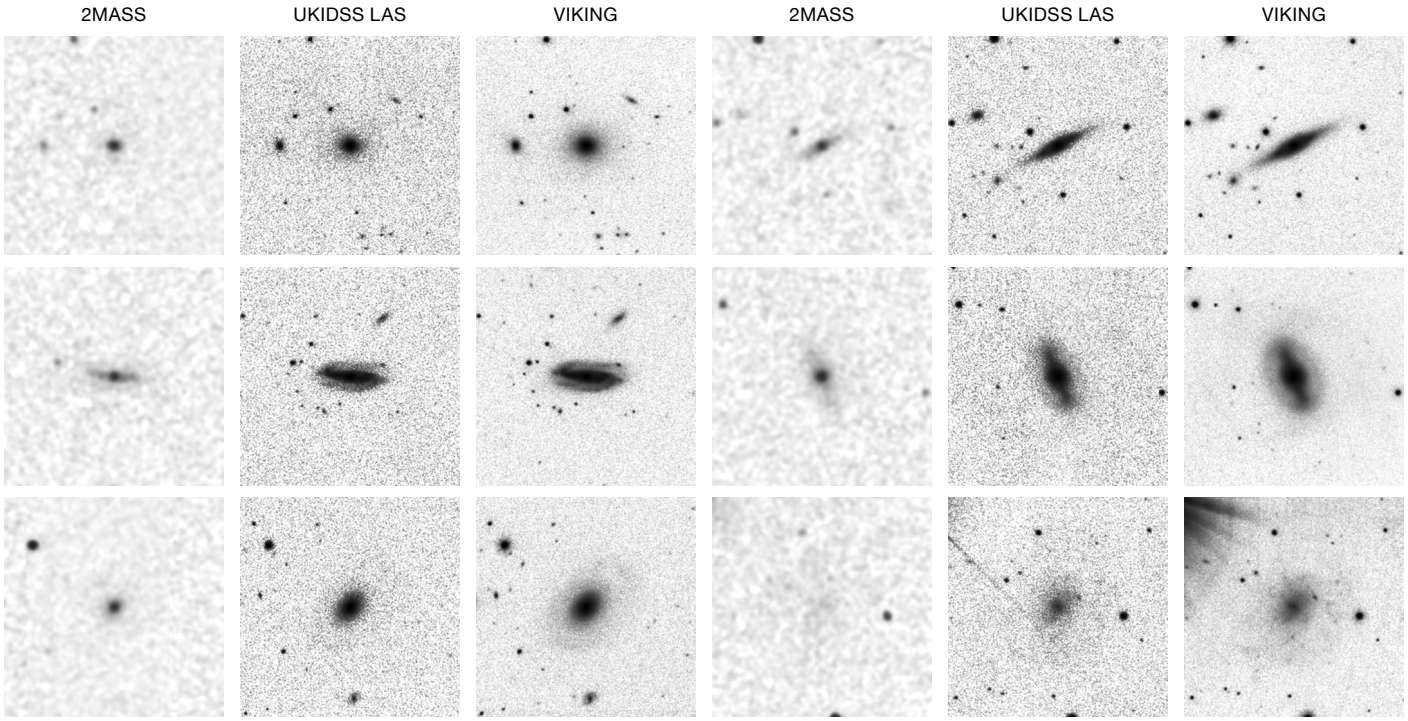

Figure 1. The 2MASS, UKIDSS LAS and VIKING images of six GAMA galaxies in the *Ks*-band. Note the extended, low surface brightness emission that only becomes clear in the deepest data. A full description of these comparisons can be found in Andrews et al. (2013).

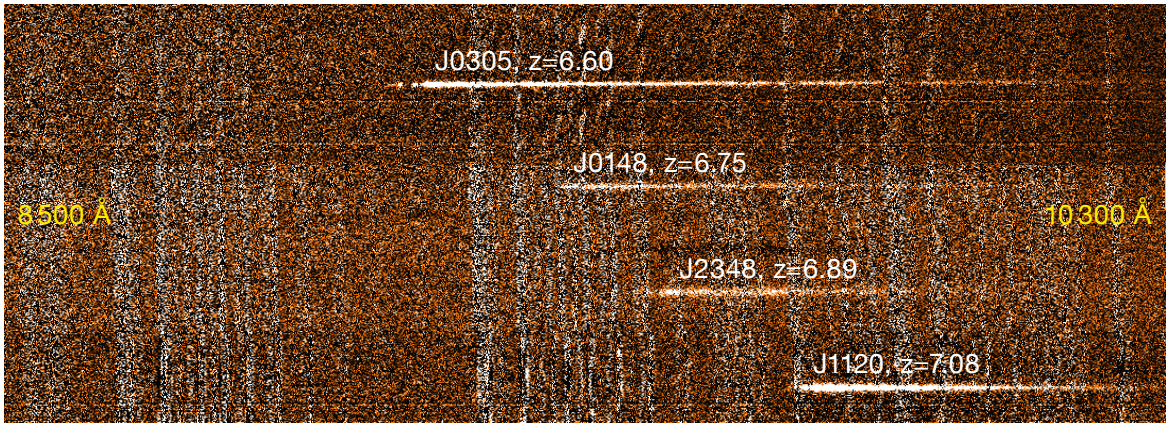

Figure 2. A montage of the 2D FORS2 spectra of the three VIKING $z > 6.5$ quasars with the $z = 7.1$ UKIDSS quasar for comparison. Note the excellent red sensitivity of FORS2 and the very abrupt cut-off blueward of the Lyman-α line in these systems.

considering the cosmological constraints that can be determined from the evolution of the cluster mass function (Eke, Cole & Frenk, 1996). VIKING will recover a significant number of the most massive clusters at $z > 1$ that are only found in small numbers in serendipitous X-ray cluster surveys, such as the XMM Cluster Survey (XCS; Mehrtens et al., 2012), or Spitzer mid-infrared surveys, such as the Spitzer Adaptation of the Red-sequence Cluster Survey (SpARCS; Wilson et al., 2009), which cover much smaller areas of sky.

In addition to clusters, VIKING will select the most massive galaxies within the survey volume and these are known to cluster particularly strongly (Kim et al., 2011). The combination of excellent photometry and the large area coverage of VIKING/KiDS will allow us to trace the angular clustering of massive galaxies at $z > 1$ (where the angular clustering scales are least affected by redshift) in a number of independent redshift slices.

Serendipity and legacy aspects

VIKING will also provide a wide margin for serendipitous discoveries of rare or extreme sources, given the overlap with many other multi-wavelength surveys. For instance, extremely obscured AGN can be selected from WISE photometry relatively easily (Eisenhardt et al., 2012), but are very faint in the optical, so NIR data are essential. VIKING photometry will fill an important niche for a number of projects that need deeper photometry than that provided by UKIDSS LAS or VISTA VHS, but wider area coverage than UKIDSS Deep Extragalactic Survey (DXS) or VISTA VIDEO.

The legacy value of the VIKING/KiDS survey will be extended with the extensive spectroscopic surveys planned in this area using the spectrographs 4MOST, MOONS and Subaru Prime Focus Spectrograph (PFS). The complementary nature of these optical and NIR surveys means that the spectral coverage will be very dense, allowing many new observational strategies related to the lensing and intervening absorption of background objects by a fully constrained foreground to be explored. The vital foundation of these surveys will be the reliable photometric catalogue that VIKING/KiDS provides.

The VIKING data will be made available through the VISTA Science Archive (VSA[1]) and the ESO Phase 3 facility[2], but the VIKING consortium will be creating an additional set of images that are optimised to match the seeing of other optical surveys (SDSS, KiDS and/or HSC) to ensure the best possible aperture photometry is extracted. These additional images will be made available to the community through the VSA. The first 226 square degrees of the VIKING data have been released through the VSA and ESO Phase 3 databases and we encourage the community to contact us if they have any questions.

References

Andrews, S. K. et al. 2013, PASA, submitted
Burton, C. S. et al. 2013, MNRAS, 433, 771
Eisenhardt, P. R. M. et al. 2012, ApJ, 755, 173
Eke, V. R., Cole, S. & Frenk, C. S. 1996, MNRAS, 282, 263
Fleuren, S. et al. 2012, MNRAS, 423, 2470
González-Nuevo, J. et al. 2012, ApJ, 749, 65
Kim, J.-W. et al. 2011, MNRAS, 410, 241
Marriage, T. A. et al. 2011, ApJ, 737, 61
Mehrtens, N. et al. 2012, MNRAS, 423, 1024
Mortlock, D. J. et al. 2011, Nature, 474, 616
Predehl, P. et al. 2009, AIPC, 1248, 543
Stanford, S. A. et al. 2012, ApJ, 753, 164
Venemans, B. et al. 2013, ApJ, 779, 24
Wilson, G. et al. 2009, ApJ, 698, 1943

Links

[1] VISTA Science Archive (VSA): http://horus.roe.ac.uk/vsa/
[2] ESO Phase 3 VIKING data release 1: http://www.eso.org/sci/observing/phase3/data_releases/viking_dr1.pdf

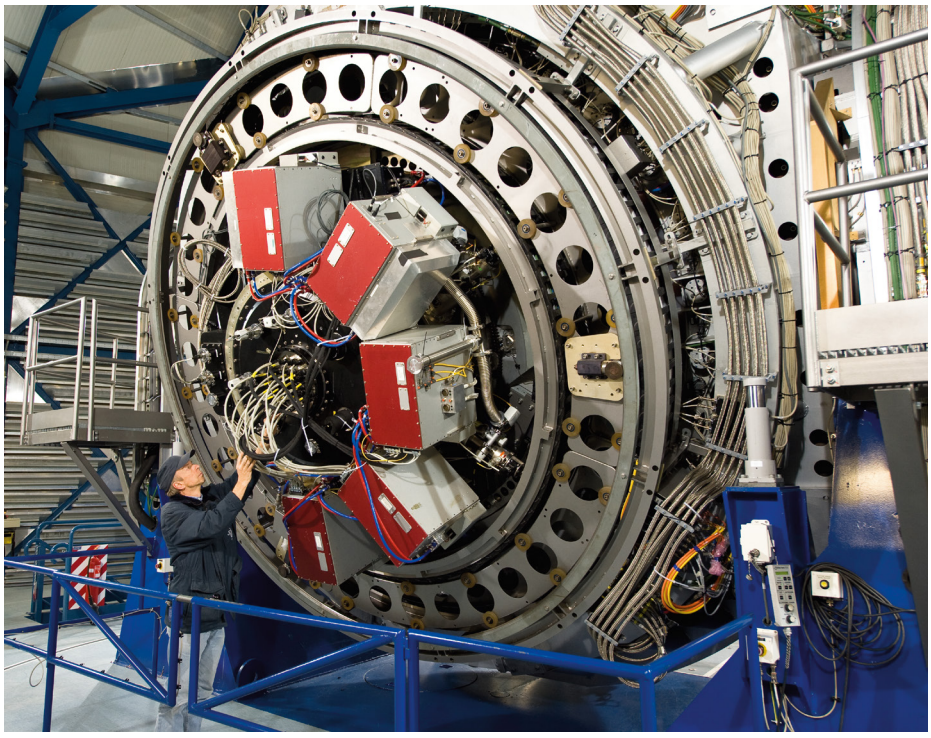

View of the Cassegrain focus of VISTA housing the VIRCAM camera. VIRCAM consists of 16 2048 square Raytheon VIRGO HgCdTe 0.84–2.5 µm detectors covering a field of 45 × 45 arcminutes (with inter-detector gaps). This image shows Paranal engineer Gerhard Hüdepohl checking VIRCAM.

First Scientific Results from the VISTA Hemisphere Survey (VHS)

Richard G. McMahon[1,2]
Manda Banerji[1,3]
Eduardo Gonzalez[1]
Sergey E. Koposov[1]
Victor J. Bejar[4,5]
Nicolas Lodieu[4,5]
Rafael Rebolo[4,5]
and the VHS collaboration

[1] Institute of Astronomy, University of Cambridge, United Kingdom
[2] Kavli Institute for Cosmology, University of Cambridge, United Kingdom
[3] Department of Physics and Astronomy, University College London, United Kingdom
[4] Instituto de Astrofisica de Canarias, La Laguna, Tenerife, Spain
[5] Departamento de Astrofisica, Universidad de La Laguna, Tenerife, Spain

The first Galactic and extragalactic results from the VISTA Hemisphere Survey (VHS) are presented. The aim of the VHS is to carry out a near-infrared survey which, when combined with other VISTA public surveys, will result in coverage of the whole southern celestial hemisphere (~20 000 square degrees) to a depth 30 times fainter than the Two Micron All Sky Survey in at least two wavebands (*J* and *Ks*). The VHS vision includes a deep optical survey over the same area and this is now being realised with the VST surveys and the Dark Energy Survey, which has recently started. A summary of the survey progress is presented, with some follow-up results on low-mass stars and high-redshift quasars.

Introduction

The goal of the Vista Hemisphere Survey (VHS[1]) is to carry out a near-infrared (NIR) survey of all of the southern hemisphere (an area of ~ 20 000 square degrees) in at least two wavebands (*J* and *Ks*), with an exposure time of 60 seconds per waveband to produce median 5σ point source (Vega) limits of *J* = 20.2 and *Ks* = 18.1. This is ~ 30 times deeper than the Two Micron All Sky Survey (2MASS; Skrutskie et al., 2006) in the same bands. This total area coverage is achieved by combining with data from other VISTA public surveys, such as VIKING.

In the South Galactic Cap, ~ 5000 square degrees will be imaged more deeply with an exposure time of 120 seconds, and also including the *H*-band to produce median 5σ point source limiting magnitudes of: *J* = 20.6, *H* = 19.8 and *Ks* = 18.5. In this region of the sky, deep multi-band optical (*grizY*) imaging data will be provided by the Dark Energy Survey (DES). The remainder of the high Galactic latitude (|*b*| > 30°) sky will be imaged in *YJHKs* for 60 s per band, to be combined with *ugriz* waveband observations from the VST ATLAS survey.

The medium-term scientific goals of the VHS include:
– the discovery of the lowest-mass and nearest stars;
– deciphering the merger history of the Galaxy via stellar galactic structure;
– measurement of large-scale structure of the Universe out to *z* ~ 1 and measuring the properties of dark energy;
– discovery of quasars with *z* > 7 for studies of the baryons in the intergalactic medium during the epoch of reionisation;
– discovery of the most luminous quasars at all redshifts in the southern hemisphere as probes of the intergalactic medium and the formation of the most massive supermassive black holes in the Universe.

In addition the VHS survey will provide essential multi-wavelength support for the European Space Agency (ESA) Cornerstone missions; XMM-Newton, Planck, Herschel and Gaia.

Survey status

Figure 1 shows the sky coverage of VHS observations completed up to 1 October 2013. A total of 5511 observation blocks (OBs) have been completed. Each OB is equivalent to a single VISTA tile and covers 1.5 square

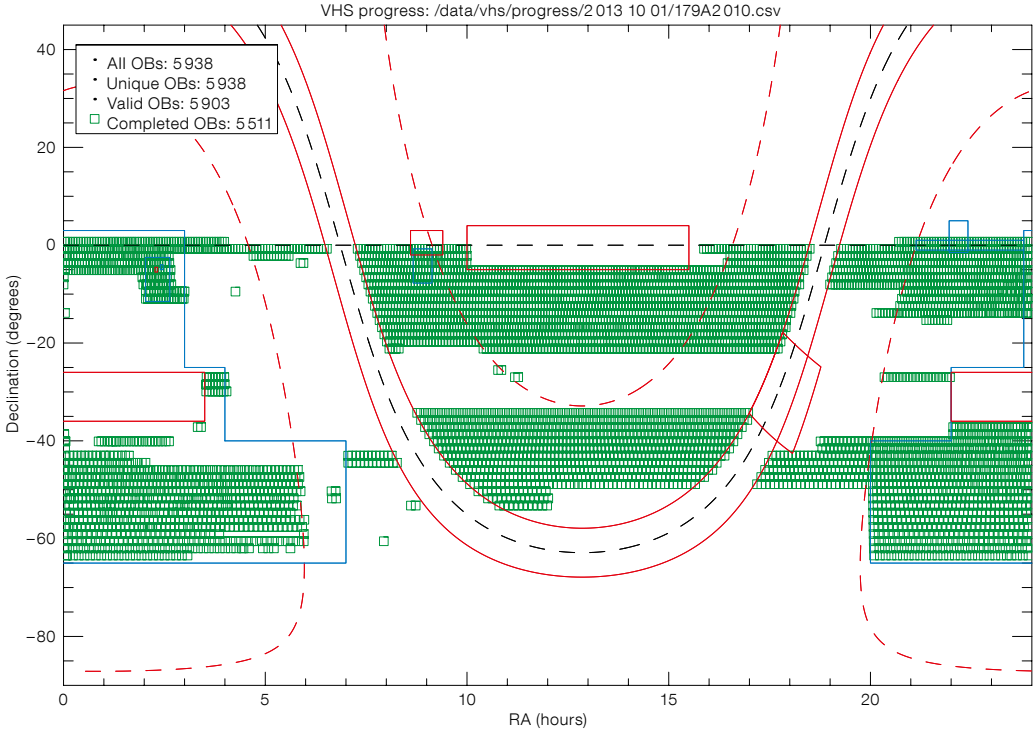

Figure 1. Sky coverage of the VHS survey completed up to 1 October 2013 based on ESO portal report tables. The green rectangles show completed tiles. The red solid lines show nominal regions outside the VHS observing footprint. The dashed red line is Galactic latitude +30, –30 degrees. The blue lines show the provisional DES footprint, circa April 2012.

degrees. The total observed area is around 8300 square degrees. All data is pipeline processed with the VISTA Data Flow System (Irwin et al., 2004; Lewis, Irwin & Bunclark, 2010; Cross et al. 2012) and the science products are available from the ESO Science Archive Facility and the VISTA Science Archive[2].

Scientific results

Many of the proposed scientific programmes for VHS require optical survey data from the VST surveys and DES. These surveys have only recently started and hence scientific exploitation has focused on science that can be carried out without optical data.

Figure 2 shows a comparison between VHS positions and the very long baseline interferometry (VLBI) radio reference frame[3]. The results are summarised in Table 1 and compared with the Sloan Digital Sky Survey (SDSS) and the UKIRT Infrared Deep Sky Survey (UKIDSS): there is a statistically significant systematic error of 0.05 arcseconds in declination. This is consistent with expected proper motions of 2MASS stars (Roeser et al., 2010) due to the ten year difference in epoch between 2MASS and VHS. Note that this systematic error varies depending on the direction in the sky of the Solar System motion with respect to an average 2MASS reference star. Proper motions will be included in future Cambridge Astronomical Survey Unit (CASU) processing based on the Fourth U.S. Naval Observatory CCD Astrograph Catalogue (UCAC4) or PPMXL catalogues (Roeser et al., 2010).

Survey (number of sources)	σ (statistical) (arcseconds)		Systematic uncertainty (arcseconds)	
	RA	Dec	RA	Dec
VHS (563)	0.11	0.09	0.011 ± 0.005	0.051 ± 0.004
SDSS (2308)	0.05	0.05	0.006 ± 0.001	0.003 ± 0.001
UKIDSS (599)	0.10	0.09	−0.031 ± 0.004	−0.068 ± 0.004

Table 1. VHS astrometry comparison with VLBI radio reference frame, contrasted with SDSS and UKIDSS.

Low-mass stars

Gauza et al. (2012) are conducting a search for very low-mass common proper motion companions of nearby (< 25 pc) stars using VHS data and the shallower but earlier epoch (baseline around ten years) 2MASS catalogue. A search around the star HD 221356, which lies at a distance of 26.1 pc, has resulted in the discovery of a new common proper motion companion star located at an angular separation of 12.1 ± 0.2 arcseconds, corresponding to a projected distance of ~ 317 astronomical units (au). Figure 3 shows the VISTA discovery image. Near-infrared spectroscopy indicates a L0–L2 spectral type. Evolutionary models combined with an effective temperature of 2100–2300 K indicate a mass of 0.079 ± 0.006 $M_{\odot}$. Since the distance and metallicity of the HD 221356 system are well known, the detailed study of this new ultra-cool companion, which is located close to the frontier between stars and brown dwarfs, can provide valuable constraints on evolutionary models and, in particular, shed light on the properties of objects at the transition from stellar to substellar regime.

Lodieu et al. (2012) are using VHS in a project to improve our current knowledge of the density of T dwarfs and the shape of the substellar initial mass function by identifying a magnitude-limited sample of T-dwarfs in the full southern sky. Lodieu et al. (2012) have used VHS data combined with longer wavelength photometric data from the Wide Infrared Survey Explorer (WISE) satellite mission (Wright et al., 2010) to select candidates with red mid-infrared colours and NIR to mid-infrared colours characteristic of cool brown dwarfs.

In this first stage of the survey, which only covers a few hundred square degrees, five new T-dwarf stars have been confirmed spectroscopically with the VLT with spectral types between T4.5 and T8 (see Figure 4). Two are estimated to be T6 dwarfs and lie within 16 pc, while a T4.5 dwarf is situated within 25 pc.

Quasars

Banerji et al. (2013) present the first results of a project that uses VHS data combined with WISE data to identify heavily reddened broad-line type 1 quasars in the redshift range 1.5 to 3. This redshift extent represents the cosmological epoch at the peak of star formation activity and accretion onto supermassive black holes as manifested by luminous quasars. Up until now it has been impossible to detect these luminous dust-enshrouded quasars, since existing NIR surveys like 2MASS are too shallow and deeper surveys have not covered enough area. Such luminous quasars

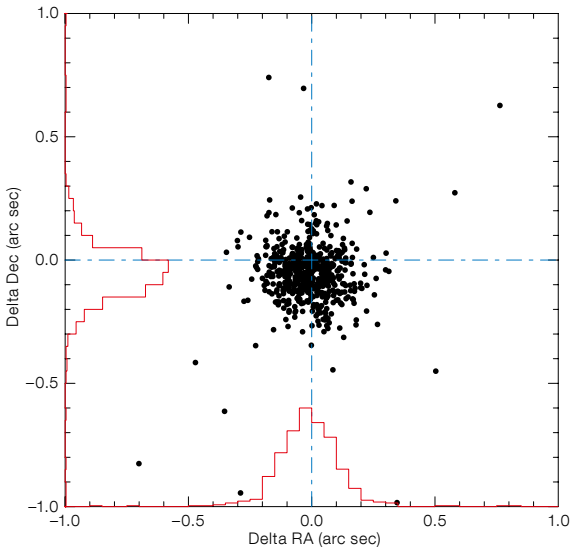

Left: Figure 2. Astrometric comparison between VHS positions and the VLBI radio reference frame[3].

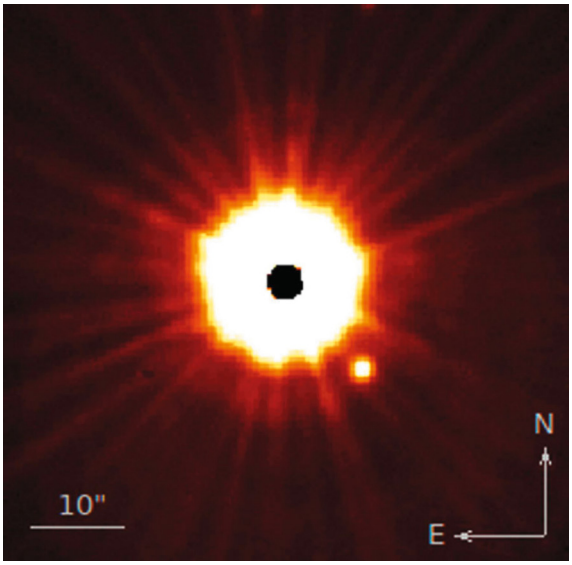

Right: Figure 3. False colour VISTA *J*-band image of HD 221356AD. The angular separation of the newly identified companion is 12.13 ± 0.18 arcseconds and the position angle 222 ± 2 degrees. Saturation in the image centre of the primary star is visible. Scale and orientation are shown.

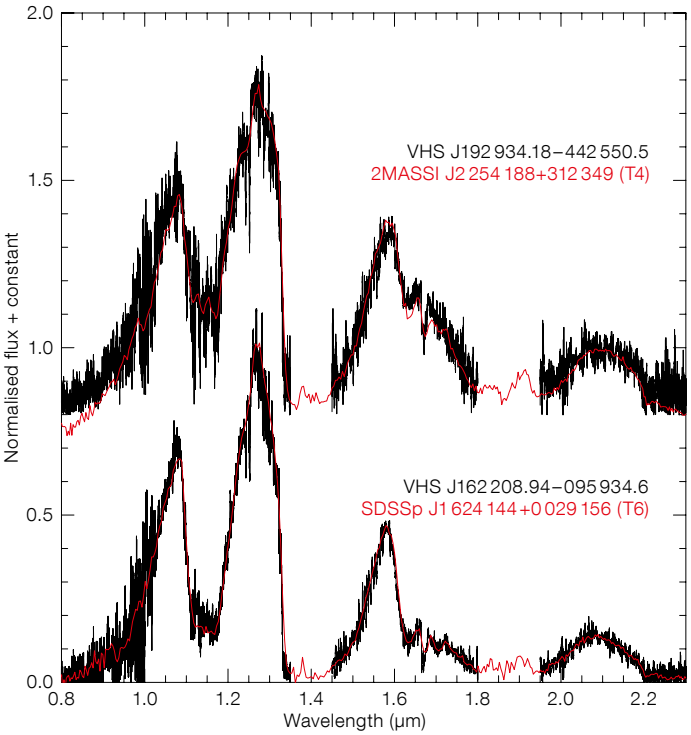

Figure 4. Near-infrared spectra obtained with VLT X-shooter and normalised at 1.265 μm. Overplotted in red are the known T-dwarf T4 and T6 templates that best fit the observed spectra.

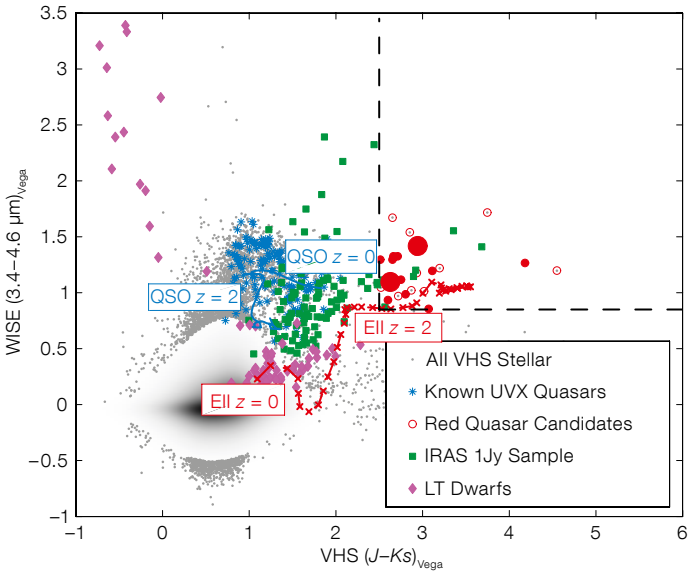

Figure 5. VHS (*J–K*) versus WISE (W1–W2) colour selection of our red quasar candidates are shown. All stellar objects detected over 180 square degrees are shown with greyscale representing the density, while the 1% of outliers in the distribution are shown as the individual grey points. Known UV-luminous quasars, local Ultraluminous Infrared Galaxies (ULIRGs) from the IRAS 1Jy sample and known LT dwarf stars have also been plotted. Also shown are the tracks of a typical unreddened quasar and an elliptical galaxy template with a formation redshift of $z = 5$. Heavily reddened quasars are marked as red circles. The small filled circles represent the spectroscopically confirmed sample from UKIDSS, the large filled circles are two newly confirmed quasars from VHS and the open circles are all candidates detected in the Banerji et al. (2013) study down to $Ks < 17$.

are expected to be in a short-lived transition phase from a heavily reddened dusty starburst to ultraviolet (UV)-luminous quasar. Optical surveys like SDSS and those with the VST are unable to detect quasars in this dusty formation phase due to the restframe UV extinction, which can be larger than 10 magnitudes at observed optical wavelengths.

With the new generation of wide NIR surveys, like UKIDSS and VHS, this field will be transformed. Luminous, heavily reddened, quasars detected by VHS will be ideally suited to follow up with the Atacama Large Millimeter/submillimeter Array (ALMA). Figure 5 shows how VHS and WISE colours are used to select the heavily obscured quasars with extremely red ($J–Ks > 2.5$ mag) colours. At high Galactic latitudes, obscured high-redshift quasars dominate this colour locus at $15 < Ks < 17$. SINFONI spectra have been used to detect broad Hα with line widths that imply supermassive black holes with masses of more than 10^9 $M_\odot$.

References

Banerji, M. et al. 2013, MNRAS, 429, L55
Cross, N. J. et al. 2012, A&A, 548, A119
Gauza, B. et al. 2012, MNRAS, 427, 2457
Irwin, M. J. et al. 2004, SPIE, 5493, 411
Lewis, J. R., Irwin, M. J. & Bunclark, P. S. 2010, ASP Conf. Ser., 434, 91
Lodieu, N. et al. 2012, A&A, 548, A53
Roeser, S. et al. 2010, AJ, 139, 2440
Skrutskie, M. F. et al. 2006, AJ, 131, 1163
Wright, E. L. et al. 2010, AJ, 140, 1868

Links

[1] VHS web page: http://www.vista-vhs.org
[2] VISTA Science Archive: http://horus.roe.ac.uk/vsa/
[3] VLBI radio reference frame: http://astrogeo.org/vlbi/solutions/rfc_2012b

VST ATLAS First Science Results

Tom Shanks[1]
Vasily Belokurov[2]
Ben Chehade[1]
Scott M. Croom[3]
Joe R. Findlay[1]
Eduardo Gonzalez-Solares[2]
Mike J. Irwin[2]
Sergey Koposov[2]
Robert G. Mann[4]
Nigel Metcalfe[1]
David N. A. Murphy[5]
Peder R. Norberg[6]
Mike A. Read[4]
Eckhard Sutorius[4]
Gabor Worseck[7]

[1] Department of Physics, Durham University, United Kingdom
[2] Cambridge Astronomical Surveys Unit, Cambridge, United Kingdom
[3] School of Physics, University of Sydney, Australia
[4] Wide Field Astronomy Unit, Institute for Astronomy, University of Edinburgh, Royal Observatory, Edinburgh, United Kingdom
[5] Instituto de Astrofísica, Universidad Catolica de Chile, Chile
[6] ICC, Department of Physics, Durham University, United Kingdom
[7] Max-Planck-Institut für Astronomie, Heidelberg, Germany

The VST ATLAS is a *ugriz*-imaging survey targeting ~ 4500 square degrees of the southern sky. It reaches similar magnitude limits to the Sloan Digital Sky Survey in the north, i.e., *r* ~ 22.5, but ATLAS has better median seeing of 1 arcsecond full width half maximum. ATLAS is a companion survey to the VISTA Hemisphere Survey, which supplies *YJHK* imaging over much of its area. In addition, the Wide-field Infrared Survey Explorer (WISE) satellite supplies a further four mid-infrared bands. Together these surveys complement each other and provide excellent multi-wavelength data for both Galactic and extragalactic science projects.

Survey description

The VLT Survey Telescope (VST) ATLAS imaging exposures are 2 × 60 s in *u*-band, 2 × 50 s in *g*-band and 2 × 45 s in *riz*-bands. The *iz* images are observed in grey time and the *ugr* in dark. The median seeing of 1 arcsecond is well sampled by the 0.21-arcsecond pixels of VST OmegaCAM. The current status of the VST ATLAS in the *ugriz* band can be queried[1]. Ultimately we are targeting most of the available high latitude sky in the northern and southern Galactic Caps. So far we have covered approximately 2200 square degrees in each band with a little less coverage in *ugr* and somewhat more in *iz*. Thus the survey which started in September 2011 is roughly at its half-way point. The survey is unique in terms of southern surveys in having *u*-band sensitivity and the ATLAS Chilean *u*-band extension (Principal Investigator [PI]: L. Infante) doubles the *u*-band exposure to four minutes. As well as VHS supplying *YJHK* imaging, ATLAS is well complemented by the WISE satellite near-infrared (NIR) survey covering 3.4–22 μm. The WISE survey depth is particularly well matched to ATLAS in the W1 (3.4 μm) and W2 (4.6 μm) bands and several of the science aims, outlined in the following sections, exploit this complementarity. The OmegaCAM Science Archive[2] will publish ATLAS data, and federate it with GALEX, WISE and the VISTA surveys, to facilitate these multi-wavelength analyses.

z < 2.5 quasar redshift surveys

ATLAS has two routes to quasar surveys at lower redshifts: via ultraviolet excess (UVX) selection by virtue of its *u*-band sensitivity; via "KX" selection using the W1 (3.4 μm) band. Both these methods distinguish the power-law spectra of quasars from the thermal spectra of stars at their respective wavelength extremes. Chehade et al. (in prep.) have made the first spectroscopic follow-up of quasars selected using ATLAS+WISE, using the Two-degree-Field Galaxy Redshift Survey (2dF) and AAOmega at the Australian Astronomical Telescope (AAT). They found that while UV selection wins at the faintest magnitudes ($g < 22.5$), NIR selection using (*g*-*i*):(*i*-W1) significantly increases the quasar number counts by around ~ 15% in the fields where it has been applied to $g < 22$, mostly comprising a population of dust-reddened quasars (see Figure 1a), leading to quasar sky densities of up to 95 per square degree. We now have a sample of ~ 10 000 quasars with which to analyse the luminosity functions and clustering in a more complete and fainter redshift survey than the best previous surveys, such as 2SLAQ. The ATLAS quasar surveys will provide future targets for the ESO 4MOST fibre spectrograph and will also gain X-ray coverage with the eROSITA satellite, soon to be launched.

5 < *z* < 6 quasar redshift surveys

The combination of WISE and ATLAS shows further potential. Findlay et al (in prep.) have shown that the (*r*-*z*):(*i*-W1) colour–colour plane (see Figure 1b) can easily distinguish $5 < z < 6$ quasars from red stars and galaxies, since previously discovered SDSS quasars in this redshift range lie in a valley between the loci of stars and galaxies. This immediately reduces background contamination for such quasar searches by about two orders of magnitude to $i = 21.5$ even before a *g*-band dropout technique is applied. Using the combination of these techniques, it should be possible to add significantly to the relative dearth of known quasars in this redshift range and so bridge the gap between the $z \sim 5$ and $z \sim 6$ quasar luminosity functions. Increasing the numbers of

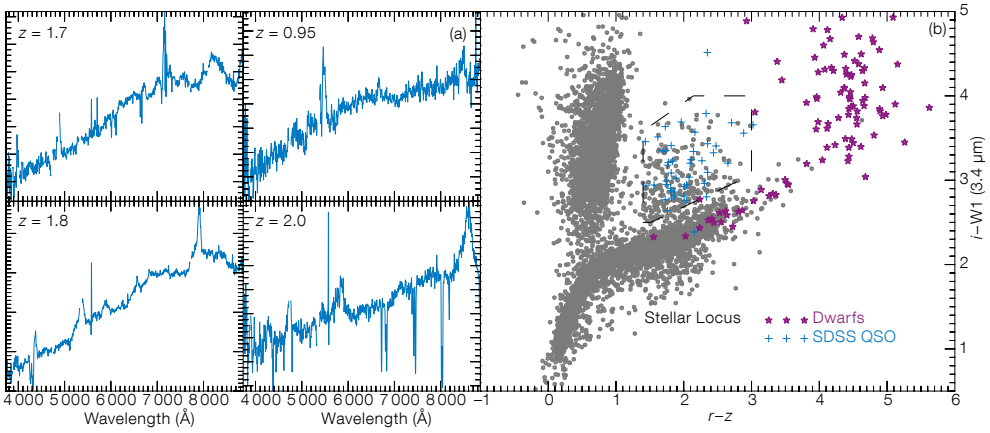

Figure 1. (a) Four examples of a new population of dust-absorbed red quasars at $z < 2.5$ selected from (*g*-*i*):(*i*-W1) colour–colour plot by a combination of WISE and ATLAS. Spectra are from AAT 2dF AAOmega. (b) WISE and ATLAS (*r*-*z*):(*i*-W1) colour–colour plot shows high efficiency in isolating previously discovered SDSS $5 < z < 6$ quasars.

$5 < z < 6$ quasars will also provide the sightlines required to characterise better the properties of the intergalactic medium (IGM) at redshifts approaching the end of reionisation.

New UV-bright quasars for helium reionisation studies

VST ATLAS provides a unique opportunity to select rare UV-transmitting high-redshift quasars to study the reionisation epoch of He. Far-UV spectra of background quasars obtained with the Hubble Space Telescope (HST) probe the redshifted Lyman-α transition of singly ionised helium, with strong absorption signalling that He is not yet fully ionised (e.g., Worseck et al., 2011). To date, very few quasars allow for such analysis due to the near-ubiquitous occurrence of strong Lyman continuum absorption by neutral hydrogen at longer wavelengths. Current quasar catalogues have been almost fully exploited, yielding high-quality helium absorption spectra of only 19 quasars. The very low predicted surface density of quasars for He absorption spectroscopy with HST (~ 6 per 1000 square degrees; Worseck & Prochaska, 2011) requires large-area surveys. Moreover, the optical colours of most of these quasars are degenerate with stellar colours (see Figure 2, upper), and only the combination with multi-wavelength photometry from the Galaxy Evolution Explorer (GALEX; UV) and WISE (mid-IR) allows their selection at high efficiency. With VST ATLAS it is now possible to extend these multi-wavelength studies to the southern hemisphere, complementing similar efforts with Sloan Digital Sky Survey (SDSS) and the Panoramic Survey Telescope and Rapid Response System (Pan-STARRS). Confirmation of quasar candidates is under way (see Figure 2, lower) to maximise the number of potential targets for He reionisation studies before the end of HST's lifetime.

Luminous red galaxy surveys out to $z \sim 1$

Using ATLAS *gri* colour cuts at $z \sim 0.35$ and $z \sim 0.55$ and *riz* cuts at $z \sim 0.68$, new catalogues containing up to one million luminous red galaxies (LRGs) can be made. One aim is to use the angular clustering of the LRGs to test the evidence for non-Gaussianity found in similar SDSS LRG samples. Again there may be a possibility to extend the LRG redshift range to $z \sim 1$ by incorporating WISE data in (*i*-*z*):(*z*-W1) galaxy colour cuts. But the prime aim is to use the ATLAS LRGs to measure the strength of the Integrated Sachs–Wolfe (ISW) effect in the southern hemisphere by cross-correlating with Planck cosmic microwave background data. Such a cross-correlation is only predicted in cosmological models with an accelerating expansion. Previously Sawangwit et al. (2010) found only a weak ISW effect at $z = 0.35$ and $z = 0.55$ and a null result at $z = 0.68$. It is therefore important to repeat this test of the accelerating expansion in the south. Since the test cannot be made at high redshift, the southern hemisphere ATLAS data will provide the only decisive independent new evidence for universal acceleration.

GAMA and VST ATLAS

The Galaxy And Mass Assembly (GAMA) project originated as a large optical spectroscopic survey on the AAT with complementary imaging data from the far-UV to the radio, via optical, NIR, mid-IR and far-IR (Driver et al., 2011). GAMA is the first multi-wavelength spectroscopic survey covering hundreds of square degrees over a 5 Gyr lookback time.

Since 2008, GAMA has executed a comprehensive and complete spectroscopic survey down to $r_{AB} = 19.8$ (i.e., two magnitudes deeper than the main SDSS survey) in five roughly equal-sized areas covering a large range in right ascension: three equatorial 60 square degree regions (G09, G12 and G15), a 50 square degree patch overlapping with the Canada France Hawaii Telescope Legacy Survey (CFHTLS) W1 (G02) and another of similar size centred within the VST ATLAS survey (G23). The latter, defined as $339 < \mathrm{RA} < 351$ degrees and $-35 < \mathrm{Dec} < -30$ degrees, is currently only 37 % complete spectroscopically, but is due to be completed by autumn 2014.

GAMA represents the highest priority target areas for the Herschel-ATLAS, VST ATLAS/KiDS, VISTA VIKING and Hyper SuprimeCam surveys. The G23 region was specifically motivated for future Australian SKA Pathfinder (ASKAP) DINGO observations free from any known bright continuum sources. Crucially, G23 enables unique science that is not possible in the other GAMA regions, as interferometric radio facilities, such as ASKAP, produce a dramatically larger, noisier beam-width at the equator due to the lack of rotation of the sky. To provide complementary UV star formation rates (SFRs), the entire G23 region has been covered in the final six months of GALEX operations to 3000 s depth (double that of the GAMA equatorial fields). G23 combined with

Figure 2. Upper: VST ATLAS *ugr* selection of candidate quasars with UV flux at lower wavelengths than the H I Lyman limit where He II 304 Å Lyman alpha absorption may be detected. Lower: The spectrum of the above candidate for helium reionisation studies.

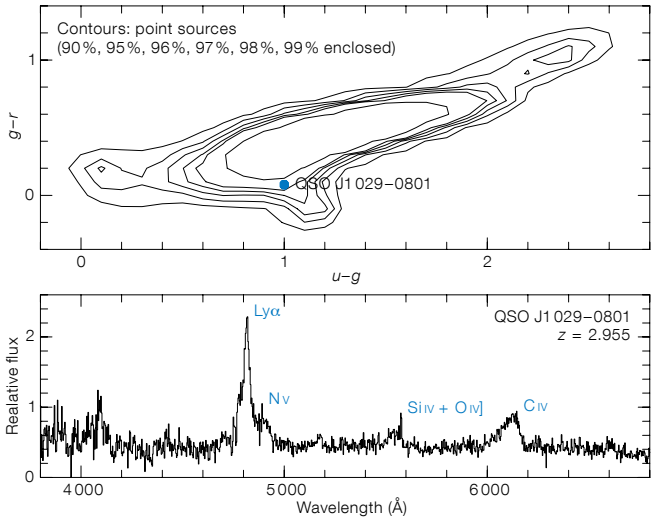

Figure 3. The spatial density variation of stellar sources in the combined *g*- and *r*-bands over part of the ATLAS survey of the southern Galactic Cap.

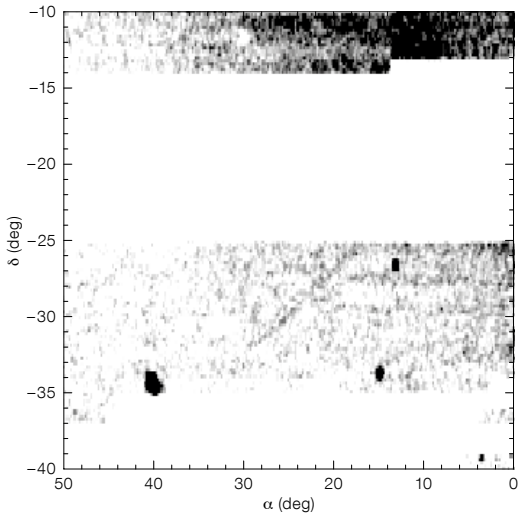

ASKAP will be capable of measuring whether the cosmic H I has remained static or declined to within a factor of two over a 4 Gyr baseline.

G23 will thereby provide a unique multi-wavelength database from the far-UV to the radio, that is not possible with the equatorial regions, for the investigation of the conversion of gas into stars as a function of redshift, stellar mass, age and metallicity. Additionally, by using a state-of-the-art group catalogue (like the one already created for the GAMA equatorial fields by Robotham et al. [2011]), a new door in extragalactic astronomy is opened on how galaxy formation processes (e.g., mass–metallicity relation, SFRs, morphologies, etc) correlate with halo mass.

Galactic archaeology with ATLAS

A simple diagnostic for the overall quality of the ATLAS photometric calibration is to examine the uniformity of stellar density maps selected from a relatively narrow colour and magnitude range. With a sensible choice of colour–magnitude loci these maps can, in addition, be used as a first pass probe of nearby Milky Way and satellite foreground populations. An example of this, cut from more extensive coverage of the south Galactic Cap available in autumn 2012, is shown in Figure 3.

In addition to the obvious density enhancements due to previously known satellites such as the Fornax and Sculptor dwarfs, toward the bottom of the map, and the globular cluster NGC 288 right of centre, are two stellar streams. The broad enhancement in stellar density from the Sagittarius dwarf southern stream is visible towards the top and a newly discovered stellar stream near the centre, pointing just south of the Fornax dwarf. This new stream can be traced quite clearly over about 10 degrees before petering out to the south and being lost to the north in a gap in coverage.

The likely nature of the stream can be inferred from its angular width and comparing on-stream *vs.* off-stream colour–magnitude diagrams; it is found to be consistent with the stream being at a distance of around 20 kpc and originating from an old metal-poor low velocity dispersion satellite. This suggests that the stream most likely comes from a disrupted globular cluster, and in the current coverage there is no sign of any obvious progenitor. When further observations for this region have been fully processed, many of the gaps in coverage should be filled and further exploration of the stream, and of other nearby stellar populations, can be made.

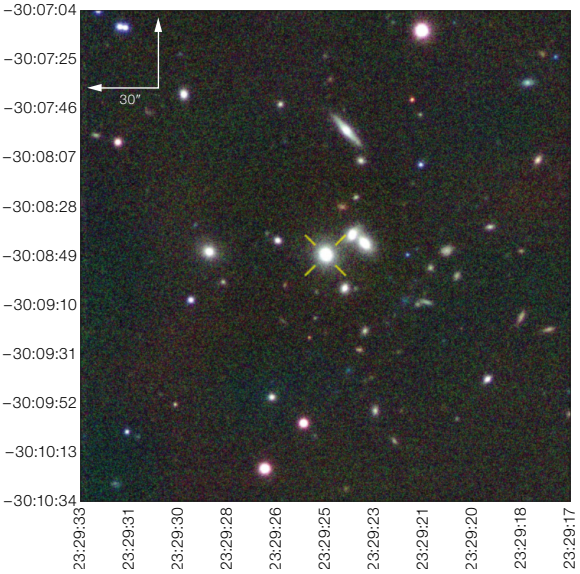

Figure 4. A *gri* composite image of a $z \sim 0.1$ galaxy group identified by ORCA in the VST ATLAS survey. The brightest group member is denoted by the yellow cross at the centre of the image.

The SAMI galaxy survey

VST ATLAS imaging has formed part of the target selection for the new survey being carried out using SAMI (the Sydney-AAO Multi-object Integral field spectrograph) on the AAT. SAMI can target 13 galaxies at once over a 1 degree diameter field of view. The target is to build a sample of 3400 galaxies, spanning a large range in both mass and environment to address key questions in galaxy formation, including: the primary physical mechanisms causing environmental suppression of star formation and morphological changes in galaxies; the frequency of inflows and outflows of gas and how they influence galaxy properties; the distribution of angular momentum in the galaxy population and how mass is built up.

SAMI is targeting galaxies in field and group environments, using the GAMA survey as input, together with clusters selected over the southern sky. VST photometry is particularly crucial for target selection in the SAMI clusters, as no other optical multi-band imaging exists over the cluster regions. The photometry, together with 2dFGRS redshifts, forms the basis for SAMI target selection, with further AAOmega redshifts being measured to give complete sampling across each cluster. The SAMI team has already observed over 100 galaxies using VST photometry for selection, and these, together with further observations, will shed light on numerous issues in galaxy formation.

Galaxy groups and clusters

Based on a pilot band-merged *gri* galaxy catalogue, a 50 square degree region of VST ATLAS has been searched for galaxy clusters. In the absence of photometric redshifts, we identify clusters via the red sequence using the over-dense red-sequence cluster algorithm (ORCA; Murphy et al. 2012). This algorithm is robust to systematic magnitude errors and does not require redshift data. The initial search yielded 93 clusters, an example of which is shown in Figure 4, but analysis suggests that some are spurious detections arising from the fragmentation of stellar haloes. Future work will reduce the level of stellar contamination in the source catalogue. Comparison against calibrated measurement of sequence normalisations in *g-r* and *r-i* from the Geach et al. (2011) ORCA cluster catalogue suggest this group has a redshift of $z \sim 0.1$. Five-band photometric redshifts will be used in the future to better determine the redshifts of VST clusters identified with ORCA.

References

Driver, S. P. et al. 2011, MNRAS, 413, 971
Geach, J. E., Murphy, D. N. A. & Bower, R. G. 2011, MNRAS, 413, 3059
Murphy, D. N. A., Geach, J. E. & Bower, R. G. 2012, MNRAS, 420, 1861
Robotham, A. S. G. et al. 2011, MNRAS, 416, 2640
Sawangwit, U. et al. 2010, MNRAS, 402, 2228
Worseck, G. & Prochaska, J. X. 2011, ApJ, 728, 23
Worseck, G. et al. 2011, ApJ, 733, L24

Links

[1] VST ATLAS status: http://astro.dur.ac.uk/Cosmology/vstatlas/
[2] OmegaCam Science Archive: http://surveys.roe.ac.uk/osa/

VST Photometric Hα Survey of the Southern Galactic Plane and Bulge (VPHAS+)

Janet E. Drew[1]
Geert Barentsen[1]
Juan Fabregat[2]
Hywel Farnhill[1]
Michael Mohr-Smith[1]
Nicholas J. Wright[1]
Eduardo Gonzalez-Solares[3]
Michael J. Irwin[3]
Jim Lewis[3]
Aykube K. Yoldas[3]
Robert Greimel[4]
Jochen Eislöffel[5]
Paul Groot[6]
Michael J. Barlow[7]
Romano Corradi[8]
Boris T. Gänsicke[9]
Christian Knigge[10]
Antonio Mampaso[8]
Rhys Morris[11]
Tim Naylor[12]
Quentin A. Parker[13]
Roberto Raddi[9]
Stuart E. Sale[14]
Danny Steeghs[9]
Yvonne C. Unruh[15]
Jorick S. Vink[16]
Jeremy R. Walsh[17]
Nicholas A. Walton[3]
Roger Wesson[17]
Albert Zijlstra[18]

[1] School of Physics, Astronomy & Mathematics, University of Hertfordshire, Hatfield, United Kingdom
[2] Observatorio Astronómico, Universidad de Valencia, Paterna, Spain
[3] Institute of Astronomy, Cambridge University, United Kingdom
[4] IGAM, Institute of Physics, University of Graz, Austria
[5] Thüringer Landessternwarte, Tautenburg, Germany
[6] Afdeling Sterrenkunde, Radboud Universiteit Nijmegen, the Netherlands
[7] Department of Physics & Astronomy, University College London, United Kingdom
[8] Instituto de Astrofisica de Canarias, La Laguna, Tenerife, Spain
[9] Department of Physics, University of Warwick, Coventry, United Kingdom
[10] School of Physics & Astronomy, University of Southampton, United Kingdom
[11] School of Physics, Bristol University, United Kingdom
[12] Department of Physics, University of Exeter, United Kingdom
[13] Department of Physics, Macquarie University, NSW 2109, Australia
[14] Rudolf Peierls Centre for Theoretical Physics, Oxford University, United Kingdom
[15] Department of Physics, Blackett Laboratory, Imperial College London, United Kingdom
[16] Armagh Observatory, College Hill, Northern Ireland, United Kingdom
[17] ESO
[18] Jodrell Bank Centre for Astrophysics, School of Physics & Astronomy, University of Manchester, United Kingdom

The VST Photometric Hα survey of the Southern Galactic Plane and Bulge (VPHAS+) is collecting single-epoch Sloan *u*, *g*, *r*, *i* and Hα narrowband photometry, at arcsecond resolution, down to point-source (Vega) magnitudes of ~ 21. The survey footprint encloses the entire southern Galactic Plane within the Galactic latitude range $-5° < b < +5°$, expanding to $b = \pm 10°$ in the Galactic Bulge. This brief description of VPHAS+ includes sample data and examples of early science validation.

Overview

VPHAS+ is the southern counterpart to two existing northern hemisphere surveys: the Isaac Newton Telescope Photometric Hα Survey of the Northern Galactic Plane (IPHAS), which covers the Northern Plane from La Palma in *r*, *i* and Hα (Drew et al., 2005; Barentsen et al. in preparation) and the UV-excess survey of the Northern Galactic Plane (UVEX), which does the same in *u*, *g*, and *r* (Groot et al., 2009). The combination of these three surveys will ultimately provide a 360 × 10 square-degree view of the entire Galactic Plane at roughly one arcsecond spatial resolution. This will result in a photometric catalogue containing approximately half a billion stars — two thirds of which will be captured by VPHAS+, surveying the denser southern Plane and Bulge.

The original motivation for IPHAS was to provide the digital update to photographic Hα surveys of the mid-twentieth century. In the south, VPHAS+ is the digital successor to the UK Schmidt Hα survey (Parker et al., 2005). However, the legacy of VPHAS+ will extend beyond the traditional Hα applications of identifying emission line stars and nebulae. For example, the survey's unique (*r*–Hα) colour, when combined with broadband colours, offers a rough extinction-free proxy for intrinsic stellar colour. This opens the door to a wide range of Galactic science applications, including the mapping of extinction across the Plane in three dimensions (e.g., Sale et al., 2009). VPHAS+ is also efficient in identifying OBA stars on the basis of their blue colours, and it enables comparative studies of clusters using homogeneous data. The final photometric catalogue is likely to achieve an externally validated accuracy of 0.02 to 0.03 magnitudes. The first data release is already available from the ESO archive[1] as images and single-band catalogues, calibrated against nightly standard-star data.

The original survey plan drawn up in 2006 envisaged contemporaneous five-band photometry per survey field, providing optical snapshots of stellar spectral energy distributions. During the commissioning of VST and the camera, OmegaCAM, it became evident that working to this ideal would not permit VPHAS+ to proceed in a timely manner. Hence it was agreed to adopt a more flexible strategy of splitting the data-taking into blue (*u*,*g*,*r*) and red (Hα,*r*,*i*) filter sets that can be combined, post-observation, using the repeated *r*-band exposures as aids to calibration and checks on variability. As a result, VPHAS+ follows an observing strategy that echoes the northern

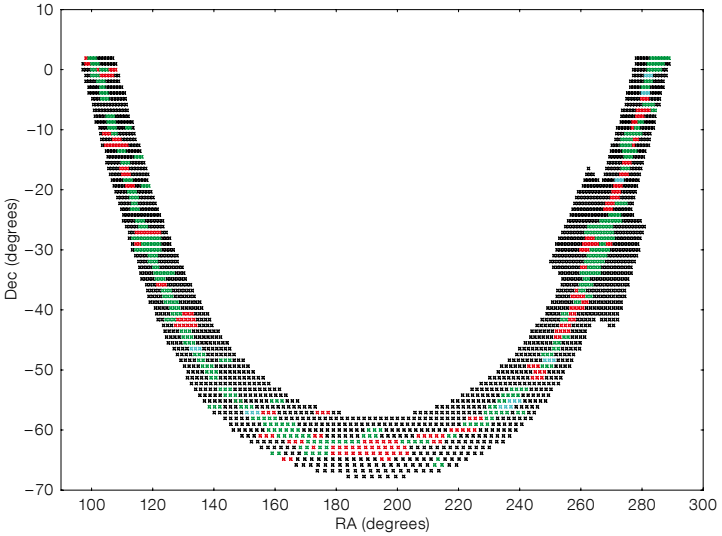

Figure 1. A map of the VPHAS+ survey footprint showing status on 30 September 2013. 2269 fields make up the survey: those shown in black had not yet been observed, while those in green have already been completed. Red is used for fields observed only in the Hα, *r*- and *i*-bands, while blue is used for those only observed in the *u*-, *g*- and *r*-bands.

Filter	Total exposure time: No. of exposures × exposure (s)	5σ (Vega) magnitude limit per exposure
u	2 × 150	21.5
g	3 × 30 or 40	22.5
r	2 × 25	21.6
Hα	3 × 120	20.8
i	2 × 25	20.8

Table 1. VPHAS+ exposures per field and sensitivity. (The shorter *g* exposure time applies to data first obtained prior to 19 February 2013.)

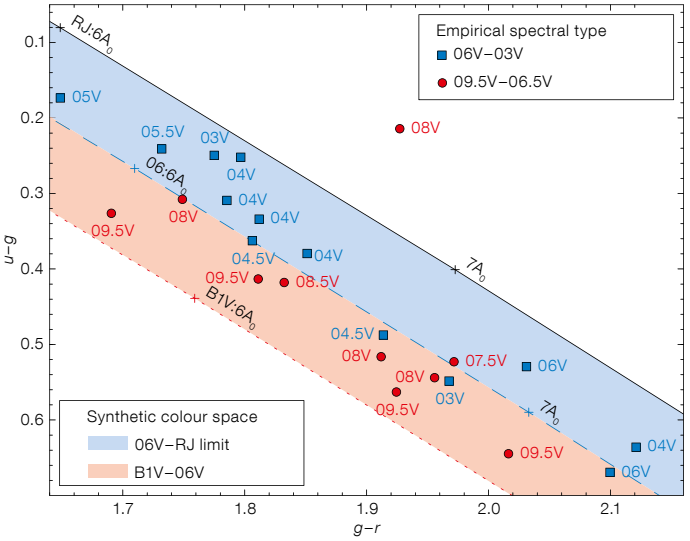

Figure 2. The VPHAS+ (*u*–*g*) *vs.* (*g*–*r*) colour–colour diagram is shown for known O stars in and close to Westerlund 2.

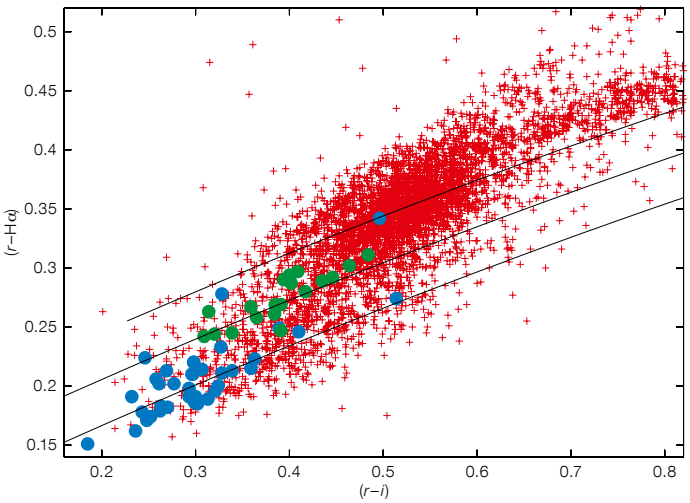

Figure 3. The (*r*–Hα) *vs.* (*r*–*i*) photometric diagram from VPHAS+ field 33 (centred on RA 06 44 16.7, Dec –00 58 04, J2000). Red points represent all stars in the field with magnitude $r < 16.5$. Blue and green points represent stars with spectroscopically determined spectral types in the range A0–3V and F0–1V respectively. The solid lines are, from bottom to top, the model reddening lines corresponding to A2V, F0V and F5V respectively.

hemisphere IPHAS and UVEX survey pair. It remains the case that each filter set delivers a robust contemporaneous colour–colour diagram, straight from the pipeline. At the beginning of October 2013, complete data had been obtained for 404 fields, out of 2269. The blue filters are progressing more slowly than the red because they require darker observing conditions. A map of the survey pointings, picking out those already executed to survey standard, is presented in Figure 1.

The quality of data delivered by OmegaCAM is, in most respects, excellent. We have set the target maximum seeing at 1.2 arcseconds for all except the densest fields, where it is 0.9 or 1.0 arcseconds. The outcome is that the median seeing in all filters, except *u*, is around 0.8 arcseconds. In *u*, the most challenging filter, the median is 0.95 arcseconds. At the same time, image quality across the full square degree of field has also been very good. Bright Moon is avoided for VPHAS+ data-taking because experience with IPHAS has taught us that the mix of diffuse Hα background and bright moonlight can become impossible to separate. Given that the southern Galactic Plane is threaded by even more Hα nebulosity than the north, this is an important precaution. There is room for improvement with respect to scattered light: presently this is significant and variable — to the extent that it has posed a challenge to the photometric calibration. We look forward to the installation of the planned baffles on the VST that should cut this scattered light down substantially.

The Hα filter procured for the VST by the VPHAS+ consortium is named NB-659 and is segmented: four 13.6 × 13.6 square-centimetre pieces of coated glass are held in place in the mount by a pair of blackened T-bars. This creates some extra vignetting — a factor that has been taken to account in our offsetting strategy. The filter's full width at half maximum (FWHM) transmission is close to 10 nm and the transmission at peak is ~ 95 percent, making the filter 20% more sensitive than its IPHAS/La Palma counterpart. Median magnitude limits achieved in all five bands are set out in Table 1. All VPHAS+ data are processed by the Cambridge Astronomical Survey Unit (CASU), via a pipeline similar to the VISTA Data Flow System that presently delivers flux-calibrated images and aperture photometry. The main features of VPHAS+ will be presented in a forthcoming paper (Drew et al., in preparation).

VPHAS+ science validation

A well-established technique for identifying O- and early B-type stars is to pick them out above the main stellar locus in the Johnson (*U*–*B*) *vs.* (*B*–*V*) diagram. The same is possible using Sloan (*u*–*g*) vs. (*g*–*r*) and we provide an example that shows that VPHAS+ is ready for the same kind of exploitation — one of the survey aims: Figure 2 shows how known and typed O stars lying within and close to the massive cluster Westerlund 2 fall in this colour–colour plane. The plotted stars range in *g* magnitude from 14 down to 18. It can be seen clearly that there is good, if not perfect, separation between the later- and earlier-type O stars, with one prominent failure — an O8V star that has escaped to above the theoretical Rayleigh–Jeans limit (only because it is in a close blend right at the heart of this very dense bright cluster — others have deblended more successfully). A more profound validation has come from comparing our data on these stars with the results of Vargas Alvarez et al. (2013) from Hubble Space Telescope (HST) data. We conclude, as they do, that the reddening law must be characterised by $R = 3.8$, and find that the mean difference in visual extinction is only 0.13 mag (Mohr-Smith et al., in preparation).

Figure 4. A 12.3 × 7.1 arcminute cut-out image from M8, the Lagoon Nebula, centred on RA 18 09 36, Dec -24 01 51 (J2000), in which *r*, *i* and Hα data are combined. Below left, a 2.5 × 2.5 arcminute zoom into some of the detail. Below right, the same detail as imaged in the *R*-band by the UKIRT Schmidt survey.

The VPHAS+ (*r*–Hα) vs. (*r* –*i*) photometric diagram can be used in a more general way to select samples of stars of different spectral types, capitalising on the sensitivity of (*r*–Hα) to intrinsic stellar colour. Figure 3 illustrates how this can be done: the colour–colour diagram for brighter stars in VPHAS+ field No. 33, centred on RA 06 44 16.7, Dec –00 58 04 (J2000) is plotted. This is a part of the sky that the CoRoT satellite has observed twice and that has also been followed up spectroscopically (Guenther et al., 2012; Sebastian et al., 2012). The blue and green points plotted in the diagram correspond to stars with MK spectral types and luminosities obtained from the spectroscopy, in the A0–3V and F0–1V ranges respectively. Their positions are compared with model reddening lines, including the A2V line which lies along the bottom of the main stellar locus (A2V stars have the strongest Hα absorption of all non-degenerate stars). From this figure it is apparent that most of the early A main sequence stars are confined to a strip ~ 0.05 mag wide, with observational error taking them across the A2V reddening line, while the F0–1V stars are mostly well-separated and cluster around the F0V line.

Nebulae and diffuse interstellar medium emission

In terms of the integrated light received, the imaging capability of VPHAS+ is not greatly different to that of the UK Schmidt Hα Survey (SHS; Parker et al., 2005). Because of the effort that was made using the SHS to search for well-resolved planetary nebulae, it is unlikely that VPHAS+ will find many more. But there is discovery space in the domain of compact nebulae — which are either very young or very far away — that other ground-based surveys have failed to resolve.

The outstanding advantage of VPHAS+ relative to SHS is the sub-arcsecond seeing commonly encountered at Paranal. Figure 4, showing a portion of M8 (the Lagoon Nebula), provides an example of the refinement of detail relative to the SHS that is apparent even in imagery combining exposures in three different filters. Ionisation fronts, dust lanes and other dynamically revealing structures at the arcsecond scale are now much more readily accessed from the ground.

Synergies with other surveys now and in the future

The VPHAS+ footprint encloses the entire Variables in the *Via Lactea* (VVV) footprint and hence will provide complementary optical coverage to this near-infrared (NIR) survey of the Galactic Bulge and inner disc. The same synergy exists with respect to the other NIR photometric surveys — the Two Micron All Sky Survey (2MASS) and the UKIRT InfraRed Deep Sky Surveys: Galactic Plane Survey (UKIDSS/GPS). On combining VST optical magnitudes with 2MASS magnitudes, particularly for early-type stars, we are already finding that we can obtain good constraints on sight-line reddening laws — such data can play a critical role in three-dimensional extinction mapping of the Milky Way (c.f., the work of Sale, 2012 and Berry et al., 2012). VPHAS+, along with IPHAS and UVEX in the north, already have achieved full optical coverage of the Spitzer and Herschel legacy surveys of the Galactic mid-plane.

The beginning of VPHAS+ data collection closely coincided with the beginning of the Gaia–ESO spectroscopic survey (GES), described by Randich et al. (p. 47). GES needs high-quality photometry of the type VPHAS+ can supply, as input to its target selections programme. There have already been transfers of photometric catalogues, particularly to support open-cluster observations. A major design effort is currently underway in connection with plans to build the next generation of massively-multiplexed spectrographs for Europe's astronomy community — notably 4MOST and MOONS. Homogeneous, astrophysically informative optical photometry will continue to be needed to feed targets to these advanced instruments. VPHAS+, as it transforms into a complete five-band survey catalogue, will be there to meet this need for Galactic Plane and Bulge science.

References

Berry, M. et al. 2012, ApJ, 757, 166
Drew, J. E. et al. 2005, MNRAS, 362, 753
Groot, P. J. et al. 2009, MNRAS, 400, 1413
Guenther, E. W. et al. 2012, A&A, 543, A125
Parker, Q. A. et al. 2005, MNRAS, 362, 689
Sale, S. E. et al. 2009, MNRAS, 392, 497
Sale, S. E. 2012, MNRAS, 427, 2119
Sebastian, D. et al. 2012, A&A, 541, A34
Vargas Alvarez, C. A. et al. 2013, AJ, 145, 125

Links

[1] VPHAS+ first data release: http://archive.eso.org/cms/eso-archive-news/first-data-release-of-vst-public-survey-vphas--imaging-data.html

The Kilo-Degree Survey

Jelte T. A. de Jong[1]
Konrad Kuijken[1]
Douglas Applegate[2]
Kor Begeman[3]
Andrey Belikov[3]
Chris Blake[4]
Jeffrey Bout[3]
Danny Boxhoorn[3]
Hugo Buddelmeijer[3]
Axel Buddendiek[2]
Marcello Cacciato[1]
Massimo Capaccioli[5]
Ami Choi[6]
Oliver-Mark Cordes[2]
Giovanni Covone[5]
Massimo Dall'Ora[7]
Alastair Edge[8]
Thomas Erben[2]
Jeroen Franse[1]
Fedor Getman[7]
Aniello Grado[7]
Joachim Harnois-Deraps[9]
Ewout Helmich[1]
Ricardo Herbonnet[1]
Catherine Heymans[6]
Hendrik Hildebrandt[2]
Henk Hoekstra[1]
Zhuoyi Huang[7]
Nancy Irisarri[1]
Benjamin Joachimi[10]
Fabian Köhlinger[1]
Thomas Kitching[11]
Francesco La Barbera[7]
Pedro Lacerda[12]
John McFarland[3]
Lance Miller[13]
Reiko Nakajima[2]
Nicola R. Napolitano[7]
Maurizio Paolillo[5]
John Peacock[6]
Berenice Pila-Diez[1]
Emanuella Puddu[7]
Mario Radovich[14]
Agatino Rifatto[7]
Peter Schneider[2]
Tim Schrabback[2]
Cristobal Sifon[1]
Gert Sikkema[3]
Patrick Simon[2]
William Sutherland[15]
Alexandru Tudorica[2]
Edwin Valentijn[3]
Remco van der Burg[1]
Edo van Uitert[2]
Ludovic van Waerbeke[9]
Malin Velander[13]
Gijs Verdoes Kleijn[3]
Massimo Viola[1]
Willem-Jan Vriend[3]

[1] Leiden Observatory, Leiden University, the Netherlands
[2] Argelander Institute for Astronomy, University of Bonn, Germany
[3] OmegaCEN – University of Groningen, the Netherlands
[4] Centre for Astrophysics & Supercomputing, Swinburne University, Hawthorn, Australia
[5] Dept. of Physical Sciences, University Federico II, Naples, Italy
[6] SUPA, Institute for Astronomy, University of Edinburgh, United Kingdom
[7] INAF – Osservatorio Astronomico Capodimonte Napoli, Italy
[8] Department of Physics, Durham University, United Kingdom
[9] Department of Physics and Astronomy, University of British Columbia, Vancouver, Canada
[10] Department of Physics and Astronomy, University College London, United Kingdom
[11] Mullard Space Science Laboratory, Holmbury St Mary, Dorking, United Kingdom
[12] Queen's University Belfast, United Kingdom
[13] Department of Physics, University of Oxford, United Kingdom
[14] INAF – Osservatorio Astronomico di Padova, Italy
[15] Astronomy Unit, School of Physics and Astronomy, Queen Mary University of London, United Kingdom

The Kilo-Degree Survey (KiDS), a 1500-square-degree optical imaging survey with the recently commissioned OmegaCAM wide-field imager on the VLT Survey Telescope (VST), is described. KiDS will image two fields in *u*-,*g*-,*r*- and *i*-bands and, together with the VIKING survey, produce nine-band (*u*- to *K*-band) coverage over two fields. For the foreseeable future the KiDS/VIKING combination of superb image quality with wide wavelength coverage will be unique for surveys of its size and depth. The survey has been designed to tackle some of the most fundamental questions of cosmology and galaxy formation of today. The main science driver is mapping the dark matter distribution in the Universe and putting constraints on the expansion of the Universe and the equation of state of dark energy, all through weak gravitational lensing. However, the deep and wide imaging data will facilitate a wide variety of science cases.

Survey design

KiDS is part of a long heritage of ever improving wide-field optical sky surveys, starting with the historical photographic plate surveys. The KiDS survey targets two areas of extragalactic sky, some 750 square degrees each, to ensure that observations can be done all year. While KiDS observes in four filters (*u,g,r,i*), the companion VIKING project on the neighbouring Visible and Infrared Survey Telescope for Astronomy (VISTA) is already covering the same area in five near-infrared bands: *z*, *Y*, *J*, *H* and *Ks*. The two fields (Figure 1) are chosen to overlap with previous and ongoing galaxy redshift surveys, which means that the foreground galaxy distribution is already mapped out, and that spectral diagnostics for several 100 000 galaxies are already available. One of the central aims of KiDS is to "weigh" these galaxies systematically as function of their type and environment.

The exposure times of KiDS (see Table 1) are chosen such that the survey will reach a median galaxy redshift of 0.7. They are also well-matched to the natural exposure times for efficient VST operations, and balanced over the astro-climate conditions on Paranal (seeing and Moon phase, see Table 1) so that all bands can be observed at the same average rate. This strategy takes advantage of the Paranal queue-scheduling system, which makes it possible to use the best seeing time for deep *r*-band exposures, for example, and the worst seeing for *u*-band. After completion of the survey, repeat observations of the full area in the *g* filter with a minimum time difference of two years are planned, allowing proper motion measurements.

Half of the KiDS area overlaps with the Sloan Digital Sky Survey (SDSS; Abazajian et al., 2009), and, since very similar filter bands are used, the KiDS photometric calibration can be checked thoroughly. All VST observations are observed in the context of a nightly calibration plan that relies on a number of large standard star fields established as part of the OmegaCAM instrument development (Verdoes Kleijn et al., 2013). As the survey grows and information from overlapping pointings is incorporated, the overall photometric accuracy will continue to improve.

Filter	Exposure time	FWHM	Moon phase
u	900 s	< 1.1″	< 0.4
g	900 s	< 0.9″	< 0.4
r	1800 s	< 0.8″	< 0.4
i	1080 s	< 1.1″	any

Table 1. KiDS exposure times, maximum point spread function size (full width at half maximum [FWHM]) and Moon phase per filter.

Science drivers

The central science case for KiDS is mapping the matter distribution in the Universe through weak gravitational lensing and photometric

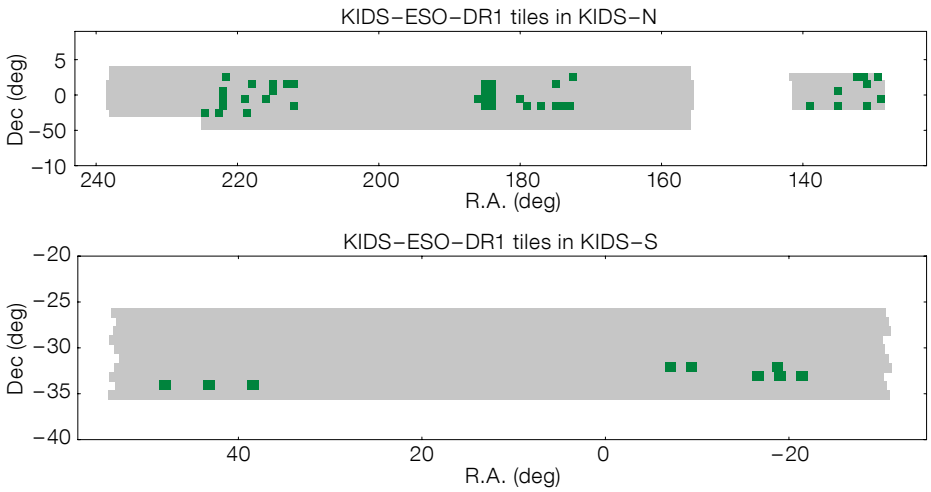

Figure 1. Layout of the two KiDS fields. The KiDS-North (upper) and KiDS-South (lower) fields are indicated in grey. Green rectangles show the pointings that are included in the first KiDS data release (KiDS-ESO-DR1).

redshift measurements. The power of using weak gravitational lensing as a cosmological probe relies on two facts: it is a very geometric phenomenon; and, it is sensitive to mass inhomogeneities along the line of sight (see e.g., Peacock et al., 2006). This makes gravitational lensing both a good probe of the growth of structure with time (redshift), as well as a purely geometrical distance measure. Both the distance–redshift relation and the rate of growth of overdensities with cosmic time depend directly on the expansion history of the Universe, and thus form the most fundamental measures of the energy content of the Universe. Weak lensing is an excellent method for making such a measurement, although the requirements on the systematics of shape measurements and photometric redshifts are challenging.

With the combination of KiDS and VIKING we have put ourselves in the optimal position to attempt this, by ensuring the best image quality in our instrument, and having a wide wavelength coverage that maximises the accuracy of the photometric redshifts. An independent measurement of the expansion history of the Universe can be made using baryon acoustic oscillations (BAO), utilising the high-precision photometric redshift measurements that will be provided by KiDS and VIKING.

However, the KiDS dataset will have many more possible applications, and the main science interests pursued by the KiDS team are briefly discussed below. Note that the primary gravitational lensing science case sets tight requirements on the astrometric and photometric calibration of the data, which is of direct benefit to other analyses as well.

Numerical simulations provide a detailed picture of the assembly and structure of dark matter haloes at large scales. At smaller scales complex baryonic physics starts to play an important role, and this is not represented realistically in current models (e.g., van Daalen et al., 2011). The relation between dark matter and baryons is crucial to our understanding of galaxy formation and evolution. Galaxy–galaxy lensing (GGL) can provide observational constraints on the relation between mass and light at scales ranging from 10 kpc to several Mpc. Since the gravitational lensing effect from single galaxies is very weak, it can only be detected statistically, by averaging over large numbers of galaxies. The size of KiDS will afford an enormous sample of galaxies, allowing the GGL effect to be studied as function of galaxy type and redshift.

Several ramifications of the current cosmological paradigm for the formation and evolution of galaxies have, until now, eluded rigorous observational testing. For example, the influence of galaxy mergers is poorly determined, and the number of known galaxy clusters at $z > 1$ is too small to constrain the models. Also here, KiDS can make an important contribution. The survey is expected to yield 10^8 galaxies with a median redshift of 0.7, and 1–2 × 10^4 galaxy clusters, 5 % of which are at redshifts greater than 1. Since KiDS also overlaps with two nearby superclusters (Pisces–Cetus and Fornax–Eridanus), the relation between galaxy properties and environment can be studied from cluster cores to the cosmic web.

To study the stellar halo of the Milky Way, photometry of faint stars over large areas of sky is required. The SDSS proved to be a milestone in Milky Way science, unveiling many previously unknown stellar streams and faint dwarf spheroidal galaxies (e.g., Belokurov et al., 2006). Although it has a smaller footprint than SDSS, KiDS is more sensitive and will provide a view of more distant parts of the halo. Because the KiDS-S area is still uncharted at the KiDS depth, new substructures may still be uncovered.

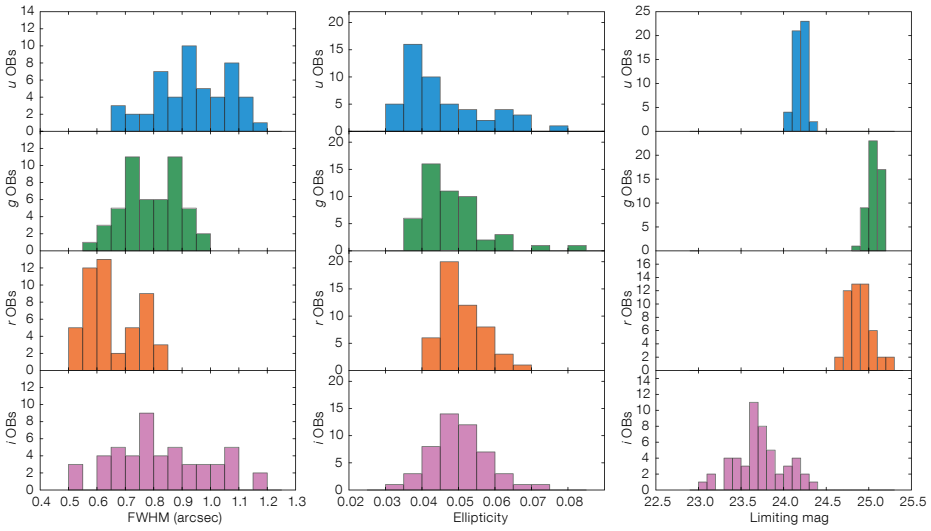

Figure 2. Histograms showing the data quality of KiDS-ESO-DR1. Left: PSF FWHM distribution. Middle: average ellipticity distribution. Right: limiting magnitude (5σ in a 2-arcsecond aperture) distribution. In all columns the panels show from top to bottom *u* (blue), *g* (green), *r* (red), and *i* (magenta) bands respectively.

Finally, the deep, multicolour object catalogues that KiDS will produce are also ideal hunting grounds for rare objects. In particular, the combination with VIKING data is ideal for detecting high-redshift quasars (see Mieske et al. p.12 and Venemans et al., 2013), while the good optical image quality benefits the search for strongly lensed systems. When the planned repeat-pass in *g*-band is completed, the proper motion information will allow the identification of nearby objects, for example brown dwarfs or ultra-cool white dwarfs.

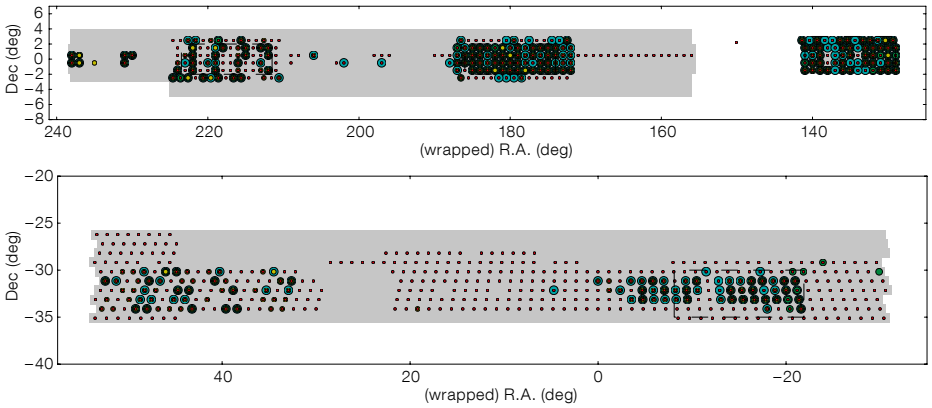

Figure 3. Status of KiDS observations at 1 October 2013. The grey areas correspond to the survey fields KiDS-North (upper panel) and KiDS-South (lower panel). Coloured circles indicate which data has been obtained successfully at each position in a specific filter: *u* = cyan, *g* = green, *r* = yellow, *i* = red. The GAMA spectroscopic survey fields are outlined with black dashed lines.

KiDS-ESO-DR1

The first public data release (DR) of the KiDS survey, dubbed KiDS-ESO-DR1, was made available through the ESO Science Archive in July 2013[1]. Since colour information is important for verifying the photometric accuracy of the data, each DR will only contain pointings that have been observed in all four filters. KiDS-ESO-DR1 comprises the 50 pointings that were completed during the first year of VST operations (15 October 2011 to 1 October 2012) and the preceding Early Science Time period. For these 50 square degrees, DR1 includes the following data products: i) photometrically and astrometrically calibrated stacked images; ii) their associated weight frames; iii) masking flag maps; and iv) single-band source lists. Data products can also be accessed via the KiDS consortium's Astro-WISE information system, which allows the full data lineage to be traced. Note that since the first year of observations, the data rate has increased substantially!

Figure 2 illustrates the data quality of KiDS-ESO-DR1. The image quality (IQ) distribution, expressed as the full width at half maximum of the point spread function, reflects the seeing constraints in Table 1. In *i*-band this distribution is very broad, because most of the bright time with seeing < 1.1 arcseconds is used for KiDS. Designed specifically to deliver good, constant image quality over the full one square degree field of view, the VST/OmegaCAM system generally performs very well, producing images with very low point spread function (PSF) ellipticity. The limiting magnitudes (5σ measured in a 2-arcsecond aperture) obtained are around 25th mag for *g* and *r*, while *u*-band is 0.8 mag shallower. In *i*-band the limiting magnitudes span a wide range due to the larger range in sky brightness.

All data products in KiDS-ESO-DR1 have been produced by the KiDS production team, using a pipeline based on the Astro-WISE astronomical data processing system (de Jong et al., 2013; McFarland et al., 2013). The pipeline version used for this release includes electronic crosstalk correction, satellite track removal, and illumination correction. By tying stellar photometry between the dithers and overlapping CCDs together, pointings are photometrically homogenised, resulting in photometry that is flat within typically 2 % over the full field of view. Absolute photometry is based on nightly calibration field observations. Due to the scattered on-sky distribution of the observations (see Figure 1), the photometry is not homogenised over the whole survey; this will be possible for future DRs encompassing more homogeneous sky coverage.

Automated masking software, dubbed Pulecenella (Huang et al., in prep), was developed for KiDS. This software produces "flag maps" that distinguish between different types of masked areas, such as saturated pixels, readout spikes, diffraction spikes, and reflection haloes. Certain other defects, for example reflections introduced by the open structure of the telescope, have been masked as well. Another stand-alone procedure was developed to produce single-band source lists, relying on SExtractor for source detection and extraction. The source lists provided in this release include star/galaxy separation and a large set of source parameters[2].

Current status

Apart from continuing to prepare and process the ongoing observations in preparation for DR2 next year, the KiDS team is also engaged in scientific analysis of the data. Much of this analysis is focussed on the opportunities that the synergy of KiDS with the Galaxy and Mass Assembly (GAMA; Driver et al., 2011) project offers. The fields of the GAMA survey, a dense spectroscopic survey on the Australian Astronomical Telescope (AAT), lie inside the KiDS areas, and they have been prioritised in the KiDS observations (see Figure 3, which shows the distribution of all data in hand at the time of writing). Combining the large-scale structure (as mapped by GAMA) with the detailed KiDS imaging of the galaxies is enabling an unprecedented study of the relation between galaxy structure, environment and, via lensing, the dark matter distribution.

To extract the cleanest possible lensing signal from the data, the team is also performing a dedicated, lensing-optimised, reduction of the data using the Bonn THELI pipeline (Erben et al., 2013) that was also used for the weak lensing analysis of the Canada France Hawaii Telescope (CFHT) Legacy Survey (e.g., Heymans et al., 2012). Initial indications are that the KiDS data are very well suited to this type of analysis.

References

Abazajian, K. et al. 2009, ApJS, 182, 543
Belokurov, V. et al. 2006, ApJ, 642, L137
de Jong, J. T. A. et al. 2013, ExA, 35, 25
Driver, S. P. et al. 2011, MNRAS, 413, 971
Erben, T. et al. 2013, MNRAS, 433, 2545
Heymans, C. et al. 2012, MNRAS, 427, 146
McFarland, J. P. et al. 2013, ExA, 35, 45
Peacock, J. A. et al. 2006, *ESO/ESA Working Group Report No. 3 Fundamental Cosmology*
van Daalen, M. P. et al. 2011, MNRAS, 415, 3649
Venemans, B. et al. 2013, ApJ, 779, 24
Verdoes Kleijn, G. et al. 2013, ExA, 35, 103

Links

[1] Access to KiDS ESO DR1: http://archive.eso.org/wdb/wdb/adp/phase3_main/form?phase3_collection=KiDS&release_tag=1

[2] For more details on the KiDS-ESO-DR1 pipeline see: http://kids.strw.leidenuniv.nl/DR1

The Gaia–ESO Large Public Spectroscopic Survey

Sofia Randich[1]
Gerry Gilmore[2]
on behalf of the Gaia–ESO Consortium

[1] INAF–Osservatorio Astrofisico di Arcetri, Italy
[2] Institute of Astronomy, University of Cambridge, United Kingdom

The Gaia–ESO Public Spectroscopic Survey has completed about one third of the data taking and continues to acquire high-quality spectroscopy, with both Giraffe and UVES, of representative samples of all Galactic stellar populations, including open clusters — young and old, nearby and distant, interior and exterior to the Sun — and field stars in the Galactic Halo, the thick Disc, the thin Disc and the Galactic Bulge. A large sample of stars in the Solar Neighbourhood, selected to include all possible ages and metallicities, is also being observed with UVES. This will be the first such large internally homogeneous study of the Milky Way stellar populations. Besides the intrinsic range of exciting scientific results, the Gaia–ESO Survey is also a pathfinder for future massive Gaia follow-up. Equally importantly, we are building an ESO-wide community of stellar spectroscopists, sharing, optimising, refining and cross-calibrating complementary approaches, strengths and experience. Internal Science Verification has started with several results demonstrating the huge potential of the survey and the first release of spectra to ESO has occurred.

An introductory overview of the Gaia–ESO survey was presented in *Messenger* 147 (Gilmore et al., 2012). Briefly, the survey is obtaining high-quality spectra with Giraffe at several wavelength settings, depending on the stellar type, high-resolution (HR) spectra (R ~ 20 000) of some 100 000 cluster and field stars down to V = 19, with parallel Ultraviolet and Visual Echelle Spectrograph spectra (UVES; R ~ 47 000) obtained in each field for brighter stars. Data-taking began at the end of 2011, and will continue for four years until the ESO progress review. A wealth of kinematic and abundance information, along with astrophysical parameters will be obtained for the bulk of our targets, facilitating the impressive range of science foreshadowed in our earlier article.

One of the special features of the Gaia–ESO survey is that a wider range of stellar types (from O- to M-type, from pre-main sequence to evolved stars, from very low to solar and super solar metallicity) is being observed than was attempted in previous large surveys, and that we are working at very much higher spectral resolution. These aspects make it necessary and desirable that a large consortium of groups is involved, implementing many spectrum analysis methods and approaches. The consortium has grown to nearly 400 members, from nearly 100 institutes. The survey project is structured in 19 working groups, each dedicated to the different aspects. Five of these groups focus on spectrum analysis and benefit from the contribution of several analysis teams. We communicate through our web page[1], newsletters, regular meetings and telecons, and with an actively used internal wiki.

Target selection and preparation of the observations are now in a routine phase. So far our efforts have been dominated by optimising the data reduction and radial velocity pipelines, as well as by the challenge of ensuring that all the many analysis approaches are internally consistent and that we are able to combine astrophysical parameters and abundances from many groups appropriately. None of these turn out to be trivial. For the Giraffe spectra, Jim Lewis at the Cambridge Astronomy Survey Unit (CASU) has developed a new special-purpose reduction pipeline, taking the data from “as acquired” to “ready for analysis” (Gilmore et al., 2013, in preparation). For UVES spectra we have been working closely with ESO, in particular with Andrea Modigliani, to remedy the difficulties with the reduction pipeline, which has now been successfully achieved (Sacco et al., 2013, in preparation). These substantial pipeline developments will of course benefit the entire ESO community. Considerable effort has also been invested in radial velocity pipelines and quality assessment, since precise radial velocities are critical for several of the top-level science goals.

An early lesson from working with many analysis teams was the critical need to have a well-understood, common, suitable line-list for the analyses, a common set of model atmospheres and a common grid of synthetic spectra. All of these have been made available to the analysis groups and are regularly updated thanks to the efforts of dedicated teams. Another (expected) challenge was that of combining, intelligently, astrophysical parameters and elemental abundances from many pipelines and for different types of stars. This remains work in progress, but one significant (planned) advance has been a focus on observations — largely in twilight — of the Gaia benchmark stars. This list of well-studied stars, with good coverage across parameter space, has been under development as part of the Gaia mission preparation. By combining our efforts, much progress has been made both with optimising the Gaia benchmark star parameters, but also ensuring that Gaia and Gaia–ESO will be calibrated onto a consistent scale (c.f., Jofre et al., 2013).

Internal as well external calibration also depends heavily on observations of many stars in many clusters, both open and globular, where we also complement our observations with re-analysis of ESO archive spectra. We are also planning synergies with other large spectroscopic surveys globally (RAdial Velocity Experiment [RAVE]; GALactic Archaeology with HERMES [HERMES/GALAH]; Baryon Oscillation Spectroscopic Survey/ Sloan Extension for Galactic Understanding and Exploration [BOSS/SEGUE]; Apache Point Observatory Galactic Evolution Experiment [APOGEE]) to share our calibrations and lead towards a new era of consistent stellar spectroscopic parameters. A further dataset, which is ideal for calibration, and of high scientific interest in meeting some of the original Gaia–ESO scientific goals, is the use of giant stars observed by CoRoT, for which asteroseismic gravities are available.

Making all this progress has taken some time, but Gaia–ESO is now in its first internal SV phase. A few scientific early highlights are noted below. However, our progress so far in so short a time makes us confident that this combination of European space and ground data for enhanced science is a small foretaste of what is to come when Gaia is combined with the current ESO imaging and planned spectroscopic surveys, and other complementary surveys. Each of these Gaia–ESO developments noted above is a major advance. All are currently being prepared for publication.

Early Science: Clusters

The top-level scientific goals for the cluster component of Gaia–ESO include the understanding of how clusters form, evolve and dissolve into the Milky Way field, to be obtained through the investigation of: internal cluster kinematics and dynamics; the calibration of the complex physics that affect stellar evolution; and the detailed study of the properties and evolution of the Milky Way thin Disc. With this aim, a very large sample of clusters and cluster stars will be observed, covering the age–distance–metallicity–position–density parameter space. Early focus has been put both on young, nearby regions and on intermediate–old more distant clusters, in order to start addressing all the main science topics in the Science Verification phase.

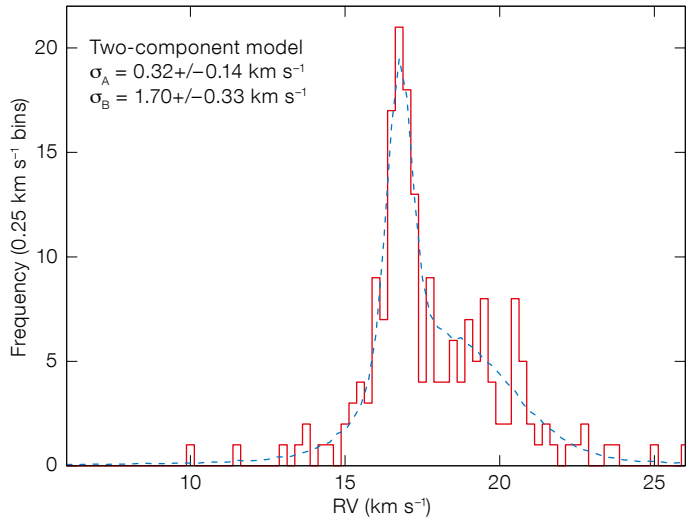

Figure 1. The radial velocity distribution of young, lithium-selected members of the γ Velorum association (red histogram), along with the best-fitting model (blue curve), consisting of two Gaussian distributions convolved with a model of the RV uncertainties and a contribution from binaries. The width of the distributions is reported in the figure.

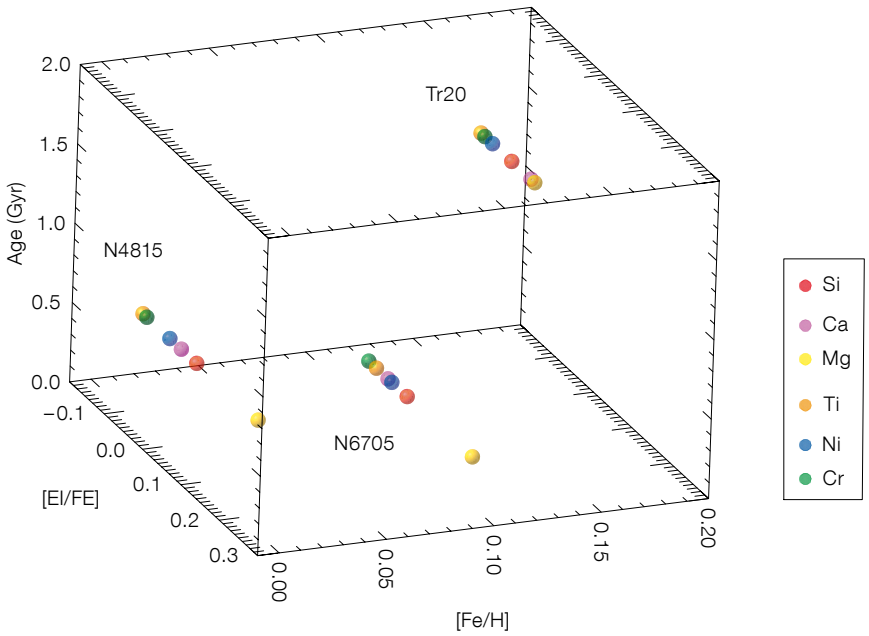

Figure 2. The three-dimensional plot shows the abundance ratios of different elements for the three open clusters NGC 6705, NGC 4815 and Trumpler 20 as a function of [Fe/H] and age. The three clusters have Galactocentric distances of 6.3, 6.9 and 6.88 kpc, respectively.

One of the currently debated issues is whether young clusters are characterised by kinematic substructures and/or radial velocity gradients. In turn this question is related to the initial conditions and the mechanism of cluster formation. Gaia–ESO observations of γ Velorum, a 5–10 Myr old, nearby association, located in the very composite Vela complex, have indeed confirmed that our radial velocity (RV) measurements have high enough precision to resolve velocity substructures (Jeffries et al., 2013, in preparation). Specifically, the RV distribution of members of the association plotted in Figure 1 shows that the excellent radial velocity precision (~ 0.3 km s^{-1}) of Gaia–ESO resolves the distribution into (at least) two sub-components, a very narrow one, probably in virial equilibrium, and a significantly broader and super-virial one. The narrower component appears to be more centrally concentrated around the massive binary star at the centre of the association. Interestingly, different tracers suggest that the low-mass stars are older than 10 Myr, while the massive binary cannot be as old as this. Whereas this result needs further investigation in the framework of different model predictions, on the one hand it implies a complex star formation history in the association and, on the other hand, it proves the potential of Gaia–ESO for this type of study.

The determination of precise abundances in open clusters represents a valuable tool for the study of the formation and evolution of the thin Disc, as clusters are rare fossils of its past star formation history. Naively, one would expect that abundances of open clusters with similar ages and positions in the Galaxy are similar, and also match those of the field stars at similar distances from the Galactic Centre. However, observations are revealing differences (see, e.g., Yong et al., 2005, 2012; De Silva et al., 2007) and these differences, if confirmed, may contain important information about, e.g., the place where the clusters were born, the homogeneity of the Disc at any Galactocentric distance at the epoch when the cluster formed, etc. In this context Gaia–ESO will allow, for the first time, a comparison of different populations based on homogeneous analysis. The first three intermediate-age/old clusters observed in the survey (NGC 6705, NGC 4815, Trumpler 20) have already enabled an initial step in this direction. Figure 2 shows that each cluster is characterised by unique features with respect to the others. These differences must be signatures of the intrinsic characteristics of the chemical composition of the interstellar medium from which each cluster was born, even if at present the three clusters are located at similar distance from the Galactic Centre. Comparison with the field population, in particular with the inner Disc stars, and with models of Galactic evolution seems to support the hypothesis that at least one of these clusters has migrated from its original birthplace (Magrini et al., 2013).

Early Science: Milky Way

The Milky Way aspects of the Gaia–ESO survey include the field star populations, and special calibration efforts. Much early focus in the Milky Way fields, driven by the available sky, was on the properties of the thick Disc. Topical issues here include the issue of discreteness between the thick and thin Disc in element ratio data at a given abundance of [Fe/H]. This has implications for the history of the Milky Way, strongly supporting the formation of the thick Disc as a discrete event early in the history of the Galaxy. All recent high-quality spectroscopic studies have shown such discreteness, though this result has been challenged by some analyses of very large low-precision surveys, especially SEGUE, where the claim is that the earlier surveys were highly biased. There is also much

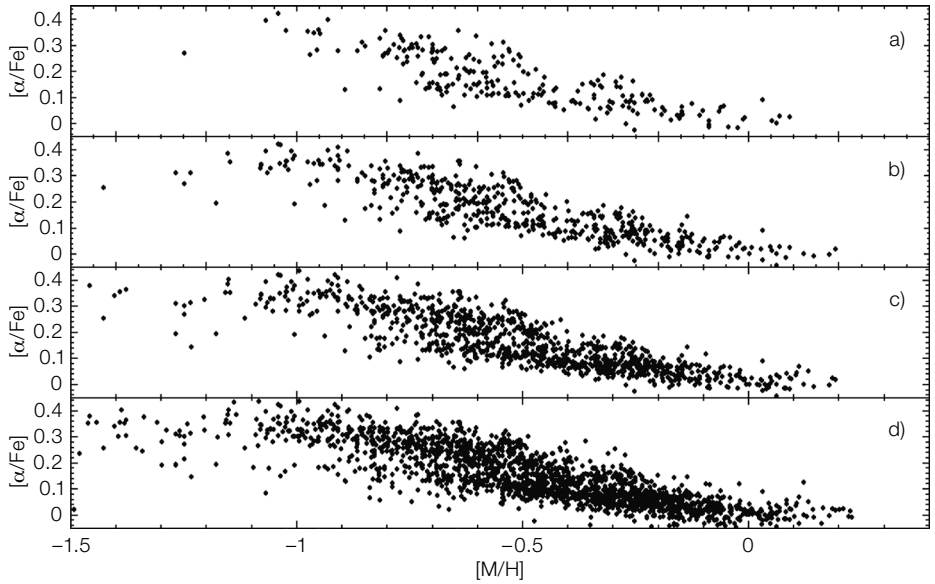

Figure 3. α-elements over iron abundance as a function of metallicity for four different sub-samples of stars with increasing errors in the abundance determination. Panel a) shows the results for stars with errors in [M/H] and [α/Fe] smaller than 0.07 dex and 0.03 dex respectively (209 stars); panel b) for errors smaller than 0.09 dex and 0.04 dex in [M/H] and [α/Fe] (505 stars); panel c) illustrates the values for 1008 stars with errors smaller than 0.15 dex and 0.05 dex respectively; panel d) shows all stars with errors in T_{eff} lower than 400 K, errors in log g lower than 0.5 dex and a spectral signal-to-noise ratio higher than 15 for the HR10 configuration (1952 stars).

ongoing confusion over the radial scale length of the thick Disc, with the answer being sensitively dependent on one's definition. Gaia–ESO has a well-defined selection function, and carefully avoids all the usual sample biases, so is ideally suited to provide a definitive result. The first Gaia–ESO results are shown in Figure 3, which shows [α/Fe] *vs.* [Fe/H] from Giraffe spectra, with the different panels selected only by measurement error. Bimodality is indeed apparent (Recio Blanco et al., 2013). A supplementary study, led by student Kohei Hattori, uses a new dynamical analysis technique to deduce the local in-plane kinematics of stars far from the Sun (Figure 4). These kinematic dispersions are directly, although non-trivially, related to population scale length. This study suggests that the high-α (thick Disc) stars do merge into a thin-Disc-like vertical scale height a few kiloparsecs exterior to the Sun.

Figure 4. Reconstructed radial profile of $\sigma_{z,0}$ (the velocity dispersion in the z-direction at the Galactic Plane) from the Gaia-ESO survey is shown (in green) for high-α (left) and low-α (right). As a reference, the curve $\sigma_{z,0}(R)$ = const. × $e^{[-R/(10\ kpc)]}$, is also shown.

Prospects

The Gaia–ESO Large Public Spectroscopic Survey has become the first large European collaboration of stellar spectroscopists, working together to identify opportunities, strengths and limitations in the way we have approached the science challenges in stellar populations, and understanding the evolution of the Galaxy and its constituents. We are learning to work as the galaxy survey community does. This opportunity to learn and respect each other, building a stronger, more expert, more efficient ESO community in a key science area, is arguably one of the most important achievements of Gaia–ESO. There are immediate community-wide quantitative benefits, in data reduction pipelines, standard stars, atomic and molecular line-lists, calibrations, and so on, which are already being realised. The impressive range of scientific papers being prepared from the available SV data will soon be public, and demonstrate the substantial scientific advances being facilitated by this ESO survey.

References

De Silva, G. M. et al. 2007, AJ, 133, 1161
Gilmore, G. et al. 2012, The Messenger, 147, 25
Jofre, P. et al. 2013, arXiv:1309.1099
Magrini, L. et al. 2013, A&A, submitted
Recio-Blanco, A. et al. 2013, A&A, submitted
Yong, D., Carney, B. W. & Teixera de Almeida, M. L. 2005, AJ, 130, 597
Yong, D., Carney, B. W. & Friel, E. D. 2012, AJ, 144, 95

Links

[1] Gaia-ESO Survey web page: www.gaia-eso.eu

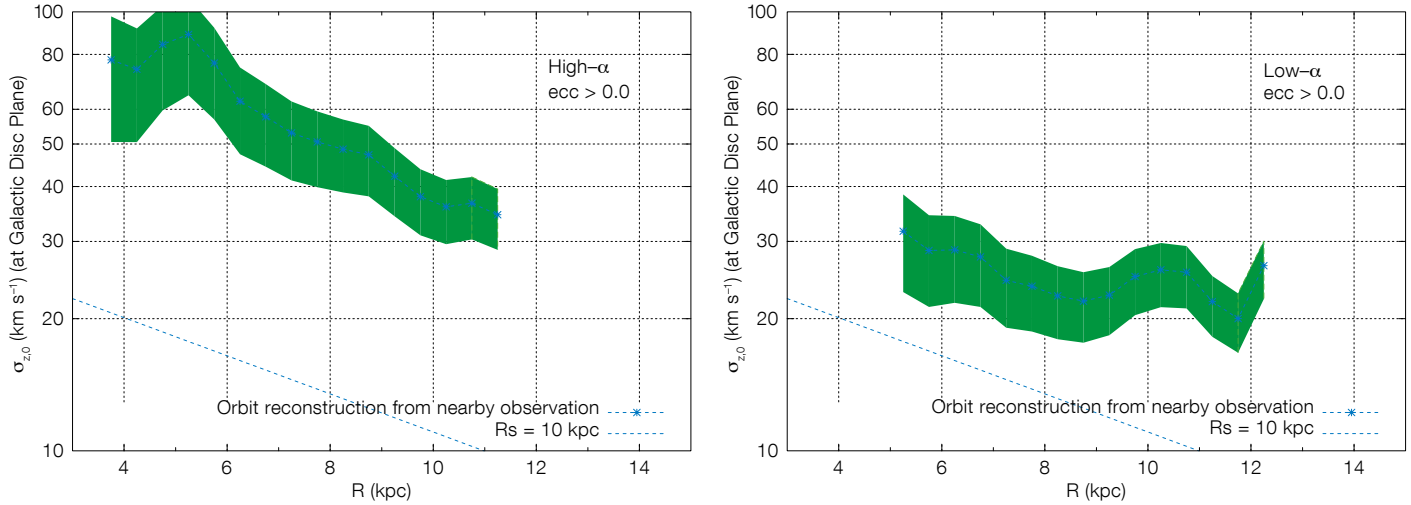

PESSTO: The Public ESO Spectroscopic Survey of Transient Objects

Stephen J. Smartt[1]
Stefano Valenti[2,3,4]
Morgan Fraser[1,5]
Cosimo Inserra[1]
David R. Young[1]
Mark Sullivan[6]
Stefano Benetti[2]
Avishay Gal-Yam[7]
Cristina Knapic[8]
Marco Molinaro[8]
Andrea Pastorello[2]
Riccardo Smareglia[8]
Ken W. Smith[1]
Stefan Taubenberger[9]
Ofer Yaron[7]

[1] Astrophysics Research Centre, School of Mathematics and Physics, Queen's University Belfast, United Kingdom
[2] Osservatorio Astronomico di Padova, INAF, Italy
[3] Las Cumbres Observatory Global Telescope Network, Goleta, USA
[4] Department of Physics, University of California Santa Barbara, USA
[5] Institute of Astronomy, University of Cambridge, United Kingdom
[6] School of Physics and Astronomy, University of Southampton, United Kingdom
[7] Benoziyo Center for Astrophysics, Weizmann Institute of Science, Rehovot, Israel
[8] INAF–Osservatorio Astronomico di Trieste, Italy
[9] Max-Planck-Institut für Astrophysik, Garching, Germany

Team members:
Joe P. Anderson[1], Christophe Balland[2], Charles Baltay[3], Cristina Barbarino[4], Franz E. Bauer[5,6,7], Sylvain Baumont[2], David Bersier[8], Sebastian Bongard[2], Maria Teresa Botticella[9], Filomena Bufano[10], Mattia Bulla[11], Enrico Cappellaro[12], Flora Cellier-Holzem[2], Ting-Wan Chen[11], Michael J. Childress[13], Alejandro Clocchiatti[5,6], Massimo Dall'Ora[9], John Danziger[14], Massimo DellaValle[9], Michel Dennefeld[15], Patrick El Hage[2], Nancy Elias-Rosa[12,16], Nancy Elman[3], Mathilde Fleury[2], Elisabeth Gall[1], Santiago Gonzalez-Gaitan[17], Laura Greggio[12], Ellie Hadjiyska[3], Wolfgang Hillebrandt[18], Simon Hodgkin[19], Isobel M. Hook[20,21], Phil A. James[8], Anders Jerkstrand[11], Erkki Kankare2[2], Rubina Kotak[11], Laurent Le Guillou[2], Giorgos Leloudas[23,24], Peter Lundqvist[23], Kate Maguire[1], Ilan Manulis[25], Steven J. Margheim[26], Seppo Mattila[22], Justyn R. Maund[11], Paolo A. Mazzali[8], Matt McCrum[11], Ryan McKinnon[3], Matt Nicholl[11], Reynald Pain[2], Joe Polshaw[11], Maria Letizia Pumo[12], David Rabinowitz[3], Emma Reilly[11], Cristina Romero-Cañizales[5,6], Richard Scalzo[13], Brian Schmidt[13], Steve Schulze5[,6], Stuart Sim[11], Jesper Sollerman[23], Giacomo Terreran1[1,12], Massimo Turatto[12], Emma Walker[3], Nicholas A. Walton[19], Fang Yuan[13], Luca Zampieri[12]

[1]ESO, [2]CNRS-IN2P3, [3]Yale Univ., [4]Sapienza Univ. Roma, [5]PUC, [6]Millennium Center for Supernova Science, [7]SSI, Boulder, [8]Liverpool John Moores Univ. [9]INAF – Obs. Capodimonte, [10]Univ. Andrés Bello, [11]Queen's Univ. Belfast, [12]INAF Obs. Padova, [13]RSAA, ANU, [14]OATS–INAF, [15]IAP, [16]ICE, Bellaterra, [17]Univ. de Chile, [18]MPA, [19]IoA, Cambridge, [20]Univ. Oxford Astrophys., [21]INAF – Obs. Roma, [22]FINCA, [23]Stockholm Univ., [24]Dark Cosmology Centre, [25]Weizmann Institute of Science, [26]Gemini

PESSTO, which began in April 2012 as one of two ESO public spectroscopic surveys, uses the EFOSC2 and SOFI instruments on the New Technology Telescope during ten nights a month for nine months of the year. Transients for PESSTO follow-up are provided by dedicated large-field 1–2-metre telescope imaging surveys. In its first year PESSTO classified 263 optical transients, publicly released the reduced spectra within 12 hours of the end of the night and identified 33 supernovae (SNe) for dedicated follow-up campaigns. Nine papers have been published or submitted on the topics of supernova progenitors, the origins of type Ia SNe, the uncertain nature of faint optical transients and superluminous supernovae, and a definitive public dataset on a most intriguing supernova, the infamous SN2009ip.

The science goal of PESSTO[1] (Smartt et al., 2013) is to extend our knowledge of unusual and rare transient events that are now challenging our understanding of the two standard explosion mechanisms which have held for several decades: core-collapse and thermonuclear. For some supernovae we are unsure whether they are thermonuclear or core collapse in origin. Supernovae in the nearby Universe ($z < 0.05$) allow critical measurements to constrain the physics, such as progenitor detections and multi-wavelength (X-ray to radio) follow-up. This offers a powerful way to probe both the explosion mechanisms and shock physics. The first important data that PESSTO takes is a classification spectrum, which gives an immediate measurement of redshift and initial supernova type. These targets are prioritised for classification if they are nearby (within about 40 Mpc, e.g., Figure 1), are discovered shortly after explosion (within a few days), are intrinsically more luminous or fainter than the bulk of the canonical supernova population, have unexplained properties (such as pre-explosion outbursts) or are fast declining supernovae. The latter are difficult to find and follow-up in detail, as all currently running optical surveys have found.

PESSTO targets and strategy

To feed PESSTO, an alliance has been made with the two major wide-field southern hemisphere surveys that have survey strategies that produce large numbers of young targets in PESSTO's sensitivity range (mag < 20.5). The La Silla QUEST survey searches for supernovae over 1000 square degrees on a 1–2 day cadence, providing PESSTO with 5–10 supernova candidates per night for classification. The rapid cadence allows for young objects to be identified for immediate follow-up and this has been the major feeder survey for PESSTO to date. The SkyMapper telescope is another powerful survey which has just started sky survey operations in earnest in September 2013 and promises a harvest of targets, and accompanying multi-colour light curves. The PESSTO science teams also scour the Catalina Sky Survey public discoveries, and, recently, the Panoramic Survey Telescope and Rapid Response System (Pan-STARRS1) survey discoveries for appropriate targets. PESSTO also welcomes early alerts from amateur supernova hunters who can inform us as quickly as possible when they find southern hemisphere and equatorial targets.

A critical component of PESSTO is communicating discovery and target details from all input surveys to ~ 120 science members, allowing them to comment, prioritise and ensure that the observers at the New Technology Telescope (NTT) get rapid and reliable information for the night's work. Speed is of the essence, as delays can lead to a scientifically critical epoch being missed. We have developed the PESSTO Marshall (based on input from Palomar Transient Factory [PTF] and Pan-STARRS1 software development) which assimilates all target information, displays interactive webpages and records comments, classifications and plans in a database. The Marshall talks to the La Silla QUEST, SkyMapper and Pan-STARRS1 databases directly, shares information and also pulls in publicly posted targets from the Catalina Sky Survey and amateur International Astronomical Union (IAU) posted targets. PESSTO developed a data reduction pipeline that allows a one command full reduction and calibration of spectra within seconds of data being taken. New classification spectra are publicly released within about 12 hours after the end of the night. These spectra are accompanied by an instant announcement to the Astronomer's Telegram, reporting target details and classifications.

The PESSTO observing team is typically made up of two observers at La Silla, and one or two people acting as a support team in Europe or Chile who take over the data release and telegram posting at the end of the Chilean night. This gives an excellent opportunity for students to be trained at the telescope in

Figure 1. The PESSTO image of SN2013ej in M74 (Valenti et al., 2013), taken with EFOSC2 on the NTT. The supernova is the bright object in the bottom left corner. This nearby SN had pre-explosion images of the galaxy, allowing a direct search for the progenitor star (ESO Picture of the Week, 2 September 2013).

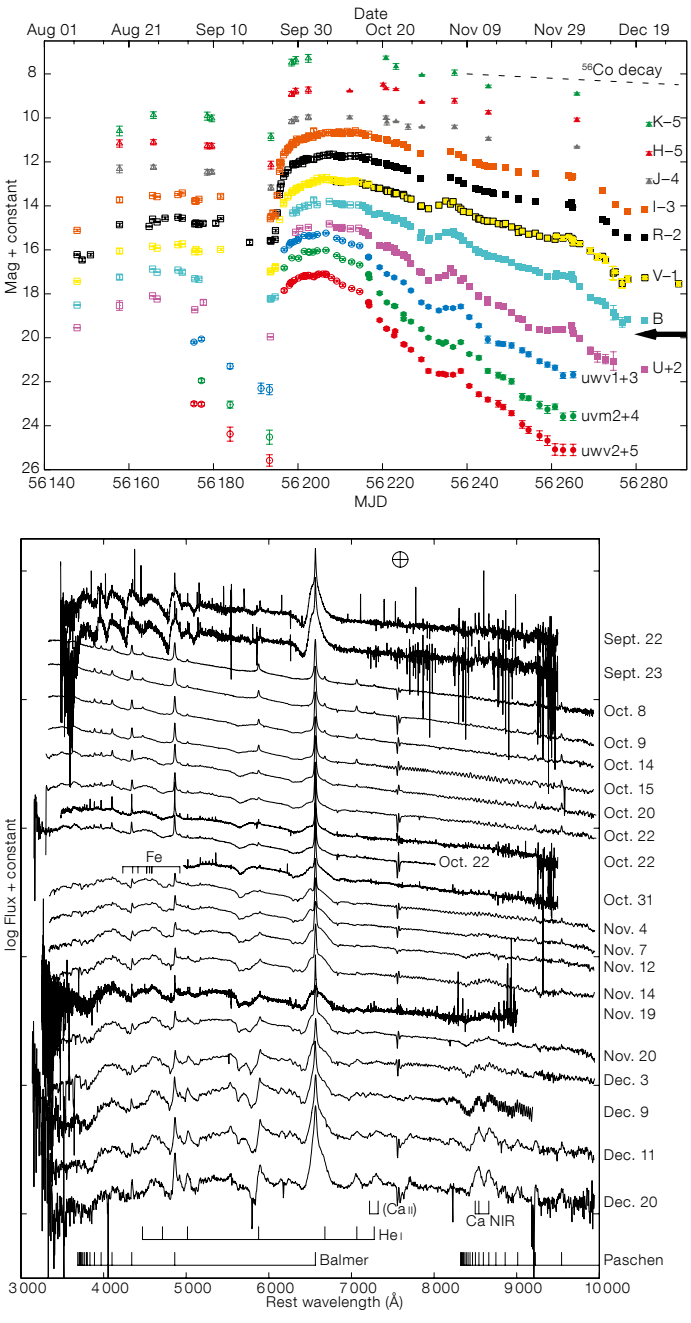

Figure 2. PESSTO light curve (upper) and spectral sequence (lower) for SN2009ip (Fraser et al., 2013), showing the initial explosion or eruption in August 2012 and rapid rise to maximum in September 2012. It is still not known if the star underwent core collapse.

making real decisions, communicating with a large science team, reducing data instantly and working out how to optimise the nights observing. PESSTO observing slots are allocated a year in advance and the younger scientists in the collaboration are keen to get this invaluable experience. PESSTO members coordinate observations with other facilities, such as the VLT, the Telescopio Nazionale Galileo (TNG), the William Herschel Telescope (WHT) and a host of 1–2-metre facilities for light-curve monitoring (e.g., Liverpool Telescope, Panchromatic Robotic Optical Monitoring and Polarimetry Telescopes [PROMPT], Small and Moderate Aperture Research Telescope System [SMARTS], Las Cumbres Observatory Global Telescope [LCOGT]).

PESSTO first-year science highlights

A successful first year of PESSTO led to the identification of 33 supernovae as scientifically interesting for detailed follow-up, and work on these is either complete or in preparation by team members. The highlight of the year was the spectacular rise in luminosity of a supernova known as SN2009ip. A transient was first discovered in 2009 in NGC 7259, which turned out to be the giant outburst of a star in the luminous blue variable stage. Although it was labelled a supernova and given the IAU name, it had not catastrophically exploded, but returned to a state of restless variability during the next three years. The star was monitored frequently (Pastorello et al., 2013) before a spectacular double peaked rise to supernova-like luminosities in August and September 2012 (Figure 2); it has been classified as a type "IIn" supernova, which means narrow hydrogen lines are visible. PESSTO monitored the outburst from the rise to peak until solar conjunction in 2013 and is now observing it during the second season (Fraser et al., 2013; Fraser et al., in prep).

This is the first time in history that a star has been monitored for years, photometrically and spectroscopically, before its explosion as a supernova. It is still not clear if the massive progenitor star has actually undergone core collapse or if the observed luminosity is powered from colliding shells which were ejected by the star in eruptive phases, such as through the pulsational pair-instability process. It is certainly a "super"-nova simply from its observed luminosity and the similarity with other type IIn explosions at larger distances. This type of instability may be quite common for these events. PESSTO produced a public optical and near-infrared dataset for SN2009ip and continues to do so with the hope that the

second season data can detect (or set limits on) the nucleosynthetic products expected if core collapse occurred.

Other PESSTO highlights include a joint VLT X-shooter project for high resolution spectra of type Ia supernovae to look for interstellar absorption signatures that could shed light on the decades long progenitor system debate (Maguire et al., 2013). The detection of an excess of blue-shifted components led Maguire et al. to suggest that this is due to mass-loss signatures in the single degenerate scenario and that there are two distinct populations of normal, cosmologically useful SNe Ia. There are a growing number of supernovae for which we are struggling to explain their physical mechanisms and in many cases it is ambiguous whether or not a core collapse or thermonuclear explosion has occurred. One example is the group of faint type I supernovae, which, by definition, have no observable hydrogen or helium, but show conflicting signs of having a massive star or white dwarf origin. PESSTO studied SN2012hn, which is a faint type I supernova that lies 6 kpc from an E/SO host (Valenti et al., 2013a). There is no sign of star formation at its location, but spectra show strong oxygen, calcium and carbon lines after 150 days which are more indicative of nucleosynthesis in core-collapse supernovae (Figure 3).

Another supernova with an ambiguous origin is SN2012ca. Studies of this object, which build on previous work, show that distinguishing between the type Ia SNe and core collapse when there is interaction with circumstellar material is not easy (Inserra et al., 2013). These events are significant for determining how many physical channels could produce the cosmologically important type Ia SNe. The new class of superluminous supernovae has caught the attention of the community as the source of the luminosity is still not understood. PESSTO classified four of these in its first year at redshifts around $z = 0.2$ and the first detailed study was submitted by Benetti et al. (2013). These supernovae cannot be powered by ^{56}Ni, which is the mechanism powering normal type Ia and Ibc SNe as they decay too fast. Two models have emerged as candidates, magnetar-powered and shock breakout from a dense and extended circumstellar shell or dense wind. Future multi-wavelength observations of the nearest events are likely to be the best way to distinguish between the models. Finally PESSTO has studied very nearby (< 20 Mpc) supernovae to determine their progenitor origins through early and frequent spectroscopic monitoring combined with archive images of the progenitor explosion site (Maund et al., 2013; Childress et al., 2013; Valenti et al., 2013b).

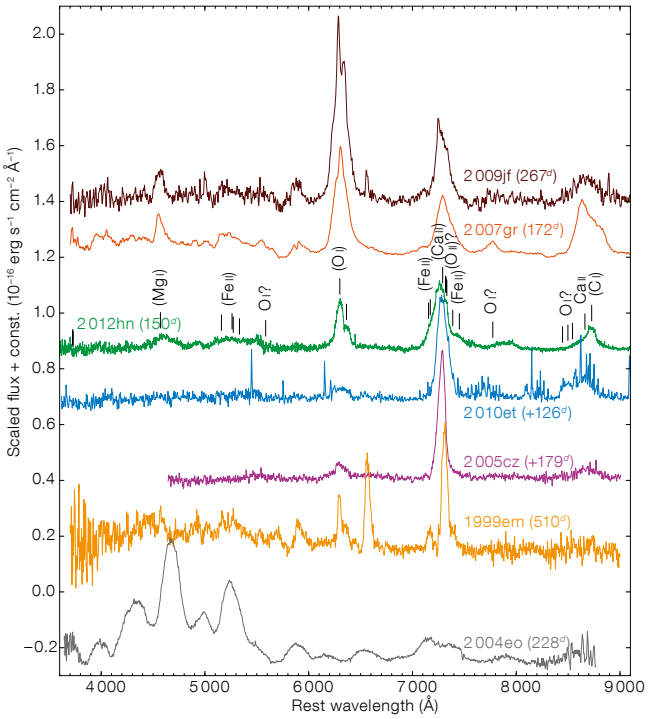

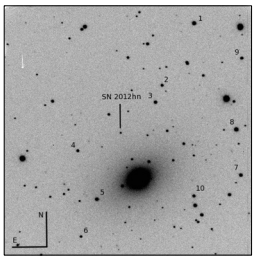

Figure 3. PESSTO image showing the position of the faint type I supernova 2012hn, at 6 kpc away from its host galaxy NGC 2272. Left: Nebular spectrum of SN2012hn (green) compared to other SNe. Prominent lines of forbidden O, Ca and Mg are visible, similar to those seen in core-collapse SNe, while the [Fe II] features typical of type Ia SNe are weak or missing; see Valenti et al. (2012a) for more details.

SSDR1 and outlook

PESSTO provides reduced classification spectra within 12–24 hours of the data being taken and releases these publicly through the Weizmann Interactive Supernova data REPository[2] (WISeREP) and an Astronomer's Telegram announcement. The final reduced data products which are now available as SSDR1 (Spectroscopic Survey Data Release 1) contain better reductions (telluric correction and fringe frame correction, more accurate flux calibration). All follow-up spectra with EFOSC2 and SOFI are available. We are also releasing all intermediate data products that may be useful to the community in the Italian Astronomical Archives (INAF IA2) in Trieste[3]. PESSTO releases 2D flux-calibrated and wavelength-calibrated frames as associated data products so that users can re-extract signal (either the transient or background galaxy) for objects with high levels of background contamination. In addition, all images taken with EFOSC2 and SOFI are reduced, astrometrically calibrated and photometrically calibrated (as far as the small fields will allow) within SSDR1.

On the technical side, the future outlook for PESSTO is to improve the absolute flux calibration of spectra (see Smartt et al., 2013) in SSDR2 and beyond. On the science side, PESSTO is trying to minimise the time between transient discoveries in the partner surveys and the first spectra being taken to look for novel signatures of the explosion mechanisms that can constrain physical models and also to probe the parameter space of rapidly varying extragalactic transients. With a large spectroscopic survey sample, statistical studies of the transient population along with host galaxy properties will be possible. With all the major ESO community supernova groups on board, PESSTO has rapidly evolved into a prodigious science survey in its first year, with great promise for its future years.

References

Benetti, S. et al. 2013, MNRAS, submitted, arXiv:1310.1311
Childress, M. J. et al. 2013, ApJ, 770, 29
Fraser, M. et al. 2013, MNRAS, 433, 1312
Inserra, C. et al. 2013, MNRAS, in press, arXiv:1307.1791
Maguire, K. et al. 2013, MNRAS, 436, 222
Maund, J. R. et al. 2013, MNRAS, 431, 102
Pastorello, A. et al. 2013, ApJ, 767, 1
Smartt, S. J. et al. 2013, A&A, in prep.
Valenti, S. et al. 2013a, MNRAS, in press, arXiv:1302.2983
Valenti, S. et al. 2013b, MNRAS, in press, arXiv:1309.4269

Links

[1] PESSTO web page: http://www.pessto.org
[2] WISeREP: http://www.weizmann.ac.il/astrophysics/wiserep
[3] INAF IA2 data archive: http://ia2.oats.inaf.it/

ArTeMiS team/Ph. André, M. Hennemann, V. Revéret et al./ESO/J. Emerson/VISTA

Composite image of the Galactic star-forming region NGC 6334 including an 350 µm image from the newly commisssioned ArTeMiS instrument on APEX. The image of the dust in emission at 350 µm is combined with a near-infrared *Y,J,H* image taken with VISTA which shows the dust in extinction. See Release eso1341 for more details.

The Milky Way's Box/Peanut Bulge: Measuring its Three-dimensional Structure Using the VVV Survey

Christopher Wegg[1]
Ortwin Gerhard[1]

[1] Max-Planck-Institut für extraterrestrische Physik, Garching, Germany

A three-dimensional map of the density of red clump giant stars (RCGs) in the Galactic Bulge has been produced from the Data Release 1 of the ESO public survey VISTA Variables in the *Via Lactea* Survey (VVV). From the magnitude distributions of the RCGs we infer line-of-sight densities and, because the VVV survey has good Bulge coverage, we can combine many line-of-sight density measurements into a complete three-dimensional (3D) map. The 3D density shows a prominent peanut shape when viewed from the side, which appears very similar to simulations of barred galaxies after the bar has buckled, and some edge-on barred spiral galaxies.

The Milky Way's barred Bulge

Despite the proximity of the Bulge of the Milky Way, our position within the disc and the intervening dust makes it difficult to ascertain its structure. We have known since the early 1990s that the Bulge of the Milky Way is barred, based on evidence from gas kinematics and near-infrared (NIR) photometry. Subsequently Cosmic Background Explorer (COBE) data and the Two Micron All Sky Survey (2MASS) star counts showed that the central Bulge had a boxy, perhaps slightly peanut-like, shape. An extensive recent review of the Galactic Bulge can be found in Rich (2013).

Recent excitement has been stimulated by the observation that along the minor axis ($l \approx 0°$) at high latitudes ($|b| \gtrsim 4°$) the distribution of red clump giants splits into separate bright and faint components (e.g., McWilliam & Zoccali, 2010). RCGs are metal-rich core He-burning stars (i.e., metal-rich horizontal branch stars) and provide a standard candle with a *K*-band dispersion ≈ 0.17 mag.

It was quickly realised that the split red clump would be a natural consequence if the Milky Way's Bulge was peanut shaped with many stars travelling along banana-shaped orbits, which, from the side, trace an X-shape. From our nearly end-on perspective of the bar, the split red clump results from looking through both arms of the "X". This type of box/peanut bulge is known to be associated with a bar (e.g., Combes & Sanders, 1981) and is commonly observed in edge-on barred spiral galaxies (e.g., Lutticke et al., 2000).

The motivation for our work was that the VVV survey covers the whole Bulge, but is also deep enough (≈ 4 magnitudes deeper than 2MASS) to allow the RCGs to be detected all through the Bulge. Therefore, because RCGs are good distance indicators and should also trace the major part of the mass, we could use VVV to obtain an approximate distribution of stellar mass in the Bulge. This is important in itself, but is also indispensable for understanding the kinematics and dynamics of Bulge stars.

Line-of-sight densities through the Galactic Bulge

Our work utilised Data Release 1 (DR1) of the VVV public survey accessible through the ESO Science Archive Facility[1]. The VVV survey was described in Gonzalez et al. (2013), along with extinction and photometric metallicity maps of the Bulge. The work described here is more thoroughly explained in Wegg & Gerhard (2013).

We downloaded the VVV DR1 source catalogue in the *J*-, *H*- and *Ks*-bands from the ESO Science Archive Facility (SAF). These source lists are available in Phase 3 format[2]. These catalogues were band matched and then extinction corrected. The extinction map was calculated directly from *J*–*Ks* reddening of Bulge RCGs in the VVV data in a similar way to the map described in Gonzalez et al. (2013).

At low Galactic latitudes, completeness becomes a significant issue for Bulge RCGs, despite the greatly increased depth of VVV compared to previous NIR surveys of the Bulge. In order to understand and correct for this we also downloaded all the VVV *K*-band images from the ESO SAF. With these images we conducted artificial star tests: modelling the point spread function (PSF), inserting stars at various magnitudes into the images, and testing whether they were detected using the same software as developed by the Cambridge Astronomical Surveys Unit (CASU) to create the original catalogues. The artificial star tests allowed us to understand and correct for these completeness issues.

Magnitude distributions were then constructed using the extinction and completeness corrected *Ks*-band data for 338 sight-lines though the Bulge region of the VVV survey (each of the 169 Bulge fields in DR1 of the VVV survey was divided into two). We excluded stars whose colour was inconsistent with being RCGs, however there is still a considerable "background" of stars which are not red clump giants in the Bulge. Fortunately this background is smooth and very close to a power law in luminosity and we therefore statistically identify Bulge RCGs as an excess over this background.

The entire process of constructing the line-of-sight density is shown for one sight-line in Figure 1. We fitted the background in the grey shaded regions giving the blue-shaded RCG magnitude distribution. This is then deconvolved from the intrinsic luminosity function (green line). The background-subtracted magnitude distribution results from both the RCGs, and the red giant branch bump (RGBB), which is less prominent and slightly fainter than the red clump in the *Ks*-band, but with a similar dispersion. We then estimate the line-of-sight density (red line) using iterative Lucy–Richardson deconvolution, stopping when our measured density produces a magnitude distribution consistent with the data (blue line).

The 3D density map

The measured line-of-sight densities for all 338 sight-lines were then assembled into a three-dimensional density map. Our 3D density is non-parametric, however we make one assumption: that the density is eight-fold mirror symmetric along the Galactic bar. This allows us to make a complete 3D map despite DR1 of VVV not yet having 100% Bulge coverage. It also has the desirable side

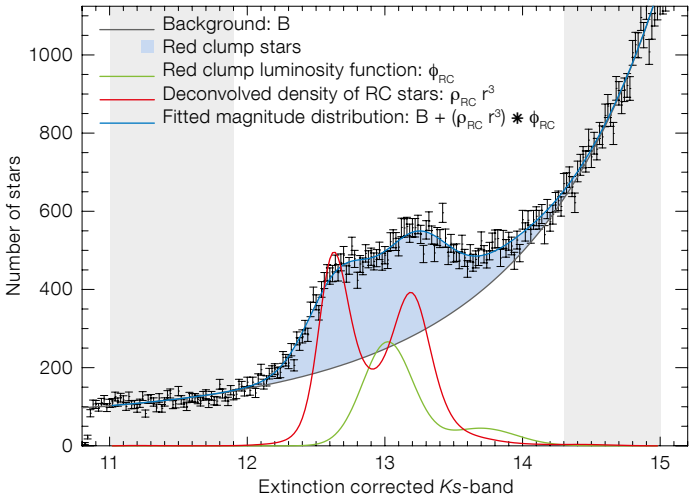

Figure 1. The process of constructing the line-of-sight density for one field at $b = -6°$, $l = 1°$ is illustrated. See text for details.

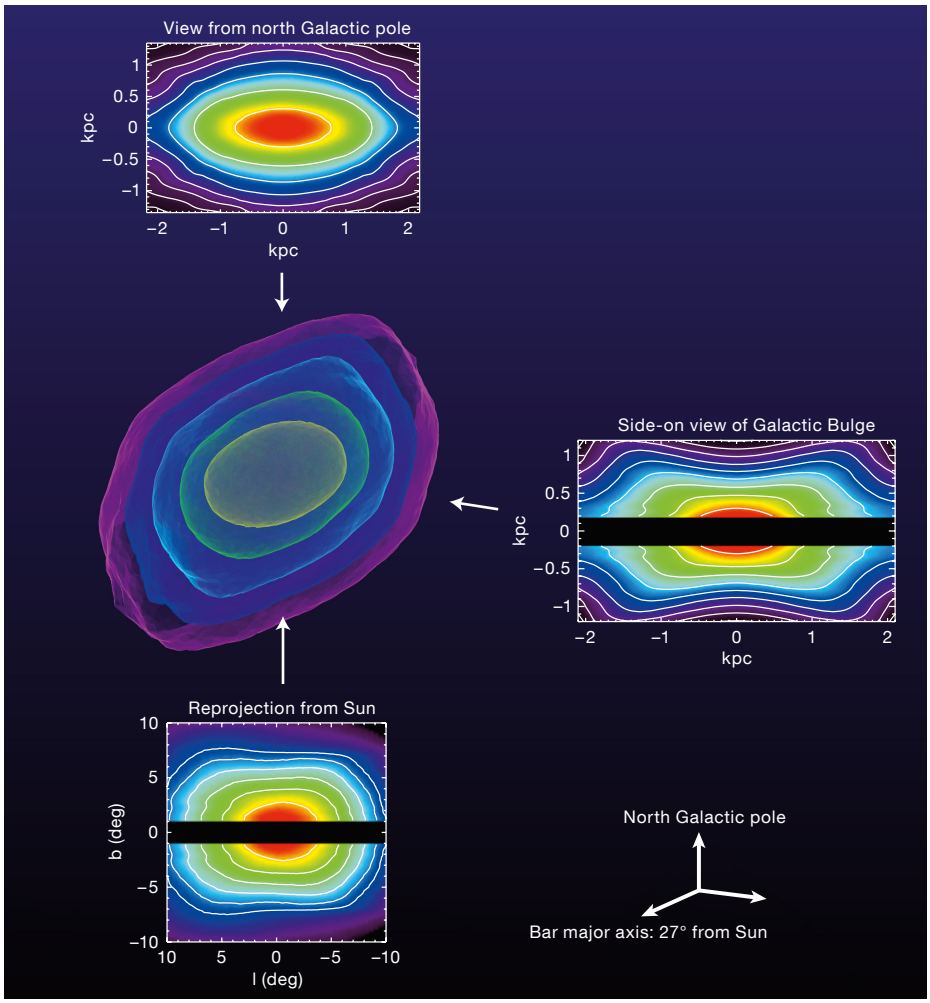

Figure 2. In the centre an image of the 3D iso-density contours of the measured Bulge density is shown, as projected by the VisIt Visualization Tool. Three projections are shown as surrounding plots: from above (i.e., from the north Galactic Pole), from the side (i.e. along the intermediate axis of the bar) and the re-projected surface density from the Sun. The three projections show the surface density of Bulge red clump stars with isophotes spaced by 0.5 mag.

effect of reducing dependence on the fitted background and intrinsic RCG luminosity function, and allows a simple error estimate for the density from the degree of departure from this eight-fold symmetry. This symmetrisation requires knowledge of the axes of the bar, which we find by minimising the differences between the eight assumed equal points. From this process we find the bar semi-major axis lies at 27° ± 2° to the Sun–Galactic Centre line-of-sight.

We graphically illustrate the properties of the resultant density map in Figure 2. From above, the measured Bulge density displays highly elongated isophotes with axis ratio ≈ 2.1:1. When viewed from the side, along the intermediate axis of the bar, the Bulge surface density shows a prominent peanut shape. The density has a short scale height in the centre of the Milky Way of 180 pc, but this scale height increases rapidly along the semi-major axis of the bar. Projecting the density measurement from the position of the Sun shows boxy isophotes, similar to the 2MASS star count maps (Alard, 2001).

Overall the density map seems remarkably similar to generic simulations of bars in which an initially thin, pure exponential disc of stars forms a bar that then buckles and evolves into a three-dimensional boxy/peanut bulge (e.g., Martinez-Valpuesta et al., 2006).

Perhaps the most interesting image is the prominent peanut shape in the side-on Milky Way projection. Cuts though this image are shown in Figure 3 together with similar cuts though NGC 128, the prototypical edge-on galaxy with a peanut bulge. The shaded regions on this plot are estimated systematic errors, formed by varying: (i) our assumptions about extinction; (ii) the intrinsic red clump luminosity function; and (iii) the form of the background distribution. The density generally seems robust at the ≈ 10% level.

Towards an understanding of the origin of the Galactic Bulge

The Galactic Bulge is unique in that we are able to study individual stars in detail in a manner impossible in other galaxies.

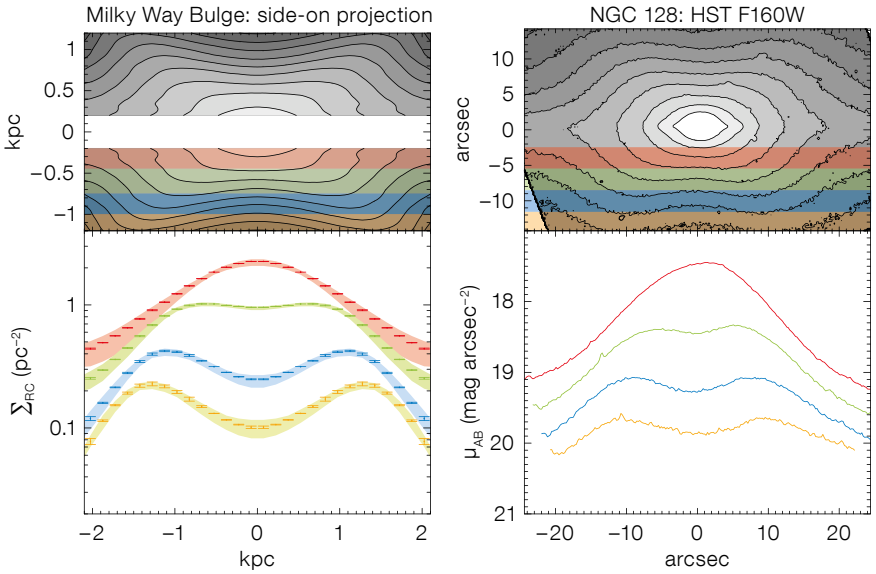

Figure 3. Cuts though the side-on projection of the Galactic Bulge density map on the left, and for NGC 128 on the right (data from Böker et al., 1999). In the upper plots isophotes are separated by 0.5 mag and the regions over which the density cuts are plotted in the lower figure are shaded. In the Galactic Bulge cuts, shown on the lower left figure, the shaded areas are the estimated systematic errors; the error bars are the internal errors of the fiducial density estimated from the departures from eight-fold symmetry. NGC 128 is the prototypical bulge with a peanut shape; although qualitatively similar it is in detail different. In particular, although the shape of the isophotes is quite similar, the Milky Way appears to be more centrally concentrated.

The density measured here, together with the kinematics which can be measured on a star-by-star basis, will allow a detailed understanding the dynamical structure of the Galactic Bulge. Meanwhile new spectroscopic surveys such as ARGOS (Ness et al., 2013) and the Gaia–ESO survey, are studying the metallicity, chemical composition, and kinematics of large numbers of stars across the Galactic Bulge. Comparing all this information to models should ultimately allow us to study and unravel its formation and evolutionary history to a level impossible in external galaxies.

Based on data products from VVV Survey observations made with the VISTA telescope at the ESO Paranal Observatory under programme ID 179.B-2002.

References

Alard, C. 2001, A&A, 379, L44
Böker, T. et al. 1999, ApJS, 124, 95
Combes, F. & Sanders, R. H. 1981, A&A, 96, 164
Gonzalez, O. A. et al. 2013, The Messenger, 152, 23
Lutticke, R., Dettmar, R. J. & Pohlen, M. 2000, ApJS, 145, 405
McWilliam, A. & Zoccali, M. 2010, ApJ, 724, 1491
Martinez-Valpuesta, I., Shlosman, I. & Heller, C. 2006, ApJ, 637, 214
Ness, M. et al. 2013, MNRAS, 432, 2092
Rich, R. M. 2013, in *Planets, Stars and Stellar Systems. Volume 5: Galactic Structure and Stellar Populations*, (Dordrecht: Springer), 271
Wegg, C. & Gerhard, O. 2013, MNRAS, 435, 1874

Links

[1] Access to VVV data: http://archive.eso.org/wdb/wdb/adp/phase3_main/form
[2] Phase 3 format: http://www.eso.org/sci/observing/phase3/overview.html

ESO/J. Borissova

The VVV survey has discovered a large number of open clusters optically heavily obscured by intervening extinction and 30 of these new clusters are shown in this mosaic. Each image cut-out is a combination of *J*-, *H*- and *Ks*-band images (coded blue, green, red respectively) taken with VISTA. See Release eso1128 for more details.

Characterising Exoplanet Atmospheres with High-resolution Spectroscopy

Jayne Birkby[1]
Remco de Kok[2]
Matteo Brogi[1]
Henriette Schwarz[1]
Simon Albrecht[3]
Ernst de Mooij[4]
Ignas Snellen[1]

[1] Leiden Observatory, the Netherlands
[2] SRON, Netherlands Institute for Space Research, Utrecht, the Netherlands
[3] Department of Physics, Massachusets Institute of Technology, Cambridge, USA
[4] Department of Astronomy and Astrophysics, University of Toronto, Canada

The search for signs of life elsewhere in the Universe requires the remote detection of molecules in the atmospheres of exoplanets. Recent progress with high-resolution infrared spectra obtained with CRIRES has led to the first ground-based detections of carbon monoxide and water in the atmospheres of hot giant exoplanets. This avenue of exoplanet characterisation has the potential to identify biomarkers in the atmospheres of Earth analogues with the European Extremely Large Telescope. The current detections not only provide evidence for how the composition of a hot giant planet atmosphere can affect its thermal structure and cloud formation processes, but also have the potential to constrain the universal mechanism for planet formation by pinpointing the birth location of the planet in its protoplanetary disc.

The importance of carbon and oxygen in hot Jupiter atmospheres

Recent studies have suggested that the balance of carbon and oxygen in hot Jupiter (HJ) atmospheres may be drastically and unexpectedly different to the composition of their host stars, with HJs being more abundant in carbon (C/O > 1; Madhusudhan et al., 2012). This surprising conclusion was proposed as a solution to the puzzling and seemingly random presence of stratospheres (i.e., temperature inversions) in HJ atmospheres. Other works have proposed either a connection between the intensity of ultraviolet (UV) light from the host star and the existence of stratospheres (Knutson et al., 2010), or a dichotomy of dusty and cloud-free HJ atmospheres (Pont et al., 2013). The latter is partly supported by Evans et al. (2013) who used the Hubble Space Telescope (HST) to detect for the first time a deep blue light reflecting from clouds in the atmosphere of an HJ.

However, measuring the C/O ratio in HJ atmospheres not only has the power to constrain their structure, but potentially has important implications for the theory of planet formation. Intriguingly, Öberg et al. (2011) showed that the C/O ratio in an HJ atmosphere could be directly linked to the location at which it formed within its protoplanetary disc, due to the different condensation temperatures of molecular ice lines for water, carbon dioxide and carbon monoxide. However, only direct evidence for the presence and abundances of the molecules involved in these theories will enable an accurate physical description of these extreme objects.

Tracing the radial velocity shift of molecular features in exoplanet atmospheres with high-resolution spectra

Robust detections of molecular features in the spectra of exoplanet atmospheres are rare because their signals are typically orders of magnitude smaller than the instrumental systematics present in both ground- and space-based observations. The treatment of these systematics has led to a debate of reported detections in the literature (see e.g., Gibson et al. [2011] for a review). However, in 2010, the first robust ground-based detection of carbon monoxide in an HJ atmosphere was made using a technique based on high-resolution spectra at 2.3 μm from the CRyogenic InfraRed Echelle Spectrograph (CRIRES) on the Very Large Telescope (VLT; Snellen et al., 2010). The detection was made by directly measuring the radial velocity shift of the planet, rather than its host star. Crucial to this success was the high spectral resolution provided by CRIRES (R ~ 100 000), which allowed the forest of spectral lines in the carbon monoxide molecular band to be individually resolved. Observing the planet continuously for the duration of approximately one of its transits traces a radial velocity change in the planetary signal on the order of km s^{-1}, which is much larger than the few m s^{-1} change in the velocity of the host star.

The cartoon in Figure 1 illustrates how the individual lines of the planet's spectrum move throughout its orbit. The large wavelength shift of the planet's signal allows it to be separated from the essentially stationary lines of the host star spectrum and from the static spectral absorption features of the Earth's atmosphere. This is achieved by using detrending algorithms. For example, the top panel of Figure 2 shows 48 spectra extracted from CRIRES observations of HD 189733 over the course of five continuous hours just before secondary eclipse, when most of the planet's dayside hemisphere was visible. Each row is a spectrum, and each column can be considered as a wavelength channel with a width of one pixel. The deep, wide absorption bands of the Earth's atmosphere (black regions) are clearly visible. Each column is subject to trends that vary smoothly during the night, such as changing airmass or seeing. By using a principal component-like analysis, such as those commonly used to de-trend transit survey light curves, trends common to all columns can be identified.

The second panel in Figure 2 shows the input to the algorithm, which is simply the extracted spectra with their median value subtracted. The most significant global trend in the columns is identified and then removed from each column (see third panel). In this specific case, the dominant trend closely followed the airmass curve of the target. The algorithm is repeated until no more significant global trends remain (see fourth panel). This column-by-column operation leaves the planetary signal relatively untouched because it is shifting in wavelength during the observations and thus does not constitute a common trend in each column. For illustration, the bottom panel of Figure 2 shows what the fourth panel would look like if we injected a strong model planet spectrum into the data before applying the algorithm. After the telluric features have been removed, the remaining data can be cross-correlated with

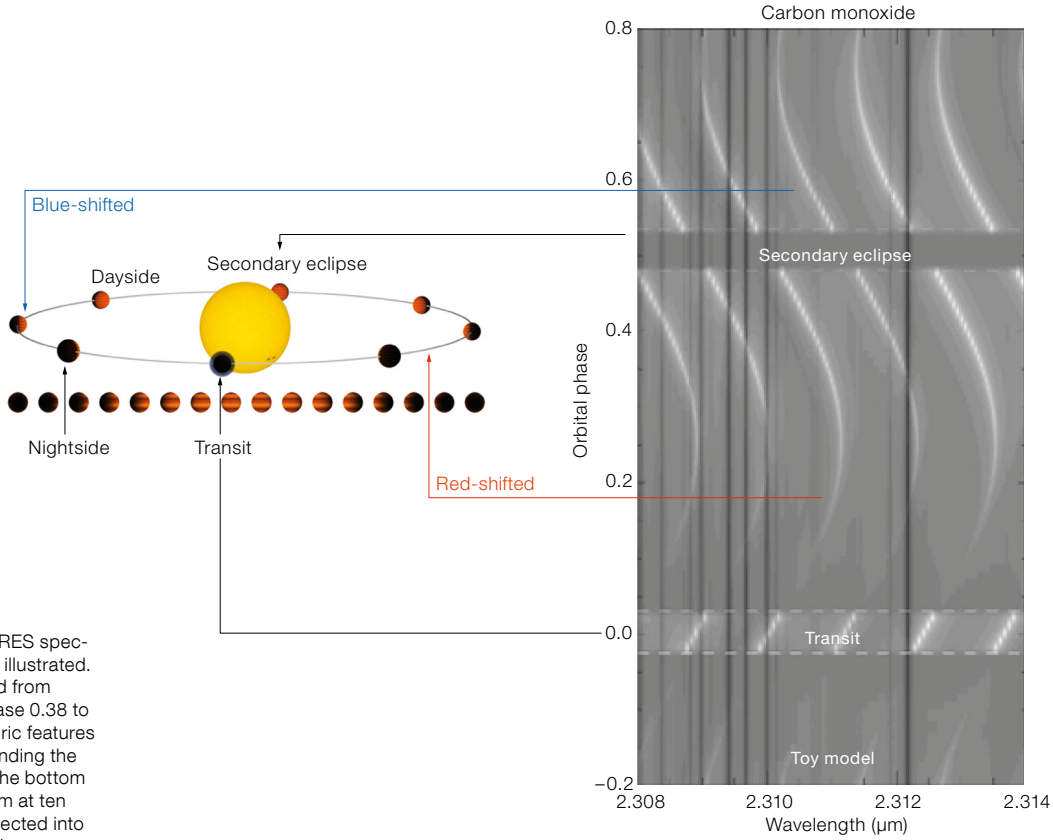

Figure 1. Schematic for detecting molecules in exoplanet atmospheres at high resolution. Each row in the right-hand panel is a spectrum. The white lines trace out the radial velocity curve of individually resolved lines in the carbon monoxide molecular band of a toy model hot Jupiter atmosphere. Throughout the orbit, the lines shift significantly in wavelength compared to the static features of the Earth's atmosphere (dark vertical lines), allowing them to be separated without destroying the planetary signal. This technique works both in transit, as starlight filters through the exoplanet atmosphere and adopts the spectral fingerprint of its molecular constituents, and throughout the phase as thermal irradiation from the planet's dayside and nightside rotate into view, depicted at left.

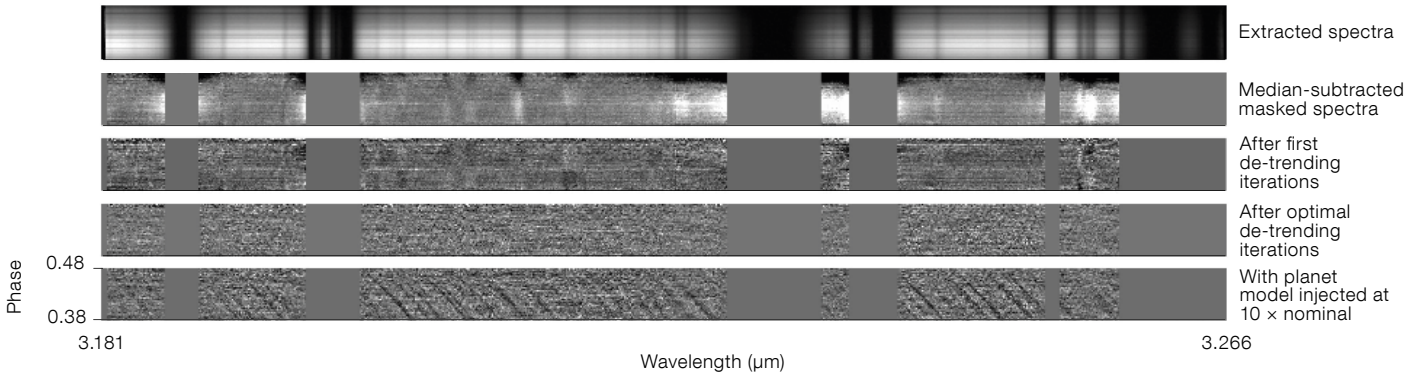

Figure 2. The process of de-trending CRIRES spectra in order to uncover the planet signal is illustrated. The top panel shows 48 spectra extracted from CRIRES observations covering orbital phase 0.38 to 0.48, where each row is a spectrum. Telluric features are removed column by column by de-trending the spectra over time (middle three panels). The bottom panel shows how a model planet spectrum at ten times its nominal value would appear if injected into the extracted spectra before the de-trending process. From Birkby et al. (2013).

high-resolution models of molecular species over a range of planet radial velocity semi-amplitudes (K_p) to trace out the radial velocity curve of the planet (see Figure 3).

In order for any signal to be considered of planetary origin, it must coincide with the total velocity of the system (V_{sys}), which is known from precision radial velocity measurements of the host star. This is a key element in the robustness of the high-resolution technique. In practice, the cross-correlation is carried out over a wide grid of K_p and V_{sys} to reliably reject spurious signals. We have since used this high-resolution technique with observations from our large ESO programme on CRIRES (186.C-0289) to produce a steady stream of ground-based detections of carbon monoxide in the daysides of both transiting and non-transiting HJ atmospheres, opening up the study of atmospheres to the full population of exoplanets (Brogi et al., 2012, 2013; de Kok et al., 2013a).

Adapting the high-resolution technique for use at other wavelengths in more obscured regions of the Earth's atmosphere that contain molecular bands of all the other major carbon and oxygen-bearing species (water, methane and carbon dioxide), has led to the first robust ground-based detection of water in an HJ atmosphere with CRIRES (Birkby et al.,

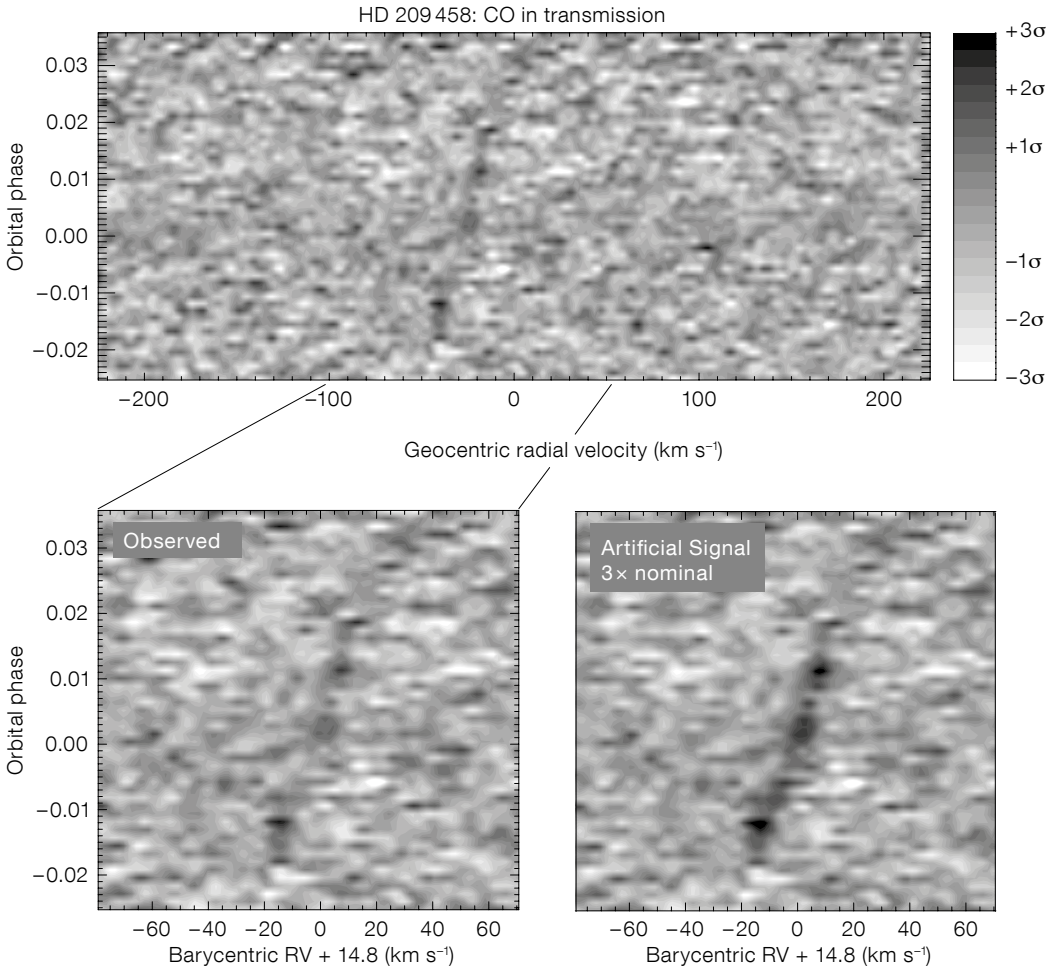

Figure 3. The radial velocity trail of carbon monoxide in the atmosphere of the hot Jupiter HD 209458 b observed during its transit. The signal is blue-shifted by 2 km s^{-1} from the expected V_{sys}, suggesting the presence of a fast, high-altitude wind blowing from the day- to the nightside of the planet. Adapted from Snellen et al. (2010).

	HD 209458 b (Transiting)	τ Boötis b (Non-transiting)	51 Pegasi b (Non-transiting)	HD 189733 b (Transiting)
Molecules detected	CO at 2.3 μm (5.6σ)	CO at 2.3 μm (6σ)	CO at 2.3 μm (6σ) H_2O 3.2 μm (4σ)	CO at 2.3 μm (5σ) H_2O at 3.2 μm (5σ)
Reference	Snellen et al. (2010)	Brogi et al. (2012)	Brogi et al. (2013)	de Kok et al. (2013a) Birkby et al. (2013)
Planet orbital velocity	140 ± 10 km s^{-1}	110.0 ± 3.2 km s^{-1}	134.1 ± 1.8 km s^{-1}	154 ± 4 km s^{-1}
System inclination	86.93 ± 0.01°	44.5 ± 1.5°	79.6° ≤ i ≤ 82.2°	85.71 ± 0.05°
Planet mass	0.64 ± 0.09 MJ	5.95 ± 0.28 MJ	0.46 ± 0.02 MJ	1.162 ± 0.058 MJ
Phase observed	Transit	Dayside	Dayside	Dayside

Table 1. Summary of detections of molecules in exoplanet atmospheres made with CRIRES. The planet masses have been independently derived from the CRIRES measurements and are actual masses, not the minimum mass usually quoted from radial velocity measurements.

2013). The cross-correlation grids showing the detection of these molecular features are shown in Figure 4 and their results are summarised in Table 1. These detections required between 5 and 18 hours of time with CRIRES, which highlights the efficiency of this instrument for exoplanet atmosphere science. Importantly, the measurement of the orbital velocity of the planet in a non-transiting system can be converted to an inclination angle and hence a true mass for the planet, unlike the minimum mass determined from stellar radial velocity measurements alone. This was the case for the well-known non-transiting hot Jupiters τ Boötis b and 51 Pegasi b. The detection of CO in their atmospheres (see Figure 4) revealed that τ Boötis b is inclined at $i \sim 45$ degrees to our line of sight (Brogi et al., 2012), and that the first exoplanet discovered around a Sun-like star, 51 Peg b, was almost a transiting system (Brogi et al., 2013).

What can we learn from high-resolution observations of exoplanet atmospheres?

The detection of molecules at high resolution in exoplanet atmospheres is in itself an important input for atmospheric modelling. In principle, detections at infrared wavelengths that probe the thermal emission of the atmosphere, also make it possible to put constraints on both the abundance of the detected gas and the temperature structure in the

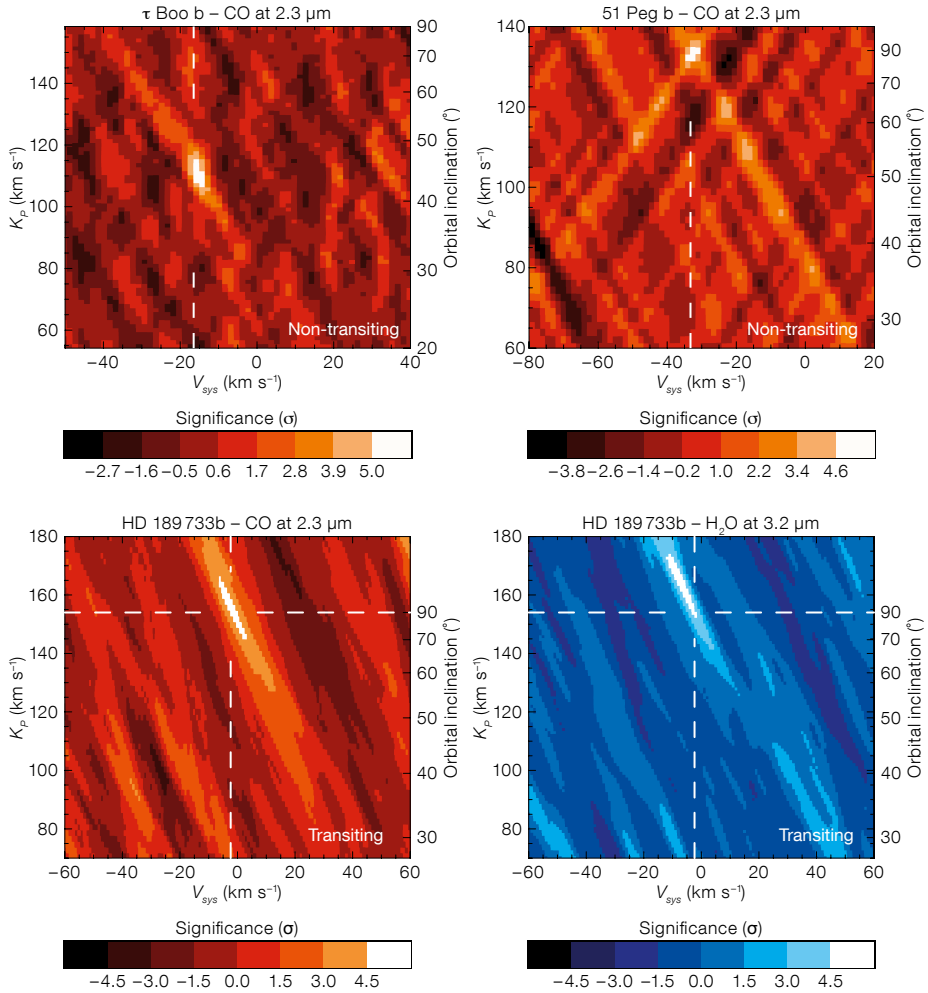

Figure 4. Carbon monoxide (CO) and water (H_2O) detected in the dayside atmospheres of several transiting and non-transiting hot Jupiters using the high-resolution spectra from CRIRES. These figures show the grid of planet radial velocity (K_p) and total system velocity (V_{sys}) explored by the cross-correlation of our processed spectra with model exoplanet atmospheres. The strongest signal is detected at the known total system velocity (dashed vertical white lines) in each case and is thus considered to have planetary origin. The orbital velocity of the planet can also be converted to a system inclination. The CO detection in τ Boötis b used three half-nights of CRIRES spectra, while 51 Peg b used two half-nights, and the detections in HD 189733 b are based on five hours observation each. The colour bars indicate the significance of the detections.

atmosphere. Such constraints can ultimately provide a measurement of the C/O ratio. However, the high-resolution technique is only sensitive to the relative depth of the absorption lines in the planet's spectrum, and not their absolute levels. As a result, many degeneracies exist between the temperature *vs*. pressure (altitude) profile of the atmosphere and the concentration of the gas in question, because different combinations can result in the same relative line depth. Furthermore, if the atmosphere is very cold in its upper layers, or has a very small change in temperature throughout the extent of its atmosphere, the relative line depths for different gas concentrations can be identical.

For transiting planets, additional constraints can be obtained at lower resolution in the same wavelength region from observations of the planet's secondary eclipse, i.e., as it passes behind its host star. This provides a measurement of the absolute flux level of the planet spectrum at the wavelength probed by the high-resolution data, and independently constrains the range of viable temperature–pressure profiles.

For non-transiting planets, where secondary eclipse measurements are not possible, further information can be gained from the simultaneous detection of several molecules in a narrow wavelength range. In this case, the lines all have a very similar continuum level, which removes some of the degeneracies in the models and allows a constraint on the relative gas concentrations. Moreover, detections of the same molecule across a range of wavelengths where the gas absorbs at different levels can further constrain the atmospheric temperature profile, the gas concentrations and even the presence of clouds.

The wavelengths at which different gases are best detected with CRIRES can be simulated in conjunction with the ESO Exposure Time Calculator (ETC). We injected model planet spectra into simulated stellar spectra spanning 1–5 μm obtained from the ETC. Using the same data reduction technique as for the real data, we assessed how well a certain planet signal can be detected at different CRIRES wavelength settings. Figure 5 shows the results of this exercise for a hot Jupiter of a given composition (based on HD 189733 b). The absorption bands in the Earth's atmosphere can clearly be seen to hinder the detection of the planet signal at e.g., 2.7 μm.

The figure also shows that there are wavelength settings that are expected to give a higher signal than the 2.3 μm and 3.2 μm regions in which we have already made carbon monoxide and water detections. In particular, the wavelength setting at 3.5 μm looks ideal for the simultaneous detection of major carbon- and oxygen-bearing gases, given its high sensitivy to water, methane and carbon dioxide, and is the target of our current observations of the dayside atmospheres of two non-transiting hot Jupiters. Interestingly, in the case of high C/O ratios or disequilibrium photochemistry, CRIRES would also be sensitive to hygrogen cyanide and acetylene in HJ atmospheres in the 3.1 μm region.

Exploring the dark side

For HJs, the nightside is expected to be colder than the dayside, as is suggested

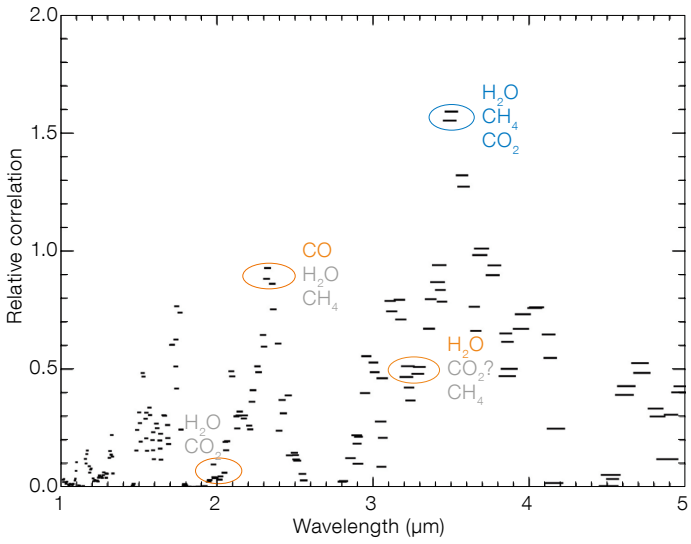

Figure 5. Simulating the sensitivity of CRIRES to different molecules in the atmospheres of exoplanets across its full range of wavelength settings. Orange circles mark regions that we have already observed; orange text denotes molecules detected; while grey text marks species with molecular bands in that region but which were not significantly detected. The blue circle and text marks the 3.5 μm region which we found to be the most sensitive to the simultaneous detection of major carbon- and oxygen-bearing species (de Kok et al., 2013b).

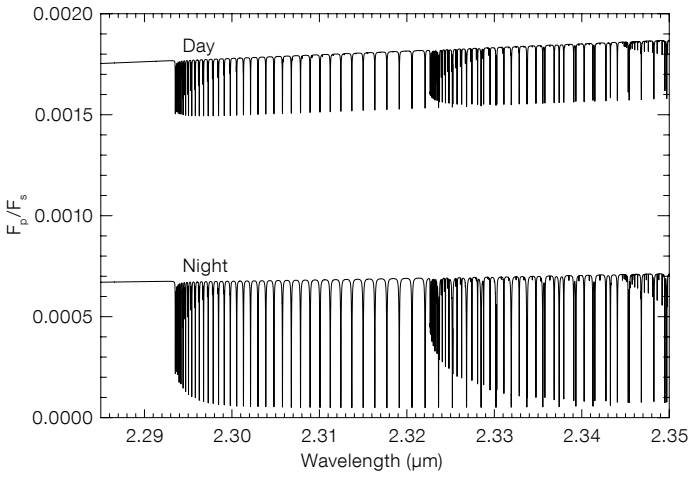

Figure 6. A high-resolution model of CO absorption lines in the day- and nightside of an HJ atmosphere expressed as a fraction of the stellar flux. The nightside produces deeper absorption features which may make it easier to detect them, despite having a lower overall flux (de Kok et al., 2013b).

by infrared phase curves from Spitzer. Despite being darker on their nightside, high-resolution observations can also be used to probe molecules at these phases in HJ atmospheres. In fact, the change in temperature with altitude on the nightside may be larger than on the dayside, and this potentially can result in deeper molecular absorption lines (see Figure 6), making the nightside perhaps even more ideal for hunting for molecules with high-resolution spectra, despite the lower overall flux. A detection of the same molecule in the same wavelength range on both day- and nightsides would allow constraints on the day-to-night heat transfer in the atmosphere, and in particular on its vertical dependence. For instance, a deeper line depth at the nightside can indicate that the highest day-to-night temperature contrast occurs at high altitudes. On the other hand, small line depths on both the dayside and nightside can indicate the presence of a thick global cloud layer.

Exoplanet atmospheres with future high-resolution instrumentation

The imminent upgrade of CRIRES to the cross-dispersed spectrograph CRIRES+ promises to yield a great improvement in the sensitivity of the high-resolution method. Its much larger wavelength coverage and upgraded detectors will greatly improve the correlation signal of detected molecules by significantly increasing the number of individual molecular lines that can be measured. It will also allow the detection of several molecules simultaneously at a relatively high signal-to-noise across a wide region of the planet's spectrum, which will provide information about the atmospheric temperature structure, the presence of clouds, and potential variations of the gas concentrations with altitude. Furthermore, it opens up the possibility of using high-resolution spectra to study the atmospheres of smaller, cooler planets such as warm Neptunes and superEarths at infrared wavelengths. In theory, high-resolution spectra at optical wavelengths can be used in a similar manner to probe for other molecules, such as metal oxides. Therefore, the high-resolution optical spectrograph, ESPRESSO, which is scheduled for first light on the VLT in 2016, will provide another compelling avenue for characterising exoplanet atmospheres.

The greatest step in sensitivity to exoplanet atmospheres with ground-based facilities will be achieved by the European Extremely Large Telescope (E-ELT). The E-ELT will potentially carry two high-resolution instruments: METIS in the infrared *L*- and *M*-bands, and HIRES at visible and near-infrared wavelengths. These E-ELT instruments will allow a detailed chemical census of the full population of exoplanets to reveal the diversity of their atmospheres. Excitingly, simulations have also shown that high-resolution spectra from the E-ELT instruments will be able to detect a potential oxygen biomarker at 0.76 μm in the atmospheres of Earth-like planets orbiting in the habitable zones of M-dwarf stars, in just a few dozen transits (Snellen et al., 2013).

References

Birkby, J. L. et al. 2013, MNRAS Letters, 436, 35
Brogi, M. et al. 2012, Nature, 486, 502
Brogi, M. et al. 2013, ApJ, 767, 27
Evans, T. et al. 2013, ApJL, 772, 16
Gibson, N. P. et al. 2011, MNRAS, 411, 2199
Knutson, H. et al. 2010, ApJ, 720, 1569
de Kok, R. J. et al. 2013a, A&A, 554, A82
de Kok, R. J. et al. 2013b, A&A, accepted
Madhusudhan, N. et al. 2012, ApJ, 758, 36
Öberg, K. I. et al. 2011, ApJL, 743, L16
Pont, F. et al. 2013, MNRAS, 432, 2917
Snellen, I. A. G. et al. 2010, Nature, 465, 1049
Snellen, I. A. G. et al. 2013, ApJ, 764, 18

The Diversity of Dusty AGN Tori: Results from the VLTI/MIDI AGN Large Programme

Leonard Burtscher[1]
Konrad R. W. Tristram[2]
and the MIDI AGN LP team*

[1] Max-Planck-Institut für extra-terrestrische Physik, Garching, Germany
[2] Max-Planck-Institut für Radio-astronomie, Bonn, Germany

The molecular gas and dust surrounding the central engine of active galactic nuclei (AGN) plays a fundamental role in understanding their physics. Due to the small angular size of this torus, direct studies of its properties require very high angular resolution. The VLTI/MIDI AGN Large Programme aims at characterising a statistical sample of AGN tori for the first time by resolving their dust emission in the mid-infrared interferometrically. Measurements of 23 sources show that most tori are very compact with sizes of 0.1 to 10 pc and emission from a two-component structure. The morphology of the torus differs significantly between individual objects and does not show the expected dependency on viewing angle (edge-on *vs.* face-on). The torus is thus significantly more complex than typically pictured, requiring new models and imaging interferometry on milliarcsecond scales to decipher the physics.

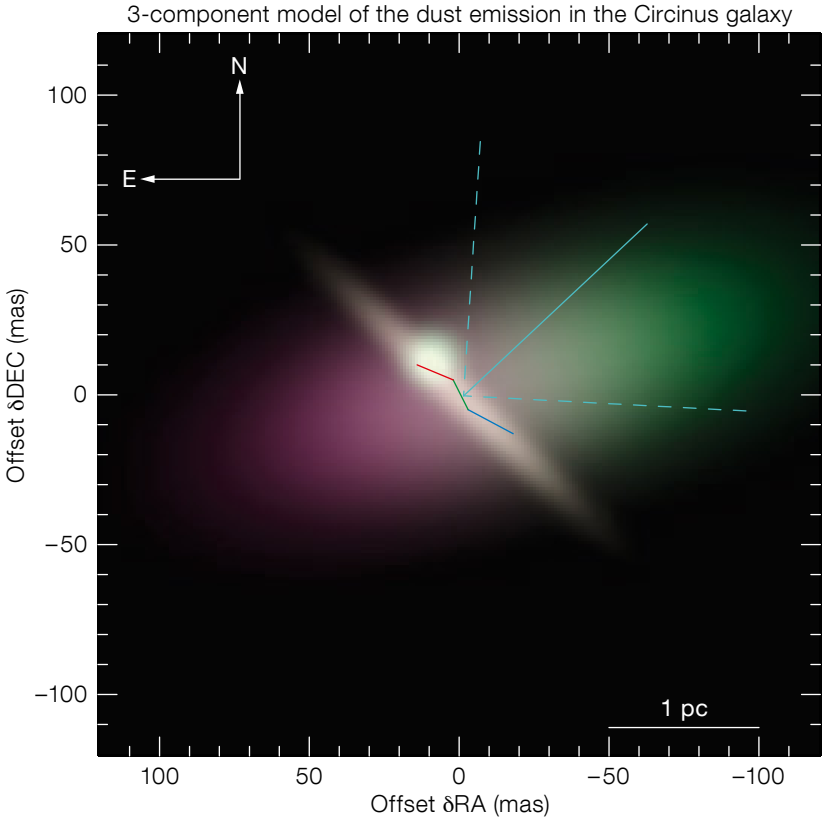

Figure 1. Colour image of the three-component model, describing over 150 individual MIDI measurements of both the visibility amplitude and differential phase from the Circinus galaxy (Tristram et al., A&A, 2013). The model components are: (1) an unresolved component; (2) a highly inclined disc, offset with respect to component (1), whose major axis is perpendicular to the ionisation cone (cyan lines) and which is coincident in orientation with water maser emission (red–green–blue line); and (3) an extended emission region roughly elongated in the polar direction with an increase of the silicate absorption towards the south-east (purple–green, with purple representing deeper silicate feature).

Motivation

The Mid-Infrared Interferometric Instrument (MIDI) at the Very Large Telescope Interferometer (VLTI) is unique worldwide in resolving what is commonly referred to as the torus in active galactic nuclei (AGNs; see Meisenheimer et al., 2008). This torus is considered to be responsible for the type 1 (broad-line) / type 2 (narrow-line) dichotomy in AGNs and perhaps plays a crucial role in feeding of the central supermassive black hole (e.g., Schartmann et al., 2009).

By interferometrically combining light from two of the large Unit Telescopes (UTs), AGNs with mid-infrared (MIR) fluxes as faint as ~ 100 mJy can be studied, and structures as small as ~ 5 milliarcseconds detected. The two brightest extragalactic southern sources in the MIR wavelength range (8–13μm) — NGC 1068 and the Circinus galaxy — have now been observed in great detail and reveal complex morphologies on (sub-)parsec scales (see Figure 1).

Although these two prominent sources have much in common, they also show marked differences. Most notably, hot dust (T ~ 800 K) on parsec scales has only been detected in NGC 1068, while the Circinus galaxy, where a similar spatial resolution is reached, seems to contain only warm (T ~ 300 K) dust. Until a couple of years ago, only a few other extragalactic objects had been studied with MIDI, but it was clear that a much larger sample was needed to build a more coherent view of the nuclear dust structures of AGNs.

This statistical sample has now been assembled by the first VLTI Large Programme (PI: K. Meisenheimer) together with two accompanying programmes and data from the archive. The questions that this programme set out to answer include:

*The MIDI AGN LP team:
K. Meisenheimer (P.I.)[1], L. Burtscher[2], K. R. W. Tristram[3], W. Jaffe[4], S. F. Hönig[5], R. I. Davies[2], M. Kishimoto[3], J.-U. Pott[3], H. Röttgering[4], M. Schartmann[3,6], G. Weigelt[3], S. Wolf[7]

[1] Max-Planck-Institut für Astronomie, Heidelberg, Germany
[2] Max-Planck-Institut für extraterrestrische Physik, Garching, Germany
[3] Max-Planck-Institut für Radioastronomie, Bonn, Germany
[4] Sterrewacht Leiden, Universiteit Leiden, the Netherlands
[5] Dark Cosmology Center, University of Copenhagen, Denmark
[6] Universitäts-Sternwarte München, Germany
[7] Institut für Theoretische Physik und Astrophysik, Universität zu Kiel, Germany

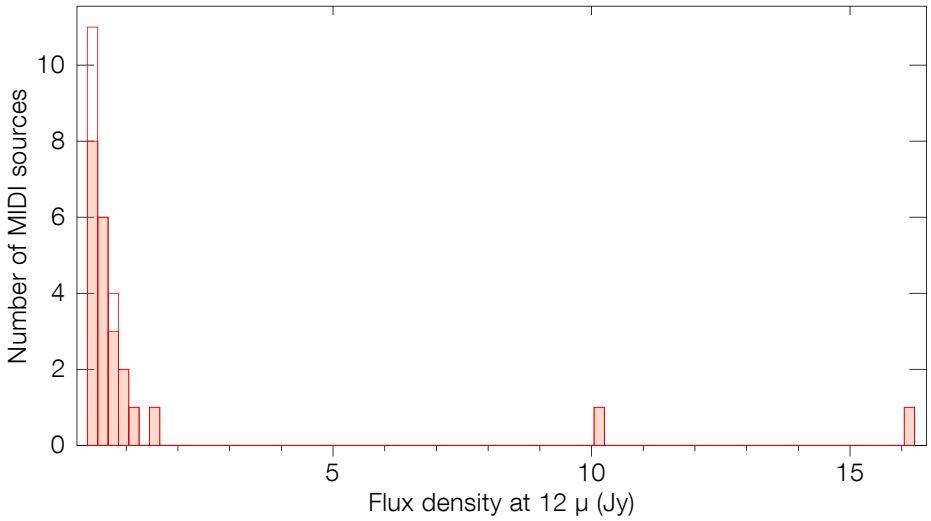

Figure 2. Histogram of mid-infrared fluxes of AGNs that have been interferometrically detected with MIDI (open bars); filled bars are for sources studied in Burtscher et al. (2013), and discussed in this article. In order to increase the sample beyond the two brightest sources, the sensitivity had to be increased by more than a factor of ten.

– What are the morphology and the size of the nuclear structures? Are type 1/2 sources intrinsically different on parsec scales? These phenomenological questions are directly addressable from the interferometric data and are the focus of this article (see Burtscher et al., 2013);
– What are the elongations of the dust structures and how do they relate to the other axes in these systems? Is the dust chemistry of the nuclear structures different to that on larger scales?
– Is there a connection between nuclear star clusters and the genesis of the torus? This more far-reaching question will be addressed using a combination of observational data (with an important constraint from the MIDI observations reported here) together with hydrodynamical simulations (Schartmann et al., 2010).

Observations

Due to the specific distribution of MIR target brightnesses (Figure 2), enlarging the sample was only possible by observing targets that were at least ten times fainter (and much more distant) than the two initially studied AGNs. NGC 1068 and the Circinus galaxy are among the closest AGNs with distances of 14 and 4 Mpc respectively. The most distant object that

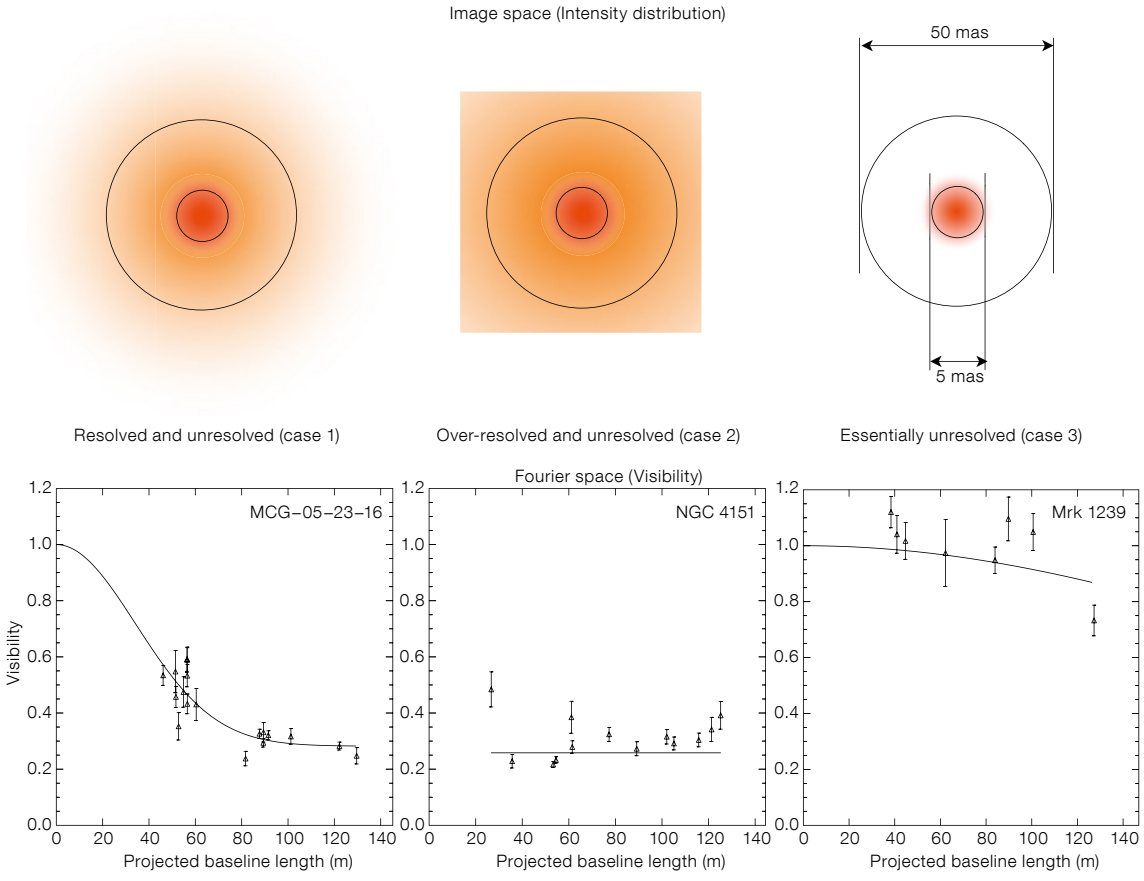

Figure 3. Nuclear morphologies of AGNs in the MIR revealed by MIDI. Left: resolved source with an additional unresolved component (visibility decreases with baseline length, but is always > 0); middle: over-resolved source with an additional unresolved component (visibility is ~ constant with baseline length and < 1); right: essentially unresolved source (visibility is ~ 1 on all baselines with only a shallow decrease). Top row: intensity distribution in image space; bottom row: radial visibility profiles of representatives of the three different nuclear MIR morphologies observed in the MIDI AGN Large Programme: MCG-05-23-16, NGC 4151 and Mrk 1239.

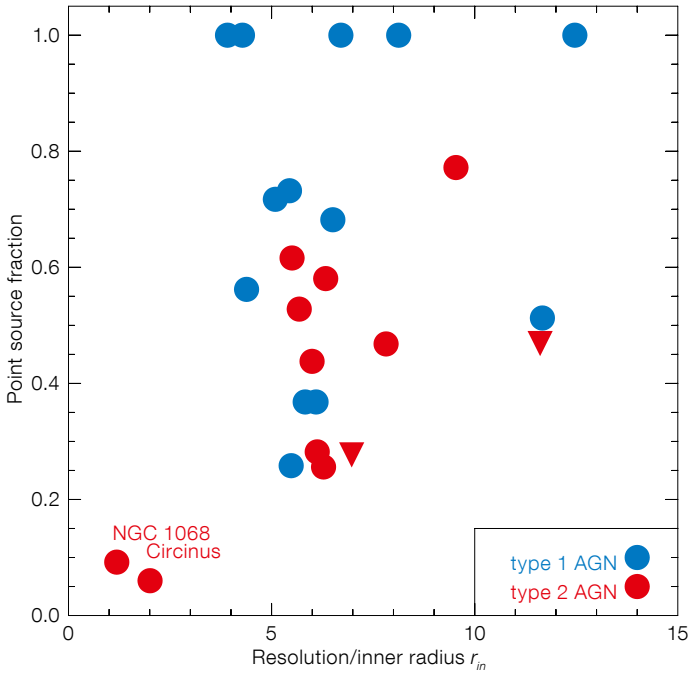

Figure 4. Point source fraction (~ minimum observed visibility) as a function of resolution. Type 1 AGNs are plotted in blue, type 2 AGNs in red; triangles show limits. To overcome resolution / distance effects in our flux-limited sample, we normalise the resolution to the inner radius of dust r_{in} (using the empirically derived relation between bolometric luminosity and r_{in}). If all tori were equal, the point source fraction would only depend on this "intrinsic resolution" — which is clearly not the case. Type 1 sources show higher levels of unresolved flux than type 2 sources (but are nonetheless statistically of the same size).

is observed with MIDI is the quasar 3C 273 at a redshift z = 0.158. It is marginally resolved.

To scientifically exploit these observations, a substantial effort was started to better understand the data reduction of the weak objects; correlation losses (that appear when the signal-to-noise ratio is very low) and calibration uncertainties were quantified (Kishimoto et al., 2011; Burtscher et al., 2012). This allowed us to consistently analyse the newly acquired data as well as all previously published archive data on AGNs with MIDI. While not complete by flux or volume, we also did not find any obvious biases in this sample.

Results

Out of the 36 galaxies for which observations have been attempted with MIDI, 27 are interferometrically detected (23 are part of this work); the few observed, but undetected galaxies either contain only feeble AGNs or were observed as back-up targets during bad conditions. Furthermore, all of the detected sources have been successfully observed on the longest VLTI-UT baseline of 130 metres — there was no galaxy that was only detected on short baselines with MIDI. In MIR-bright AGNs, therefore, a substantial fraction of the nuclear 12 µm emission must originate from very compact (0.1–10 pc) scales, that are only partially resolved even on the longest baselines with MIDI.

This finding was somewhat unexpected, since scaling relations, derived from near-infrared (NIR) dust reverberation mapping and interferometry, predicted more extended dust structures if based on the bright sources that had been initially studied with MIDI. Instead most AGNs were only partly resolved with median visibility well above 50 %. The visibility is a measure of how well resolved a source is: unresolved sources show a visibility of 100 % and resolved sources show very low visibilities.

On the one hand, high visibilities are easier to observe and are the reason for the success we had in observing AGNs with MIDI; on the other hand, the high visibilities imply that fainter AGNs are largely unresolved and therefore their substructure (see Figure 1) is not revealed. But even at these high visibility levels, we were able to discriminate three different morphologies (see Figure 3):

1. Resolved sources, where the visibility decreased with baseline length;
2. Over-resolved sources, where the visibility was less than 100 %, but no change of visibility with baseline or position angle was observed; and
3. Essentially unresolved sources.

Most of the resolved (case 1) and all of the over-resolved (case 2) sources show clear signs of a two-component structure, where the larger component is (at least) several tens of milliarcseconds in size (about 1 pc in the nearest galaxies — 30 pc in the most distant ones) and the compact, unresolved point source is less than about 5 milliarcseconds in size.

The low-resolution spectra obtained with MIDI generally show an almost featureless continuum with only the broad silicate feature imprinted in absorption or emission. Here we show only the visibilities at 12 µm (Figure 3) since the sources are best resolved at this wavelength.

A large sample of (partly) resolved AGN tori

Apart from the generally high level of visibility in the weak sources, another surprising result was the large diversity in morphology among the sources. This is most readily seen when looking at the lowest visibility measured for each source (we call this the “point source fraction”). If the tori in the sources were all of equal size, we would expect that the point source fraction depends only on the resolution with which the source is observed. This is clearly not the case, as Figure 4 demonstrates. Except for the two bright sources (NGC 1068 and the Circinus galaxy) that are more highly resolved than all of the faint sources, no clear trend between resolution and point source fraction can be seen.

Since the radial profiles of most sources show that they are composed of at least two components (perhaps they correspond to the extended component and the disc in the well-resolved sources?), we derive a half-light radius to characterise the extension of the entire nuclear emission in a single number. This radius can then be compared to the inner radius of dust as derived with dust reverberation mapping and NIR interferometry. For this inner radius of dust, it is now well

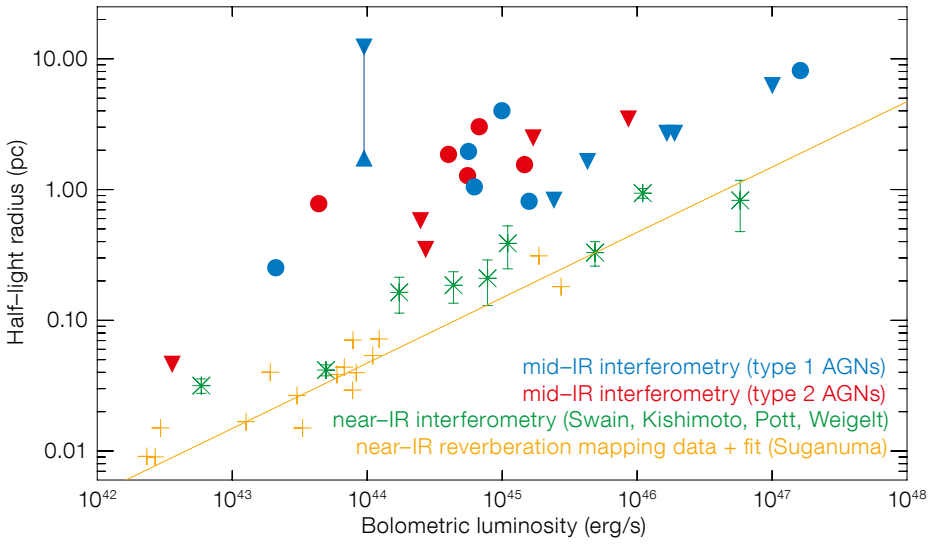

Figure 5. Size–luminosity relation for AGNs probing different regions of the torus: blue/ red points are MIDI measurements from the MIDI AGN Large Programme + archive for type 1/type 2 sources (statistical errors are smaller than symbol sizes); green crosses are NIR interferometry with both the Keck-Interferometer and AMBER/VLTI; orange pluses are from NIR dust reverberation mapping. Filled triangles show limits. Taking both the limits and the determined half-light radii into account shows that the mid-infrared size is less strictly correlated with luminosity than the innermost radius of dust that is seen in the NIR.

accepted that it scales with $\sqrt{L}$ where L is the bolometric luminosity of the AGN. For the MIR, due to the small and biased samples that were available prior to the MIDI AGN Large Programme, such a relation was claimed from some early data (Tristram et al., 2009), but later Kishimoto et al. (2011) found the relation to be essentially flat at 12 μm. With the large sample available now, we show that the torus does scale with luminosity roughly as $\sqrt{L}$, but we also find that this relation shows more scatter than the NIR relations (Figure 5), possibly because of the two-component structure discussed above.

In our sample, there are about the same numbers of type 1 and type 2 sources. The type 1 sources are at greater distances, i.e., have higher luminosities in our flux-limited sample. Otherwise, the two populations are indistinguishable. This is in contradiction to expectations from clumpy torus models, in which type 2 tori are expected to appear larger than type 1 tori. It shows that torus orientation cannot be the only factor in creating the different optical characteristics of AGNs.

Further results and future perspective

So far we have used only simple axisymmetric models for the brightness distribution, although the best-studied sources (NGC 1068, Circinus galaxy, NGC 424, NGC 3783) show considerable elongations in their dust distributions. While these axisymmetric models provided good fits to all faint targets, the residuals for some of the weak sources (see Burtscher et al., 2013) show indications for elongations. This, as well as an analysis of the full spectral information, is ongoing work.

In conclusion, the MIDI AGN Large Programme (+ archive) provides a sample of 23 (partially) resolved AGN tori, analysed in a uniform way. It has shown that the differences that were already known between the two MIR brightest AGNs are not a peculiarity of these sources, but indicative for the whole population. Even at more or less constant intrinsic resolution, AGN tori appear very diverse.

On the other hand, a two-component structure of the nuclear MIR morphology seems to be a common trait in most AGNs. We found both a very compact (< 0.1 pc in the most nearby sources) and a more extended component in the majority of sources. While all torus models predict that type 2 tori appear larger than type 1 tori, we cannot find such a dichotomy in our sample of 23 (partly) resolved AGN tori. This calls for a new set of torus models to explain the now well-studied nuclear dust morphologies in a large sample of active galaxies.

VLTI/MIDI observations have shown how complex the nuclear dust morphologies of AGNs are. In the near future, the second generation VLTI instruments GRAVITY and MATISSE will allow interferometric observations on six baselines at a time and provide both high signal-to-noise visibilities and phases. This will allow us to reconstruct real images of the torus from the inner edge to the main body with resolutions of a few milliarcseconds that are needed to decipher the physics at work.

Acknowledgements

The authors would like to thank the VLT(I) crew for their excellent support during many years of observations.

References

Burtscher, L. et al. 2012, Proc. SPIE, 8445, 84451G
Burtscher, L. et al. 2013, A&A, 558, A149
Kishimoto, M. et al. 2011, A&A, 536, A78
Meisenheimer, K. et al. 2008, The Messenger, 133, 36
Schartmann, M. et al. 2009, MNRAS, 393, 759
Schartmann, M. et al. 2010, MNRAS, 403, 1801
Tristram, K. R. W. et al. 2009, A&A, 502, 67
Tristram, K. R. W. et al. 2013, A&A, in press (arXiv:1312.4534)

To mark the 50th anniversary of ESO's presence in Chile, a gift of ESO's first atomic clock was presented to Sebastián Piñera, the President of Chile (right) by the Director General Tim de Zeeuw (left). Also shown is Fernando Comeron, the ESO Representative in Chile. See Announcement ann13092 for more information.

The new extension to the ESO Headquarters was inaugurated on 4 December 2013 and hosted its first ESO Council meeting on 4–5 December. To the left the new technical building is visible. See Release eso1350 for more details.

Report on the ESA–ESO Conference

Science Operations 2013: Working Together in Support of Science

held at ESAC, Madrid, Spain, 10–13 September 2013

Francesca Primas[1]
Nicolaus Hanowski[2]

[1] ESO
[2] ESA

This first conference aimed at establishing closer communication and synergy of ground- and space-based operations for astronomy and Solar System science is summarised by the two chairs. The main topics covered the organisation and management of science operations, science and instrument planning, instrument handling and calibration, data processing and archiving, and support services.

Continuing the effort of establishing new synergies between space- and ground-based astronomical facilities, back in 2012 the European Space Agency (ESA) and ESO thought that it would be worthwhile to bring their communities together and compare their operational methodologies, processes, procedures and interfaces. The authors were tasked with defining and structuring the broad content of the meeting. The objective of the resulting conference — Science Operations 2013 — was clear, i.e., to present and discuss the various approaches to science operations in spacecraft missions and ground-based facilities for astronomy and Solar System science. Through a more direct comparison of operational approaches, the meeting was also intended to improve our current processes and use of resources, as well as to foster innovations and establish/intensify collaborations.

With the contributions of the Programme Organising Committee (see Table 1), which included representatives of both space- and ground-based facilities (mostly European), all details of the content of the programme were discussed and finalised once all abstract submissions had been received. Thanks to a broad range of contributions, the programme[1] took shape and was naturally arranged following the chronology of project phases, from initial concept developments to legacy products. The following aspects were addressed:

– Science operations organisation and management
– Science and instrument planning
– Instrument handling and calibration
– Science data processing
– Community support and services
– Science data archiving and product generation.

With approximately 150 attendees (see Figure), the meeting took place at ESAC (European Space Astronomy Centre; ESA's establishment for science operations), near Madrid, and ran over a total of three days, with a full programme of oral contributions and a parallel poster session.

Science operations

The welcome presentations were given by Martin Kessler (ESA, Head of ESA Science Operations Department) and Andreas Kaufer (ESO, Director of Operations), who summarised the highlights and challenges of ESA and ESO science operations at large, respectively. The programme then started with the most extensive session of the entire meeting, on science operations. This session was intended to provide overview presentations on science operations schemes for a wide spectrum of projects and was organised following a timeline, from past, or ongoing, to future missions. In the end, it ranged from operational overviews of ground-based facilities (Isaac Newton Group, ESO Very Large Telescope [VLT], Gemini and the Atacama Large Millimeter/submillimeter Array [ALMA]) and space missions (Herschel, Planck — High Frequency Instrument [HFI], Picard, Gaia, the Laser Interferometer Space Antenna and the James Webb Space Telescope), to lessons-learned type presentations, where critical evaluations of how things had gone for a given (part of a) mission were presented (e.g., INTEGRAL) or how a successful operational model was evolved for the succeeding mission (e.g., from SOlar Heliospheric Observatory [SOHO] to Solar Orbiter). An interesting presentation, falling between ground and space, was the one about the Stratospheric Observatory for Infrared Astronomy (SOFIA), with all the challenges an airborne observatory has to face.

An aspect that emerged early from this first session was the comparison of operational set-ups between ground-based observatories (self-contained and operating multiple telescopes on the same site) and the more decentralised schemes

Table 1. Composition of the Programme Organising Committee.

Member	Affiliation
Paola Andreani	ALMA Europe (ESO ARC, Germany)
David Barrado	Calar Alto Observatory, Spain (now Centro de Astrobiologia [CAB], Spain)
Chris Benn	Isaac Newton Group of Telescopes (ING, Spain)
Françoise Genova	Centre de Données Astronomiques de Strasbourg (CDS, France)
Paolo Giommi	Agenzia Spaziale Italiana (ASI, Italy)
Nick Hanowski (Chair)	ESA (ESAC, Spain)
Danny Lennon	ESA (ESAC, Spain)
Thierry Levoir	Centre National d'Etudes Spatiales (CNES, France)
Roberto Neri	Institut de Radioastronomie Millimétrique (IRAM, France)
Francesca Primas (co-Chair)	ESO (Germany)
Wolfgang Schmidt	Kiepenheuer-Institut für Sonnenphysik (KIS, Germany)
Tilman Spohn	Deutsches Zentrum für Luft-und Raumfahrt (DLR, Germany)
Mike Watson	XMM-Newton Science Survey Centre (XMM-SSC, United Kingdom)

of space missions, where operations are often distributed and typically involve numerous institutes in several different countries. The closest ground-based approach to this is probably the set-up of the European ALMA Regional Centre (ARC) nodes, where different participating member countries provide operational support via a dedicated node or expertise centre to specific operational tasks and phases. The session also included presentations on the organisation of operational centres that serve multi-mission purposes or are working in close collaboration with each other (e.g., the Centre d’Opérations des Missions Scientifiques for the French Instrument Mars Operation Centre [COMS/FIMOC] facility), and on some sociological aspects that surfaced in the following sessions (e.g., best practices in the collaboration between astronomers and engineers). In addition, an overview of the challenges in setting up a new mission, with all its technical, financial and operational constraints (such as closing the loop on the lessons learned, the balance between conservative *vs*. daring approaches) was provided.

Instrument handling

The next session on instrument handling was actually split into two sub-sessions: “Planning and Scheduling” and “Calibrations and Operations”.

The first part included a mix of talks — some focusing on how the use of an instrument is planned and its science is scheduled (with Herschel as an example), others focusing on the implementation of the most efficient use of telescope/instrument science time. It is clear that this latter is a challenging task that both communities face and has the same ultimate goal: to ensure reliable long-term scheduling (where “long” can refer to a full observability season or shorter periods of time) for which a robust but flexible short-term scheduling can provide the operators/observers with the best trade-off between observations, external conditions, minimisation of idle time, time criticality constraints, etc. In this group of presentations, it was interesting to learn the details of how telescope scheduling is currently carried out at ESO (for the La Silla Paranal and Atacama Pathfinder EXperiment [APEX] facilities) and the exploratory investigations carried out by two independent projects.

The Cherenkov Telescope Array (CTA), is planned to begin construction next year and represents the next generation of ground-based very high energy γ-ray instrumentation. For their final scheduler, the CTA is investigating the application of neural networks (specifically a guarded discrete stochastic neural network) coupled with constraint propagation techniques. The other ongoing investigation presented at the meeting is related to one of the ESA M3 mission candidates currently being assessed, the Exoplanet Characterisation Observatory (EChO). The complexity of the multi-dimensional space (target visibility, time and duration of events, number of events to be observed, target priority), combined with the huge number of possible combinations that have to be looked through to find the optimal solution, makes the scheduling exercise impossible for human planners and motivated the EChO team to look into genetic algorithms. This approach tries to reproduce the evolution of a problem/environment by combining all potential solutions using different types of operators (selection, combination and mutation). Preliminary results look promising, showing higher operational efficiencies than more standard (heuristic) approaches.

The second part of this session, covered best practices in calibrating a given facility/instrument and some operational challenges. The VLT Quality Control Loop and how it has evolved over the years was presented in detail, as well as the challenges that our ALMA colleagues are facing in calibrating all the antennas. More on the operational side, one presentation described the “evolutionary transfer” of the successful operational model behind the Planck low-frequency instrument (LFI) to the Euclid near-infrared spectrometer and photometer (NISP). Another nice presentation, touching upon lessons learned and operational evolution, focused on laser guide star (LGS) operations at the Keck Observatory. Again, the challenges presented in this talk were found to be common with other observatories that offer LGS-supported observations.

Science data processing and conservation

Of the three remaining sessions, two focused on different aspects related to science data, respectively Science Data Processing and Science Data Archiving & Data Legacies. Since they both deal with data, we will summarise the content of both sessions together, leaving the summary of the fifth session for the end of this report. There were of course notable differences in the main focus of these two sessions, namely the basic processing principles applied to science data and their operational implementations on the one side, data archiving/archives and their content at the other end. A few talks dealt with several data-related aspects (e.g., combining multi-frequency, multi-messenger, multi-temporal data or archive, grid, interactive and pipeline processing). Otherwise, we learned how back-end operations are, or will be, implemented (respectively at ESO’s La Silla Paranal Observatory and for the Euclid mission) and what is, and will be, the raw and processed content of current and future archives (from ground- to space-based facilities/missions, like ESO, ALMA, INTEGRAL, VENUS-EXPRESS, HEAVENS).

The highlights here were probably the major infrastructure developments that have taken place in recent years to serve large and complex datasets (Astro-WISE, ESO Advanced Data Products and its new Phase 3 interface, the MUSE–WISE [Wide-field Infrared Survey Explorer] set-up to handle massive MUSE-IFU [integral field unit] datasets and the ESA Multi-Mission Archive). This is a clear and prompt response to the shift that we have witnessed (and are still seeing) within the astronomical community and the way the top scientific questions are posed and tackled. The trend is to deeper and bigger, with large teams proposing public survey (hence legacy) projects that combine efforts in order to collect huge data volumes and tackle the most ambitious scientific quests. These are not projects that can be managed and handled by a few individuals; they are gigantic efforts that require dedicated infrastructure and data centres, able to process huge amounts of data, making them available to the community at large in almost real time. In turn, this also brings more

requests from the community to enhance the content of the more standard data archives. Because of this overwhelming data flow, archive architectures are evolving (e.g., at ESA), independent data centres are being set up (e.g., the European University Institute Data Centre at the Royal Observatory of Belgium) and interoperability among different archives remains an important item on the agenda of future efforts.

Community and user support

The final session to be reviewed here is the one on Community and User Support. This was a session heavily dominated by presentations (seven out of ten) on tools and user-support schemes implemented at ground-based (as opposed to space-based) facilities. ALMA and VLT/I user support implementations were compared in detail, including the main sets of tools that are provided to the users to prepare their observations. All other contributions were geared more towards user services for data processing, handling and distribution. We learned about the challenges that the APEX facility had to overcome in making the data available rapidly (i.e., within two days) to its users via the ESO Archive and which services and interfaces the AGILE Science Data Centre at the Italian Space Agency provides to its user community (especially in terms of web-based tools for quick-look and online data analysis).

At the end of the day, what really counts is how successful a facility/mission is or has been. This is rather challenging to assess: it clearly relies on a variety of — if not all — the operational aspects that were scrutinised during the meeting, from the call for ideas and conception of a new mission/instrument to the detailed definition and implementation of ancillary tools/interfaces that make the new facility as user-friendly as possible. Yet, the loop needs somehow to be closed so that we can measure the research output of a facility/observatory/mission as one of the possible indicators of success. One such attempt was presented in the presentation on the ESO telescope bibliography telbib, aimed at correlating scientific productivity to the amount of time invested in science observation. A huge but very rewarding effort!

Towards a follow-on conference

As the first attempt in gathering people involved in science operations at large, the success of the meeting was not guaranteed from the start. However, a large majority of the attendees agreed in declaring this event a success and something worth pursuing further. Overall, more open discussions on specific operational topics would have been beneficial; on the other hand this meeting provided a very detailed overview of all ongoing and future projects, both ground- and space-based (though mostly European). This, now common, understanding is essential for further exploration of synergies. There was a clear push from the audience in continuing this forum and we hope that the next such meeting will be able to take advantage of what we all learned this time, so that it can foster more concrete innovative developments and strengthen collaborative efforts.

Links

[1] Conference website and programme: http://www.sciops.esa.int/sciops2013

Announcement of the ESO Workshop

Herbig Ae/Be stars: The missing link in star formation

7–11 April 2014, ESO Vitacura, Santiago, Chile

This workshop on Herbig Ae/Be stars is dedicated to the formation and pre-main sequence (PMS) evolution of intermediate-mass stars. These stars bridge the transition between the distinctly different scenarios for the formation of low- and high-mass stars. Over the past 20 years, new instruments have opened up the milli- and sub-milliarcsecond spatial scales where the disc physics takes place and planetary formation processes occur. ALMA will complement spatially, and advance spectrally at high resolution, the connection between the inner discs and the outer, dusty discs as observed by space-based observatories. The workshop aims to elucidate the evolution of the circumstellar material from the formation phases, during the star's PMS contraction, and into the dispersal and debris phases. Topics include stellar interiors and surface physics accretion and ejection processes, evolution of the discs and the connection with debris discs and planet formation.

The workshop format will consist of invited reviews, contributed talks and posters. There will be ample time for discussions. The conference venue has the capacity for 100–120 participants.

The ESO 2014 Herbig AeBe workshop will commemorate of the life and works of George H. Herbig (2 January 2 1920 – 12 October 2013). George Herbig pioneered the field of star formation, especially that of young stars and their nebulous surroundings. His legacy includes the identification and first description of the Herbig Ae/Be stars and the Herbig–Haro objects.

Full details can be found on the workshop web page:
http://www.eso.org/sci/meetings/2014/haebe2014.html
or by e-mail to: haebe2014@eso.org

The abstract and registration deadline is 31 January 2014.

Fellows at ESO

Roger Wesson

Like many people in astronomy, I became interested in the subject at a very young age and have followed that interest all the way through to the heady world of professional science. But perhaps unlike many people, I've made several attempts along the way to escape from this world of sleepless nights and deadlines and constantly finding new things not to understand, only to find myself suddenly back in it, as if attached to it by some giant metaphorical bungee rope.

1985 saw A-Ha's *Take On Me* topping the charts around the world, Halley's Comet become visible to the naked eye for the first time in 75 years, and a young me develop an interest in astronomy. A local astronomy society had an open evening about the comet, and my dad took me along. And even though we did not see the comet at all from the light-polluted south of England, for several years I had an insatiable interest in everything astronomical.

Later my interest waned, and really the next time I thought about astronomy was when I was thinking about going to university. Browsing a thick book listing all the courses you could do at all the universities in the UK, I found "Astrophysics" fortuitously close to the start of the book. My interest in the Universe was reawakened in a flash, and so I went to University College London (UCL) to study astrophysics. There I had my first experience of observational astronomy using a 6-inch refractor at the University of London Observatory, looking at the Moon and Saturn through the suburban murk. Later, I used the 24-inch Radcliffe Telescope there, one of the largest working refractors in the world today, and measured the stellar wind velocity of P Cygni. And then in my third year, we went on a field trip to the Observatoire Haute-Provence for a most awesome week of science and fun. They had a really good coffee machine there and by the time we left I was addicted both to caffeine and to observational astronomy.

But the end of my degree saw my first escape attempt. My life plan was to travel for a long time, and then think of a life plan. Unexpectedly, an opportunity to do a PhD arose, and I decided it would be

Roger Wesson

silly to spurn it. So I returned from the jungles of the Yucatan to UCL once again, and spent three great years studying chemical abundances in planetary nebulae.

Then came escape attempt number two, this one a little more successful. The pain of frustrated *wanderlust* had been with me for three years and I decided it had to go away. But after seven years of impoverished studenthood in London, I needed some money. Quite randomly I found a job in the UK Home Office, where I worked in the department responsible for overseeing policing. I drafted replies to be given to questions asked by MPs in the House of Commons, wrote speeches for government ministers, and helped to develop policies, guidelines and legislation.

It was all good fun, but it was a means to an end, and the end was travelling. I headed to South America, spending four months travelling from Buenos Aires to Quito via Tierra del Fuego. I spent a long time in Chile, seeing most things between the Straits of Magellan and the Atacama. I liked Santiago straight away, and I remember thinking "I could live here", without imagining that I ever actually would.

The journey ended and I found myself back in London one cold winter morning. I got another civil service job but it was much less fun than the last one had been, and I felt the pull of the bungee rope. Luck was on my side and I managed to get a postdoc back at my old haunt of UCL.

I spent a few more fantastic years in London, before finally having the great opportunity to move to Chile to carry out duties at the Very Large Telescope, and I've been here now since October 2011. On Paranal I like to take a few minutes whenever possible to get out under the stars and see the true spectacle of a clear dark sky, which blows me away every time I see it, and convinces me that I've probably made the last of my escape attempts. Once you've connected with the Universe in the way you can at Paranal, it's hard to see how any other line of work could be as satisfying as this.

Farid Rahoui

My journey to astrophysics was long and tortuous. I was born and grew up north of Paris, in a family with a clear literary background. I am actually the only one among four siblings who embraced a scientific career, with the understanding that addition and subtraction were already science for the other three. As a child, I was not particularly interested in astronomy and could not have cared less about celestial objects such as stars, planets or galaxies. And, well, the sky in Paris is usually cloudy, which does not help. In truth, I was not really into natural sciences, which were too concrete and too empirical for me. Anyway, the experiments were usually not very co-operative, with all those chemical solutions turning red instead of blue!

No, despite a family curse, I wanted to be a mathematician. The situation evolved quite a bit when I started doing more quantitative physics in high school. I discovered that nature could be put into equations, that real-life phenomena could be well described by exponentials and other abstract functions. For the first time, teachers were telling me about all those exotic concepts, such as black holes, time dilation, subatomic particles, the Big Bang ... my choice was made, I would become a theorist.

I stuck to that plan for five years and managed to convince the University of Grenoble to give me a Masters degree in theoretical particle physics. But then, just before starting my PhD, I realised that I wanted to know something different from academia and started a real-life job as an engineer, working on signal processing for a multinational company. I quickly realised that I would not spend my life there (that's actually an understatement), but I had the great opportunity to work

Farid Rahoui

with fantastic people who taught me a lot. This is where I developed a taste for experimental work and the first time that I really used tools to build or fix things. I also had the chance to travel to several countries for my work, which was a strong incentive to stay. I eventually resigned after two years and settled down for a while in South Korea and South Africa.

Back to France, I enrolled in a Masters degree in Space Sciences at the Meudon Observatory, where I did astronomy-related things for the very first time, although my training was more focused on space missions. From then on, everything went smoothly. I did my Masters' internship at ESO Chile, working with Olivier Hainaut on simulations for extrasolar planet detection with extremely large telescopes, which were supposed to be 100 metres in diameter at that time. I had my first experience with astronomical observations there, starting with the New Technology Telescope! I liked ESO a lot, Chile even more, and I decided to stay for a PhD that I undertook in collaboration with CEA Saclay in Paris. I worked under the supervision of Felix Mirabel and Sylvain Chaty on multi-wavelength observations and modelling of neutron star and black hole X-ray binaries. These sources are very interesting because their bolometric emission is the sum of that of different components (stars, accretion discs, outflows, jets, dust, etc.) that are strongly interdependent. They allow us to apprehend physical phenomena in extreme environments, whether strong gravitational fields or intense ionising emission. They are however strongly variable on short timescales and in all spectral domains, which forces us to observe them quasi-simultaneously with a large range of space- and ground-based instruments, which is challenging.

After my PhD, I worked for three years with Julia Lee at Harvard University, where I extended my work to active galactic nuclei and radiative transfer modelling. I now have the great honour to start my second year as an ESO Fellow in Garching before, I hope, getting a research position in France and continuing to work in astrophysics.

Personnel Movements

Arrivals (1 October–31 December 2013)

Europe	
Bethermin, Matthieu (FR)	Fellow
Dhawan, Suhail (IN)	Student
Galametz, Maud Muriel (FR)	Fellow
Ginsburg, Adam (US)	Fellow
Guerou, Adrien (FR)	Student
Husemann, Bernd (DE)	Fellow
Mc Leod, Anna Faye (FR)	Student
Pfeffer, Joel Leslie (AU)	Student
Saturni, Francesco Gabriele (IT)	Student
Zafar, Tayyaba (PK)	Fellow

Chile	
Anderson, Joseph (GB)	Fellow
Beamin, Juan Carlos (CL)	Student
Deschamps, Romain (FR)	Student
Diener, Catrina (CH)	Student
Ertel, Steve (DE)	Fellow
Lorca, Rodrigo (CL)	Procurement Officer
Marsset, Michaël(FR)	Student
Perrault, Florence (FR)	Contract Officer
Yang, Bin (CN)	Fellow

Departures (1 October–31 December 2013)

Europe	
Bayo Aran, Amelia Maria (ES)	Fellow
Bramich, Daniel (GB)	Astronomer
Costigan, Gráinne (IE)	Student
Feltre, Anna (IT)	Student
Huckvale, Leo (GB)	Student
Kains, Noe (BE)	Fellow
Sanchez, Joel (MX)	Student
Scicluna, Peter (GB)	Student
Stoffer, Christina (CH)	Administrative Assistant
Urrutia-Viscarra, Paula Maria Fernanda (CL)	Student

Chile	
Bascunan, Rogelio (CL)	System Engineer
Carter, John (FR)	Fellow
Ebensperger, Carlos (CL)	Drawing Designer
Fluxa, Juan Carlos (CL)	Electronic Engineer
Guzman, Leonardo (CL)	Contract Officer
Lavin, Octavio (CL)	Mechanical Engineer
Miccolis, Maurizio (IT)	System Engineer
Nakos, Theodoros (GR)	Test Scientist
Pauwels, Evert (NL)	Product and Quality Assurance Programme Manager
Saulder, Christoph (AT)	Student

ESO, the European Southern Observatory, is the foremost intergovernmental astronomy organisation in Europe. It is supported by 15 countries: Austria, Belgium, Brazil, the Czech Republic, Denmark, France, Finland, Germany, Italy, the Netherlands, Portugal, Spain, Sweden, Switzerland and the United Kingdom. ESO's programme is focused on the design, construction and operation of powerful ground-based observing facilities. ESO operates three observatories in Chile: at La Silla, at Paranal, site of the Very Large Telescope, and at Llano de Chajnantor. ESO is the European partner in the Atacama Large Millimeter/submillimeter Array (ALMA) under construction at Chajnantor. Currently ESO is engaged in the design of the European Extremely Large Telescope.

The Messenger is published, in hard-copy and electronic form, four times a year: in March, June, September and December. ESO produces and distributes a wide variety of media connected to its activities. For further information, including postal subscription to The Messenger, contact the ESO education and Public Outreach Department at the following address:

ESO Headquarters
Karl-Schwarzschild-Straße 2
85748 Garching bei München
Germany
Phone +49 89 320 06-0
information@eso.org

The Messenger:
Editor: Jeremy R. Walsh;
Design, Production: Jutta Boxheimer;
Layout, Typesetting: Mafalda Martins;
Graphics: Roberto Duque.
www.eso.org/messenger/

Printed by Color Offset GmbH,
Geretsrieder Straße 10,
81379 München, Germany

ISSN 0722-6691

Contents

Front cover: An aerial view of the Paranal Observatory taken in 2013 looking west towards the Pacific Ocean. The four VLT Unit Telescopes, the four 1.8-metre Auxiliary Telescopes and the VLT Survey Telescope (VST) are situated on Cerro Paranal and the nearby VISTA survey telescope on the peak in the foreground. Credit: G. Hüdepohl (atacamaphoto.com)/ESO